Fresh groundwater in large beach nourishments

Growth of freshwater resources in coastal areas

Zoet grondwater in grote zandsuppleties

Groei van zoetwatervoorraden in kustgebieden

(met een samenvatting in het Nederlands)

PROEFSCHRIFT

ter verkrijging van de graad van doctor aan de Universiteit Utrecht op gezag van de rector magnificus, prof. dr. H.R.B.M. Kummeling, ingevolge het besluit van het college voor promoties in het openbaar te verdedigen op 26 april 2019 des middags te 12:45 uur.

door

Sebastian Huizer

geboren op 17 mei 1985, te Gorinchem

Promotor
Prof. dr. ir. M.F.P. Bierkens

Co-promotor
Dr. ir. G.H.P. Oude Essink

This work was financially supported by the Dutch Technology Foundation STW, which is part of the Netherlands Organisation for Scientific Research (NWO), and is partly funded by the Ministry of Economic affairs (project number 12686).

Utrecht Studies in Earth Sciences 183

Fresh groundwater in large beach nourishments

Growth of freshwater resources in coastal areas

Sebastian Huizer

Utrecht 2019

Department Physical Geography
Faculty of Geosciences - Utrecht University

Promotor
Prof. dr. ir. M.F.P. Bierkens

Co-promotor
Dr. ir. G.H.P. Oude Essink

Examination committee
Prof. dr. M. Bakker
Delft University of Technology, The Netherlands
Prof. dr. A. Kemna
University of Bonn, Germany
Dr. H.A. Michael
University of Delaware, USA
Prof. dr. B.G. Ruessink
Utrecht University, The Netherlands
Prof. dr. S.E.A.T.M. van der Zee
Wageningen University, The Netherlands

ISBN 978-90-6266-537-2

Published by Faculty of Geosciences, Universiteit Utrecht, The Netherlands, in: Utrecht Studies in Earth Sciences (USES), ISSN 2211-4335

Printed by: ProefschriftMaken || www.proefschriftmaken.nl

Contents

1 Introduction

1.1 Background

Fresh groundwater is an important to vital resource for billions of people, and constitutes a primary source of high-quality fresh water for domestic, industrial or agricultural purposes. As highlighted by many researchers in recent years, the availability of fresh groundwater around the world is under threat: excessive groundwater abstractions, continuing population growth, sea-level rise, (long) droughts, land subsidence, and increases in the frequency and intensity of storm surges threaten the access to (reliable) fresh groundwater of numerous people (Famiglietti, 2014; Ferguson and Gleeson, 2012; Gleeson et al., 2012; Rotzoll and Fletcher, 2012; Taylor et al., 2013; Wada et al., 2010; Wong et al., 2014).

The most vulnerable areas are coastal lowlands and small islands, because of their susceptibility to coastal flooding and frequent reliance on groundwater as a source of freshwater (McGranahan et al., 2007; Neumann et al., 2015; Terry and Falkland, 2010). For example, Gingerich et al. (2017) reported that the fresh groundwater supply of small low-elevation oceanic islands can become unpotable for several months after a flood event, even when the infiltrated volume of seawater is small. Besides the risks for fresh groundwater resources, these areas are prone to land loss or degradation, due to (extensive) land-surface inundations or (long-term) coastal erosion (FitzGerald et al., 2008; Nicholls, 2011; Zhang et al., 2004).

To protect coastal communities and their livelihood, a coastal management strategy should be developed and implemented for all vulnerable areas (Nicholls and Cazenave, 2010). Coastal managers generally have three adaptation options to consider (Nicholls, 2011):

1. (Planned) Retreat: minimize the impact of inundations or flooding by moving landwards, abandoning the human use of the affected area
2. Accommodate: minimize the impact of inundations or flooding by adjusting the use (e.g. warning systems, insurance)
3. Protect: prevent or reduce inundations and flooding by 'soft' or 'hard' engineering solutions (e.g. beach nourishment, groins, seawalls)

All options result in a safer environment for the inhabitants, but in the option '(Planned) Retreat' and 'Accommodate' the land-surface inundations or coastal flooding continue to occur. In both of these options the previously described threats to the availability of fresh groundwater and land loss are not prevented or resolved. The only potential response that can simultaneously prevent or reduce the loss of land and fresh groundwater resources is the implementation of coastal protection.

Coastal protection takes the form of artificial defences that vary from 'hard' (e.g. groins, seawalls or offshore breakwaters) to 'soft' (e.g. beach nourishments, dune constructions or the creation of salt-marshes). Both engineering solutions have been widely applied in developed countries, such as the Netherlands, Italy, Australia, and the United States (Armstrong et al., 2016; Cooke et al., 2012; Keijsers et al., 2015; Pranzini, 2017; Sterr, 2008). However, in recent decades concerns for the environment have led to discussions on the sustainability of (hard) engineering solutions (Cooper and McKenna, 2008). One possible answer for these concerns is a 'new' approach that tries to integrate coastal protection strategies and natural processes, which is called 'Building with Nature' (Slobbe et al., 2013). One prime example of this coastal protection strategy is the Sand Engine (also called Sand Motor, or 'Zandmotor' in Dutch), which is the name of a very large and concentrated beach nourishment of 21.5 million m^3 that has been applied on the Dutch coast in 2011 (Figure 1.1). Natural forces (i.e. wind, waves and currents) gradually transport the replenished sand along the retreating coast, compensating loss by coastal erosion and simultaneously supporting natural dune growth (Stive et al., 2013).

Figure 1.1 Photo of the Sand Engine in 2011.

This beach nourishment is part of a (pilot) research project in which this method is evaluated with respect to the current practice in the Netherlands of large-scale distribution of smaller volumes of sand (Luijendijk et al., 2017). The Sand Engine is also one of a few coastal adaptation approaches that additionally might help to preserve or even increase the available volume of fresh groundwater.

1.2 Research questions and thesis outline

Since the Sand Engine is the first of its kind, little is known about the influence of a large beach nourishment on fresh groundwater resources. In theory, a seaward displacement of the shoreline would lead to an increase of the fresh groundwater volume (Oude Essink, 2001). As shown for comparable coastal environments such as (small) islands, the size and shape of this fresh groundwater lens will likely be controlled by three key factors: (1) the physiographic and hydrogeological properties of the aquifer (e.g. geometry, hydraulic conductivity, heterogeneity), (2) hydrodynamic and dispersive processes (e.g. tidal forcing, coastal flooding), and (3) external forces – such as groundwater recharge or groundwater abstractions – that modify the inflow, discharge and boundary conditions (Schneider and Kruse, 2003; White and Falkland, 2010; Holding and Allen, 2015b; Werner et al., 2017; Gingerich et al., 2017). However, the combination of the dynamic nature of the coastal system and design of such a large and concentrated nourishment make the Sand Engine considerably more vulnerable to morphological changes and coastal flooding (Stive et al., 2013). This led to the main objective of this thesis: What is the impact of large and concentrated beach nourishments as the Sand Engine on coastal fresh groundwater resources?

The impact of the Sand Engine on fresh groundwater resources can be categorized into two groups:

1. *During the construction of the beach nourishment*
   The Sand Engine was constructed by depositing, pumping and spraying a mixture of sand and seawater from sand pits in the North Sea on the project site. Seawater that accompanies the sand led to a salinization of the nourishment and its immediate vicinity (e.g. shore, beach).

2. *Throughout the lifespan of the Sand Engine*
   During the lifespan of the Sand Engine, the seaward expansion of the beach leads to a displacement of the (direct) influence of the North Sea towards the newly created shoreline. Combined with the likely growth of dunes, the local extension of beaches and dunes leads to a growth of the volume of fresh groundwater. This growth is driven by precipitation, groundwater flow from the dunes to the site, and a local areal shift in the impact of the North Sea.

Where the direct impact of the construction of the Sand Engine on fresh groundwater is relatively predictable and limited in extent, the long-term impact of the creation of the Sand Engine is complex and extensive. The complexity is a result of the morphological evolution of the Sand Engine and the exposure to tides, waves, and storm surges. In other words, the eventual growth of fresh groundwater resources is to a large extent controlled by highly dynamic processes, which are harder to predict.

To map the growth of fresh groundwater resources and to determine the impact of the various coastal processes in more detail, extensive field measurements and model simulations were conducted on the Sand Engine. To answer and specify the various aspects of the impact of the Sand Engine on fresh groundwater resources, the research question was split into four sub-questions:

1. *What is the potential increase in fresh groundwater resources over a long period?*

In chapter 2 we investigated the potential effect of the long-term morphological evolution of the large sand replenishment and climate change on fresh groundwater resources from 2011 to 2050. The potential effects on the local groundwater system were quantified with a calibrated three-dimensional (3-D) groundwater model, in which both variable-density groundwater flow and salt transport were simulated.

2. *What is the impact of tides, waves and storms on the fresh groundwater lens in the Sand Engine?*

In chapter 3 we investigated the impact of tides and storm surges on coastal groundwater on the Sand Engine. To monitor changes in groundwater salinity under a variety of conditions, we performed automated time-lapse measurements with electrical resistivity tomography (ERT) for a period of 2 months between November 2014 and January 2015.

3. *What were the changes in the volume of fresh groundwater in the study area since its construction, and which processes drove these changes?*

In chapter 4 we have examined the impact of coastal forcing (i.e. natural processes that drive coastal hydro- and morphodynamics) and groundwater recharge on the growth of the fresh groundwater lens between 2011 and 2016. Measurements of the morphological change and the tidal dynamics at the study site were incorporated in a local, calibrated, 3-D and variable-density groundwater model of the study area.

4. *Which coastal sites are potentially suitable for large-scale beach nourishments, with regard to the growth of coastal fresh groundwater resources?*

In chapter 5 we have made a first attempt to assess the potential suitability of coastal sites for large beach nourishments, from the perspective of the the attainable growth in fresh groundwater resources. With 2-D model simulations with variable-density groundwater flow the impact of groundwater recharge, hydraulic conductivity, specific yield, beach slope, tidal dynamics, and morphodynamics on the volume evolution of fresh groundwater was evaluated. The outcome of this analysis was used to map the potential suitability for the growth of fresh groundwater resources with large-scale beach nourishments at a global scale.

At the end of this thesis (chapter 6) answers to the research questions are summarized. This final chapter also includes recommendations for future research. As a final note, the individual chapters of this thesis are direct copies of the journal papers. Consequently, there is some overlap between the chapters.

2 Fresh groundwater resources in a large beach nourishment

Based on: Huizer, S., Oude Essink, G. H. P., and Bierkens, M. F. P. (2016), Fresh groundwater resources in a large sand replenishment, Hydrology and Earth System Sciences 20, 3149–3166, doi:10.5194/hess-20-3149-2016.

Abstract

The anticipation of sea-level rise and increases in extreme weather conditions has led to the initiation of an innovative coastal management project called the Sand Engine. In this pilot project a large volume of sand was placed - also called sand replenishment or nourishment - on the Dutch coast. The intention is that the sand is redistributed by wind, current and tide; reinforcing local coastal defence structures and leading to a unique, dynamic environment. In this study we investigated the potential effect of the long-term morphological evolution of the large sand replenishment and climate change on fresh groundwater resources. The potential effects on the local groundwater system were quantified with a calibrated three dimensional groundwater model, in which both variable-density groundwater flow and salt transport was simulated. Model simulations showed that the long-term morphological evolution of the Sand Engine results in a substantial growth of fresh groundwater resources, in all adopted climate change scenarios. Thus, the application of local sand replenishments such as the Sand Engine could provide coastal areas the opportunity to combine coastal protection with an increase of the local fresh groundwater availability.

2.1 Introduction

Global sea-level rise poses a risk for coastal areas, especially when combined with an increase in the frequency and intensity of storm surges (Michael et al., 2013; Nicholls et al., 2010; Wong et al., 2014). Particularly small islands (Chui and Terry, 2013; Holding and Allen, 2015a; Mahmoodzadeh et al., 2014), and low-lying deltas (Giosan et al., 2014; McGranahan et al., 2007; Oude Essink et al., 2010) are vulnerable to rising sea-levels. Many low-lying deltas such as the Mekong Delta (Vietnam) and the Ganges-Brahmaputra delta (Bangladesh) are already frequently subjected to extensive floods, leading to considerable economic losses, property damage, and in severe cases loss of life (Few and Matthies, 2006; de Sherbinin et al., 2011). In addition, many ecosystems and inhabitants of deltas are threatened as a result of high subsidence rates, over-exploitation of fresh groundwater resources, and contamination of coastal aquifers (Crain et al., 2009; de Sherbinin et al., 2011; Syvitski et al., 2009).

Sea-level rise and storm surges will enhance the pressure on these coastal regions (Kooi et al., 2000; Yang et al., 2013, 2015), and will likely exacerbate the loss of agricultural land, damage of ecosystems and the salinization of fresh groundwater resources (Hoggart et al., 2014; Nicholls et al., 2010; Wong et al., 2014).

2.1.1 Coastal management

In order to protect the livelihood of densely populated coastal areas against climate-related impacts, a growing number of studies recognizes the need for the adoption of coastal defense strategies (Giosan et al., 2014; Nicholls et al., 2010; Temmerman et al., 2013; Wong et al., 2014). Fortunately, the awareness of the threats posed by climate change is growing, and coastal defence in a number of countries - especially developed countries - have been intensified, specifically at vulnerable locations (Goodhew, 2014; Kabat et al., 2009; Sterr, 2008). One example is the Netherlands - a vulnerable low-lying country - where coastal defence systems have been reinforced on several occasions, in accordance with its long history of intensive coastal protection (Charlier et al., 2005). Centuries of continuing erosion, flooding and subsidence led first to the implementation of hard engineering methods (e.g. groynes and sea walls), and later soft engineering methods (e.g. sand replenishment or nourishment, (van Koningsveld et al., 2008)). Since 1990 the application of sand nourishments, particularly beach and shoreface nourishments, has become the dominant coastal defence strategy. Sand nourishments are applied on an annual basis - where necessary - to maintain the position of the coastline (Keijsers et al., 2015; de Ruig and Hillen, 1997).

2.1.2 Pilot project: Sand Engine

Since 2001, the position of the entire Dutch coastline is successfully maintained with 12 million m^3 of sand nourishments per year. However, the future annual volume of sand nourishments should increase if the coast is to rise with the sea-level (Deltacommissie, 2008). Research suggests that the annual nourishment volume should be raised to 20 million m^3 yr^{-1} in the nearby future; in order to sustain the Dutch coastline in the long run (Giardino et al., 2011; de Ronde, 2008). The anticipation of a substantial growth in the annual nourishment volume incited discussions about the effectiveness of the current large-scale distribution of sand. These discussions led to the idea that concentrated (mega) nourishments could be more cost-effective than current practices, and may provide opportunities for natural dune growth, and recreation (Slobbe et al., 2013).

The effectiveness, benefits and drawbacks of concentrated (mega) nourishments are currently being investigated with a pilot project named the Sand Engine (also called Sand Motor) (Mulder and Tonnon, 2011; Stive et al., 2013). In this project a mega-nourishment of 21.5 million m^3 was constructed at the Dutch coast in 2011: a few kilometres west from the city of The Hague (Figure 2.1). The replenished sand will gradually be distributed along the coast by wind, waves and currents, thus incorporating natural forces in engineering methods (so called 'Building with Nature') (Slobbe et al., 2013; de Vriend et al., 2014).

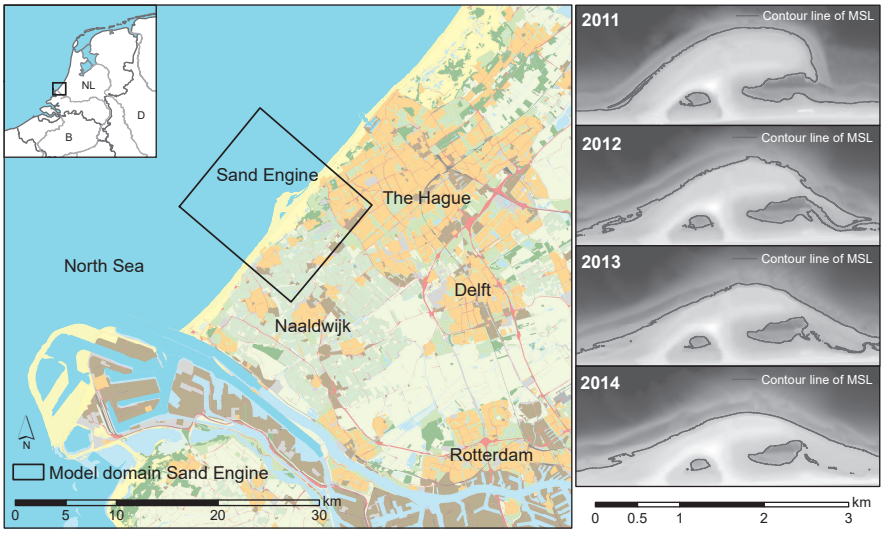

Figure 2.1 Situation of the Sand Engine and morphological development in 2011-2014.

The effectiveness of the Sand Engine is investigated by extensive research and intensive monitoring: the surface elevation (including bathymetry) is measured frequently to gain detailed knowledge of the volume and direction of sediment transport at this local mega-nourishment (Ebbens and Fiselier, 2010; Tonnon et al., 2011). Recent measurements show that the outer perimeter of the 'hook-shaped' peninsula retreated, and the alongshore extent increased (de Schipper et al., 2016; Stive et al., 2013). Initially the Sand Engine extended approximately 1 km into the sea and was nearly 2 km wide at the shoreline, while in September 2014 it extended approximately 800 m into the sea and was more than 3 km wide at the shoreline (Figure 2.1).

2.1.3 Study objectives

The primary objective of this study is to quantify the potential effect of the Sand Engine on the regional groundwater system, particularly on fresh groundwater. During the life span of the Sand Engine the (direct) influence of the North Sea is diminished, because of the seaward displacement of the shoreline – and possibly growth of adjacent dunes. The extension of the beach-dune system and the reduction in seawater intrusion may lead to a growth of fresh groundwater resources. In combination with an increase of groundwater levels, the construction of the Sand Engine may also lead to a decline in the upwelling of saline groundwater and a decreased salt load in adjacent low-lying areas.

The long-term morphological evolution of the Sand Engine – powered by coastal and aeolian sediment transport – will also affect to local groundwater system with time. Erosion and deposition of sand will alter the position of the shoreline and the surface elevation with time, which simultaneously gives rise to dynamic changes in seawater intrusion and submarine groundwater discharge. The morphological evolution of the Sand Engine and the dynamic nature of this coastal system will probably lead to considerable changes in groundwater head and divide, the direction and velocity of groundwater flow, and the stored volume of fresh groundwater.

One of the innovative aspects of this study is to incorporate detailed predictions of the long-term morphological evolution of the Sand Engine in a 3-D numerical model, which simulates variable-density groundwater flow. At the moment no studies have investigated the influence of local mega-nourishments on groundwater systems, and only a few groundwater modelling studies have incorporated a changing morphology in their calculations (Delsman et al., 2014). We also assess the effect of climate change (e.g. sea-level rise) on fresh groundwater resources in the study area, in combination with the morphological evolution of the Sand Engine. To our knowledge, no other studies have integrated the effect of the morphological evolution of coastal areas and climate change on fresh groundwater resources, and the number of quantitative studies that investigate the possibility to combine coastal defence with the protection of fresh groundwater resources are scarce (Oude Essink, 2001). However, studies on small islands have shown that great losses in the volume of fresh groundwater can occur as a result of decreases in groundwater recharge and sea-level rise, and especially small and thin lenses seem vulnerable to salinization (Chui and Terry, 2013; Holding and Allen, 2015a; Mahmoodzadeh et al., 2014). In relation to the morphological dynamics of coastal regions, studies have shown that the erosion and accretion of sand can lead to substantial changes within the beach-foredune area (Bakker et al., 2012; Keijsers et al., 2014), and that climate change might exacerbate coastal erosion (FitzGerald et al., 2008; Zhang et al., 2004). Morphological developments in coastal areas can therefore have a substantial effect on fresh groundwater resources, and coastal management strategies that compensate, limit, or counteract coastal erosion or seawater intrusion may help to protect fresh groundwater resources.

The paper first describes the construction of the Sand Engine and the characteristics of the study area. It then reviews the methodology for the development of the regional groundwater model, and the model scenarios. Next, the model calibration and model results are described and examined as well as the impact of different climate scenarios on simulated fresh groundwater resources. Finally, the methodology and results are discussed, emphasizing on the limitations and implications for fresh groundwater resources.

2.2 Site description

2.2.1 Study area

The construction of the Sand engine was commissioned and designed by the executive branch of the Ministry of Infrastructure and the Environment (Rijkswaterstaat) and the provincial authority of South-Holland (Provincie Zuid-Holland) (Mulder and Tonnon, 2011). Large trailing suction hopper dredgers were used to extract sand from several sand pits in the North Sea and to transport this sand to the project site. The dredged material was stored in the hopper and deposited on the project site with three different techniques: by opening the bottom valves of the vessel on-site ("depositing"), by pumping a mixture of sand and water to the site through a pipeline ("pumping"), and by spraying a mixture of sand and water from the vessel's bow to the site ("rainbowing"). When the construction of the Sand Engine was completed (in July 2011), the area above MSL was 1.3 km^2 with a maximum surface elevation of 7 m MSL (Slobbe et al., 2013).

The Sand Engine peninsula is connected to the mainland by a sandy beach, and is bounded by a coastal dune area called Solleveld. Solleveld is relatively small dune area (circa 2 km^2; Figure 2.2) with surface elevations ranging from 2 to 16 m MSL, and is used for the production of drinking water. From the start of the groundwater abstractions in 1887 the demand and abstraction of drinking water gradually increased from a maximum of 1 million m^3 per year before 1970, to a maximum of 7.5 million m^3 per year after 2008 (Draak, 2012). However, to be able to extract these increasing volumes of groundwater without salinization, the drinking water company started with the infiltration of surface water in 1970. The infiltrated volume of surface water is approximately equal to the volume of fresh groundwater that is extracted from the dunes. Currently the groundwater is extracted from the phreatic aquifer with almost 300 vertical pumping wells, which are located on the sides of twelve elongated infiltration basins (Figure 2.2; Zwamborn and Peters, 2000).

Beyond the dunes the area gradually transforms into urban area and low-lying agricultural areas (polders). The low-lying polders have surface elevations of -1 to 1 m MSL, and act predominantly as a groundwater sink, while the urban areas are generally situated in higher areas with surface elevations between 1 and 3 m MSL. The dominant groundwater flow in the upper aquifers flows from the higher urban areas and coastal dunes toward the North Sea and the polders. The relatively low drainage level in the polders also leads to the attraction of deep saline groundwater, in addition to the drainage of local fresh groundwater.

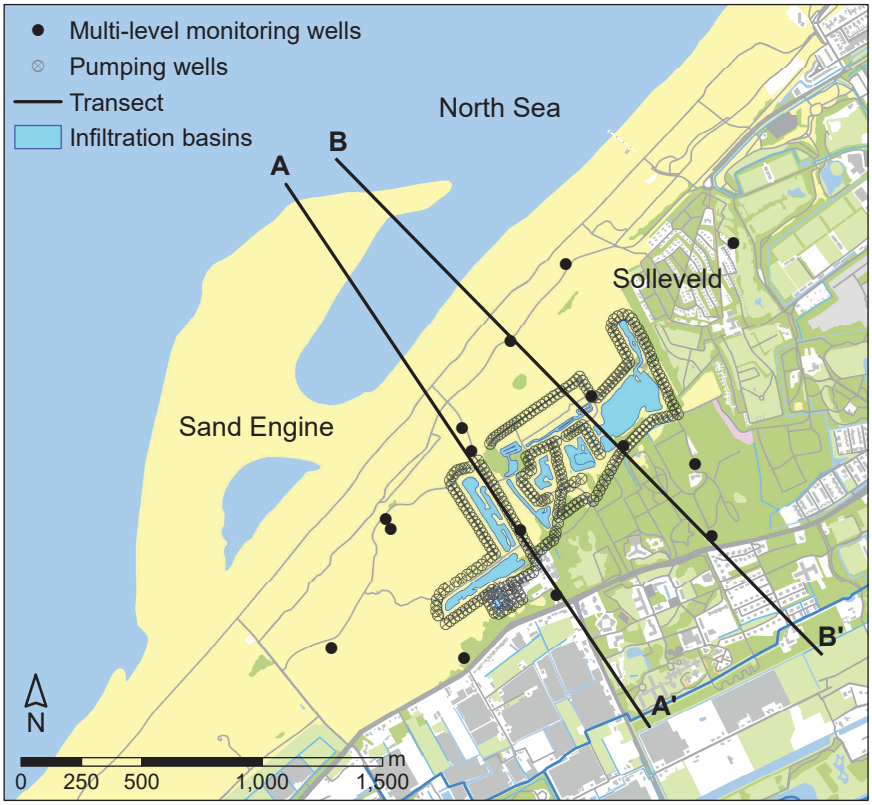

Figure 2.2 Map of the dune area Solleveld with multi-level monitoring wells and pumping wells, including transects A and B (geological profiles in Figure 2.3).

2.2.2 Hydrogeology

The subsoil consists of unconsolidated sediment of predominantly fluviatile and marine origin, as illustrated by two geological profiles in Figure 2.3. The upper part of the subsoil (10 to 30 m) consists of sand, clay and peat, which were deposited during the Holocene: primarily fine- to medium-grained sand in the higher situated dunes and urban areas, and primarily sand and clay in the low-lying areas. However, the lower section of the Holocene deposits (between -15 and -20 m MSL) consists in both areas mainly of clay and peat deposits. The underlying thick layers of fluviatile and marine sediment were deposited during the Pleistocene. It should be noted that the geological schematization of the aquifers and aquitards beneath -40 m MSL are based on a limited number of boreholes.

The conceptual fresh-brackish-saline groundwater distribution (blue striped lines; Figure 2.3) are based on chloride measurements, performed at multi-level monitoring wells. Chloride measurements in Solleveld indicate that the boundary between fresh and brackish groundwater (1 TDS g L^{-1}) is situated between -20 and -40 m MSL, and the boundary between brackish and saline groundwater (10 TDS g L^{-1}) is situated between -40 and -60 m MSL. The depth of the fresh groundwater lens and the extent of seawater intrusion are controlled by head differences.

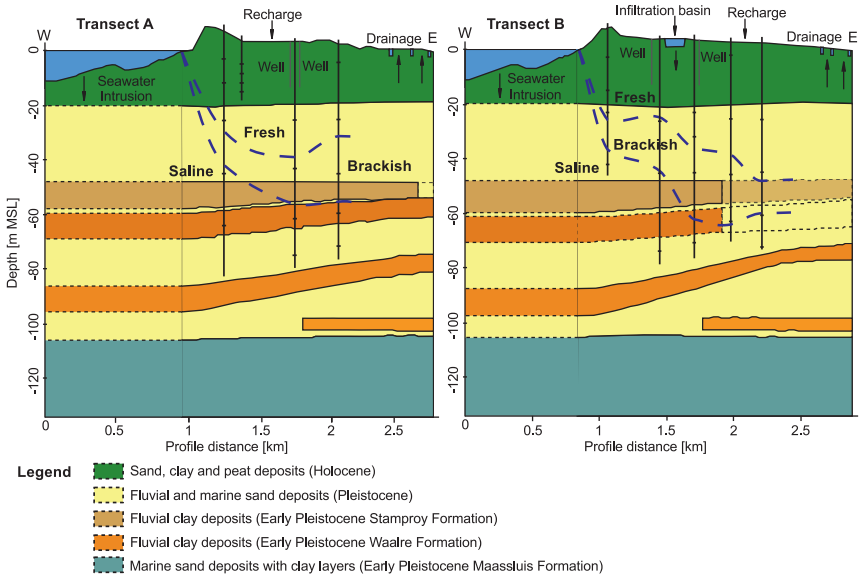

Figure 2.3 Geological profiles (based on databases of the Geological Survey of the Netherlands) across the model domain, with the conceptual freshsalt groundwater distribution (locations are shown in Figure 2.2).

2.2.3 Monitoring

In order to timely observe changes in groundwater level, flow and quality an extensive monitoring network was implemented in Solleveld. After the construction of the Sand Engine this monitoring system was expanded and intensified in the western part of the dune area. The aim of the expansion of the monitoring system was to observe long-term changes in groundwater level, flow and quality and to observe hydrogeological effects caused by the Sand Engine and previous small-scale nourishments (Buma, 2013). The current monitoring system consists of more than 300 observation wells, where the groundwater level is measured with varying frequency (ranging from wells with hourly frequency to wells that are only read off every three months).

The groundwater salinity is measured twice every year in at least 50 monitoring wells, with various methods: groundwater data loggers with measurement of electrical conductivity, electro-magnetic measurements, and analyses for chloride (Buma, 2013). Apart from measurements within the monitoring system, groundwater level measurements of 61 additional (onshore) monitoring wells were available in the national database of the Geological Survey of The Netherlands.

In addition to the expansion of the monitoring system, additional measures were taken to prevent salinization of fresh groundwater in the dunes. On the western base of the dunes a line of 28 interceptor (pumping) wells was installed in 2012 to maintain the groundwater level, and prevent any (negative) impact of the Sand Engine and previous nourishments on the extracted fresh groundwater in the dunes. These interceptor wells were not included in our study, because of a lack of information on the pumping rates and the expectation that the effects on the regional scale are small to negligible.

In order to gain specific information on the geohydrological dynamics within the Sand Engine, eight additional monitoring wells were installed with shallow filters (2 to 10 m below surface) and four monitoring wells with deep filters (16 to 20 m below surface). Since May 2014 the groundwater levels in the monitoring wells are continuously monitored with groundwater data loggers. The salinity of the groundwater is monitored with electro-magnetic measurement within all eight monitoring wells.

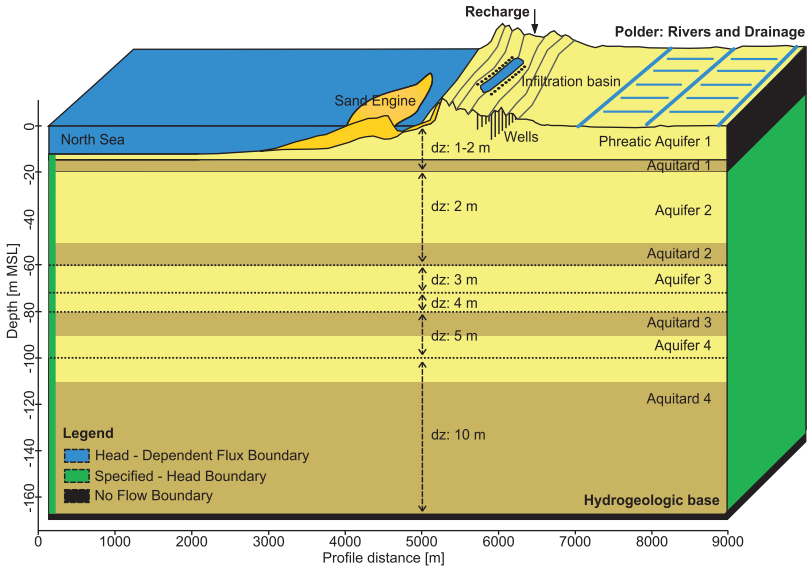

Figure 2.4 Conceptual representation of a slice of the model with layer thicknesses and boundary conditions.

2.3 Method

2.3.1 Variable-density groundwater model

For the quantification of fresh groundwater resources in the study area we constructed a regional three-dimensional groundwater model, in which variable-density groundwater flow was simulated with the computer code SEAWAT (Langevin et al., 2008). SEAWAT has been developed by the United States Geological Survey (USGS), and numerous studies have used the code to simulate variably-density, transient groundwater flow (Heiss and Michael, 2014; Herckenrath et al., 2011; Rasmussen et al., 2013). In SEAWAT the governing flow and solute transport equations are coupled and solved with a cell-centred finite difference approximation. The model domain was discretized in 234 rows, 234 columns, and 50 layers, with a uniform horizontal cell size of 50 m and a varying layer thickness of 1 to 10 m (smallest thickness in upper layers, increasing in underlying layers; Figure 2.4). The discretization and extent of the model were based on three criteria: minimise the effect on simulated groundwater heads and salinities in the study area, limit computation time, and optimise the calculation of the fresh groundwater volume. For the justification of the temporal and spatial discretization we have performed a grid convergence test (Section 2.4.2).

The model boundaries, as visualized in Figure 2.1, were defined either perpendicular to the coastline (the SW and NE sides of the model), or parallel to the coastline (the NW and SE side of the model). Model boundaries that were defined perpendicular to the coastline, lie parallel to the dominant groundwater flow direction in the coastal area, and were therefore defined as no-flow boundaries. The other model boundaries were defined as illustrated in Figure 2.4: 'specified-head' and 'head-dependent flux' boundary conditions (taking into account density differences), which represent the North Sea and local groundwater system, respectively. The 'specified-head' boundary conditions equalled the average level of the North Sea, and were applied to the sea-floor. Local groundwater conditions were defined by a previous model simulation of the southwest of the Netherlands (Oude Essink et al., 2010). The base of the model was defined equal to the hydrogeological base of the model domain, which is approximately -170 m MSL and assumed to be a no-flow boundary.

The subsoil of the model was schematized to four aquifers and three aquitards (Figure 2.4), based on borehole data, and the national geological databases REGIS II.1 (Vernes and van Doorn, 2005) and GeoTOP (Stafleu et al., 2013) of the Geological Survey of The Netherlands. The upper part of the phreatic aquifer (above -10 MSL) was subdivided into two hydrogeological zones with distinct hydraulic conductivities, because the geological data showed systematic differences in the sediment composition within the model domain: one zone coincides with most of the low-lying polders and contains predominantly clay, loam and fine sand deposits; the other zone contains most of the elevated areas of the model domain, where mainly fine to coarse sand was deposited during the Holocene.

Table 2.1 Hydrogeological parameters used in the simulations, where the upper part of the phreatic aquifer (1a: above -10 m a.m.s.l.) was subdivided in two hydrogeological zones (1: fine to coarse sand; 2: clay, loam, and fine sand).

Layer	$\mathbf{K_H}$ **(m d^{-1})**	$\mathbf{K_V}$ **(m d^{-1})**	η_e **(-)**
Phreatic aquifer 1a	10/1	1/0.1	0.3
Phreatic aquifer 1b	1	0.1	0.3
Aquitard 1	0.01	0.001	0.1
Aquifer 2	30	10	0.3
Aquitard 2	2	0.2	0.1
Aquifer 3	5	2	0.3
Aquitard 3	1	0.1	0.1
Aquifer 4	15	3	0.3
Aquitard 4	10	0.03	0.1

The aquifer parameters and layer elevations were defined uniform for each hydrogeological unit, based on parameter estimations in the national hydrogeological database (Table 2.1). The molecular diffusion coefficient was set to 10^{-9} m^2 s^{-1}, and the longitudinal dispersivity was set to 0.2 m with a ratio of transversal to longitudinal dispersivity of 0.1. These values are similar to comparable groundwater models in the same region (Eeman et al., 2011; de Louw et al., 2011; Vandenbohede and Lebbe, 2007, 2012).

Other model parameters such as recharge, and surface water levels were defined by spatially distributed and time-average values of the current situation. The average monthly precipitation and reference evapotranspiration between 1981 and 2000 (Royal Netherlands Meteorological Institute, KNMI) were used to estimate the average seasonal (DJF, MAM, JJA, and SON) precipitation and evapotranspiration. Crop and interception factors were used to estimate the actual evaporation in different land use classes (e.g. forest, agriculture, urban areas) (Droogers, 2009; Hooghart and Lablans, 1988; Meinardi, 1994). Water levels, depths and widths of canals and ditches were provided by the Delfland Water Authority, and drainage levels were based on local knowledge and estimations from the Netherlands Hydrological Instrument model (de Lange et al., 2014). Information on the abstraction of groundwater and the infiltration of surface water in the dune area Solleveld was provided by the drinking water company Dunea.

In the model simulations we have used TDS, where TDS equals salinity (g TDS L^{-1}), and in the classification of the groundwater salinity we have focused on three classes: fresh (0 - 1 g TDS L^{-1}), brackish (1 - 10 g TDS L^{-1}), and saline (10 - 30 g TDS L^{-1}). For the conversion of chloride to TDS we have used the linear relation between chloride and TDS in the North Sea; 1 g TDS L^{-1} = 0.55 g Cl L^{-1} (Millero, 2003).

The North Sea TDS in the model domain was estimated at 28 g TDS L^{-1} for all model simulations (density of 1020 kg m^{-3}), based on geo-electrical measurements in the North Sea near Ter Heijde between 1973 and 1997 (Rijkswaterstaat, 2012). This salinity concentration is smaller than the general North Sea concentration (30 – 35 g TDS L^{-1}), because of the nearby freshwater discharge from the river Rhine. The TDS concentrations on the SE side of the model were defined by previous model calculations of the southwest of the Netherlands (Oude Essink et al., 2010). The TDS concentration of infiltration basins, canals and ditches were set to 0.2 g TDS L^{-1}, which is the average TDS concentration found in surface water within the study area. The spatial variation in the salinity of the groundwater recharge was estimated with semi-empirical equations, which were developed to predict the effects of sea spray deposition in coastal areas (Stuyfzand, 2014). Based on meteorological measurements of the wind speed and wind direction at the measurement station in Hoek van Holland in the period 1971 – 2015, the estimated annual mean TDS concentration varied between 0.121 g TDS L^{-1} at the coastline to 0.023 g TDS L^{-1} at a distance of 5000 m from the high water line.

2.3.2 Calibration of pre-development conditions

The purpose of the model calibration was to generate a valid representation of the pre-development conditions of the Sand Engine (prior to March 2010). In order to exclude anomalous effects of recent sand nourishments on groundwater heads and concentrations, only observations prior to 2010 were included in the model calibration. We considered three calibration criteria:

1. The error between the observed and simulated groundwater head and concentration should be similar or smaller than the observed variations in groundwater head (the average standard deviation of observations is 0.4 m) and concentration (the average standard deviation of observations is 0.7 g TDS L^{-1})
2. The error should be randomly distributed in space
3. The simulated distribution of the (groundwater) concentrations should correspond with literature (Stuyfzand, 1993).

The calibration comprised sensitivity analyses, (restricted) manual model parameter calibration, and comparisons of simulated groundwater heads and TDS concentrations with averaged observations of recent years. Historical processes that promote or diminish seawater intrusion were included in the calibration, because a salinity distribution often takes decades to hundreds of years to reach an equilibrium (Delsman et al., 2014; Webb and Howard, 2011). Examples of historical processes that have substantially influenced the groundwater salinity in the Dutch coastal area are coastal erosion, sea-level rise, and groundwater abstractions (Post et al., 2003). These processes were therefore included in the model simulations to attain a better match between simulations and observations, and the method of incorporation of the processes is briefly described in Table 2.2 and visualised and in Figure 2.5.

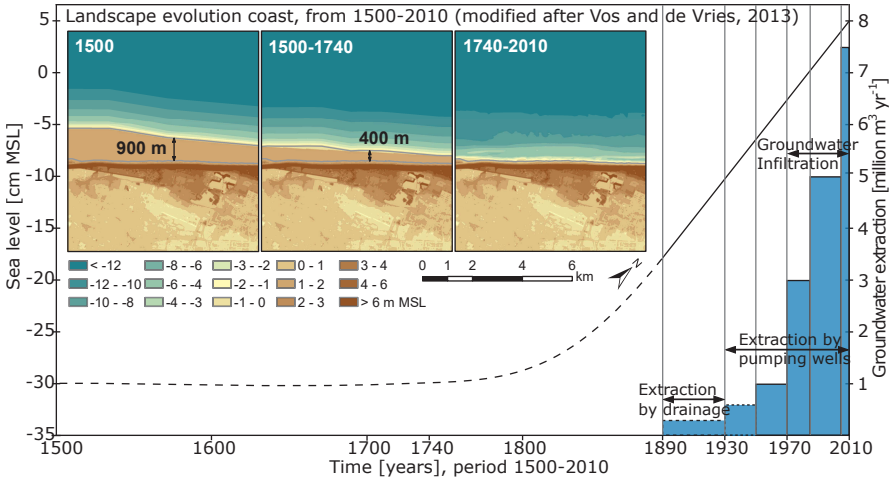

Figure 2.5 Simulation of historical coastal erosion (based on palaeogeographic maps of (Vos and de Vries, 2013), sea-level rise (black line) and groundwater abstraction (blue bars) in the period 1810–2010; dashed lines indicate estimates, and vertical grey lines refer to stress periods.

Other historical changes in for example groundwater recharge and subsidence were not included, because measurements and historical data indicate that these processes probably have a negligible impact on the current head and concentration distribution in the study area (Hoofs and van der Pijl, 2002; CBS et al., 2016). The simulation was restricted to the period 1500–2010, because the focus of this study lies on the present conditions, and we assume that the most substantial effects on the present salt distribution will probably occur in this period. Before the simulation of the period 1500–2010, a transient simulation of the approximate conditions in AD 1500 was executed until the model converged to a dynamically stable state in terms of both groundwater heads and salinity.

In order to attain an optimal calibration result with a limited number of model simulations, model parameters were manually adjusted with small increments from an initial best guess. The adjustments were performed on a selection of the model parameters: (horizontal and vertical) hydraulic conductivity, drainage resistance, stream bed resistance of canals and ditches, and (longitudinal and transverse) dispersivity. Other parameters such as groundwater recharge and surface water levels were based on measurements, maps or expert knowledge, and were excluded from the calibration. The optimised model parameters that were implemented for the model scenarios are described in subsection 2.3.1.

Table 2.2 Simulation of processes and method of incorporation in groundwater model.

Process	**Source/simulation**	**Method of incorporation**
Historical coastal erosion (1500-2010)	Literature and palaeogeographic maps of AD 1500 and 1850; Beets and van der Spek (2000); Beets et al. (1992); Vos and de Vries (2013)	Delineation of the shoreline was incorporated in three phases: 1500, 1500-1740, 1740-2010. Phasing based on literature (Figure 2.5)
Historical sea-level rise (1500-2010)	Literature containing time series and predictions of historical sea-level rise; Jensen et al. (1993); Wahl et al. (2013)	The period 1500-2010 was divided in eight stages, enforcing the average sea-level for each stage (stages are indicated with vertical lines in Figure 2.5)
Groundwater abstraction (1890-2010)	Literature on historical groundwater abstraction in Solleveld; Draak (2012); time series of groundwater abstraction and infiltration volumes.	The period 1890–2010 was divided in six stages, enforcing the average abstraction for each stage (see blue bars in Figure 2.5)
Morphological evolution Sand Engine (2011-2050)	Simulated with Delft3D; Lesser et al. (2004); with computations of the hydrodynamics, waves, sediment transport and bed change; Mulder and Tonnon (2011); Tonnon et al. (2009)	For every 3 month period in 2011-2050 the simulated bathymetry was enforced to the groundwater model; by changing the topography, area of inundation, and recharge.
Sea-level rise (2011-2050)	Climate projections of sea-level rise in 2030 and 2050; KNMI (2014)	The projected sea-level rise in 2030 and 2050 were linearly interpolated. The average sea-level was implemented for every 3 month period.

2.3.3 Morphology and climate scenarios

The effect of the Sand Engine on fresh groundwater resources will primarily depend on the morphological evolution of the coastal area. To assess the potential effect of the mega-nourishment on coastal groundwater, we performed model simulations containing projections of the morphological change of the Sand Engine during the period 2011–2050 (Table 2.2). The morphological development of the Sand Engine in this period was simulated with the hydrodynamics and morphodynamics model code Delft3D (Lesser et al., 2004). This numerical morphodynamic model was calibrated for the period 2005–2010 and validated for the period 1990–2005, prior to the construction of the Sand Engine (Fiselier, 2010; Tonnon et al., 2009).

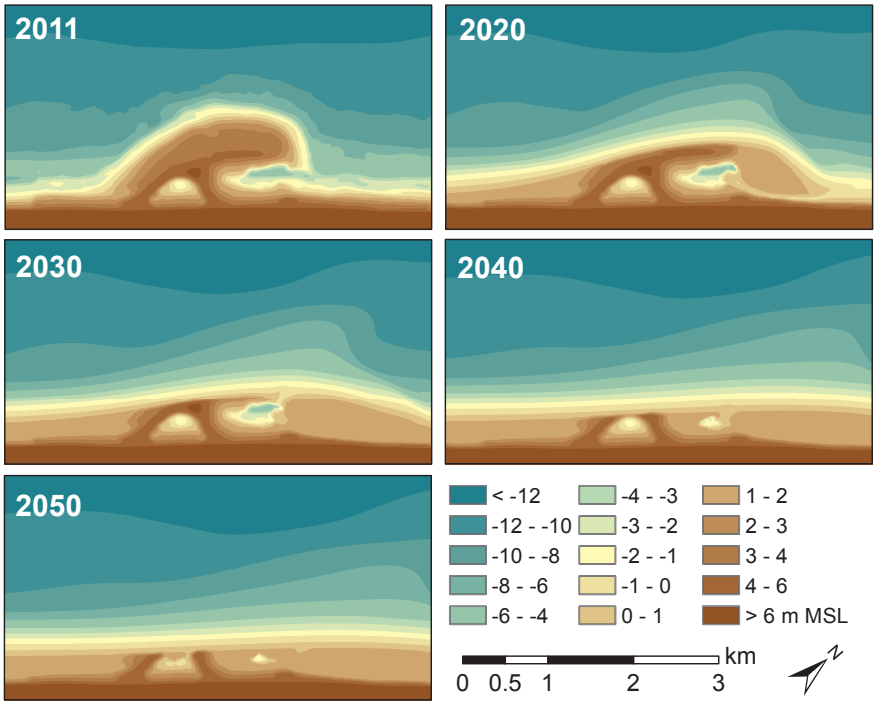

Figure 2.6 Simulated morphological development of the Sand Engine from 2011 to 2050, illustrated by contour maps with the terrain elevation (m a.m.s.l.).

Based on representative tidal boundaries and wave conditions of the current situation, the morphodynamic model was used to simulate the change in bathymetry from 2011 to 2050 (Figure 2.6). The simulated changes in the bathymetry were incorporated in the groundwater model by sequential grid regenerations of the model grid, for every three months (viz. season) in the simulation period. Subsequent changes in the area of inundation, groundwater recharge and thickness of the phreatic aquifer were also adapted in the associated model input files. Estimations of the change in the mean water level in the lagoon (at the northern side of the Sand Engine), which result from the morphological changes, were also included in the model scenarios (de Vries et al., 2015). The expected maximum mean water level in the lagoon equalled 0.9 m MSL in the simulation period.

In addition to the morphological development of the Sand Engine, climate change may also have an impact on coastal groundwater. For the assessment of the potential impact of climate change on fresh groundwater resources, we have used the KNMI'14 climate change scenarios G_L, G_H, W_L and W_H (KNMI, 2014). These scenarios contain climate projections for the Netherlands for the years 2030, 2050 and 2085, based on global climate models as described in the 5th IPCC Assessment report (IPCC, 2014). The climate projections of sea-level rise, precipitation and potential evapotranspiration for 2030 and 2050 in these scenarios were used to assess the effect of climate change as summarised in Table 2.3.

All climate change scenarios were simulated for a reference case without the Sand Engine, and the current situation with the Sand Engine including the projected morphological evolution. The reference case serves primarily as a comparison to the simulations with the morphological evolution of the Sand Engine. The dissimilarity between both situations represents the total impact of the construction of the Sand Engine on local fresh groundwater resources. In turn, the climate change scenarios show the response and sensitivity of local fresh groundwater resources to alterations in sea-level rise, precipitation and evapotranspiration.

Table 2.3 Model climate change scenarios for the period 2011 - 2050, with two rates of SLR, starting at 0.05 m a.m.s.l. and seasonal variation in groundwater recharge (DJF, MAM, JJA, SON).

Climate scenario	**Sea-level rise**	**Precipitation 2050 (given per season)**	**Potential evaporation 2050 (given per season)**
No climate change (NoCC)	No sea-level rise (0.05 m a.m.s.l.)	Equal to present: period 1981-2010	Equal to present: period 1981-2010
G_L	+3.75 mm yr $^{-1}$ [2050: 0.20 m a.m.s.l.]	+3% (DJF), +4.5% (MAM), +1.2% (JJA), +7% (SON)	+2.9% (DJF), +1.3% (MAM), +3.9% (JJA), +2.7% (SON)
G_H	+3.75 mm yr $^{-1}$ [2050: 0.20 m a.m.s.l.]	+8% (DJF), +2.3% (MAM), +8% (JJA), +8% (SON)	+2.4% (DJF), +2% (MAM), +7.5% (JJA), +2.8% (SON)
W_L	+6.25 mm yr $^{-1}$ [2050: 0.30 m a.m.s.l.]	+8% (DJF), +11% (MAM), +1.4% (JJA), +3% (SON)	+3.2% (DJF), +1.7% (MAM), +4.4% (JJA), +5.8% (SON)
W_H	+6.25 mm yr $^{-1}$ [2050: 0.30 m a.m.s.l.]	+17% (DJF), +9% (MAM), –13% (JJA), +7.5% (SON)	+2.7% (DJF), +2.9% (MAM), +10.6% (JJA), +4.5% (SON)

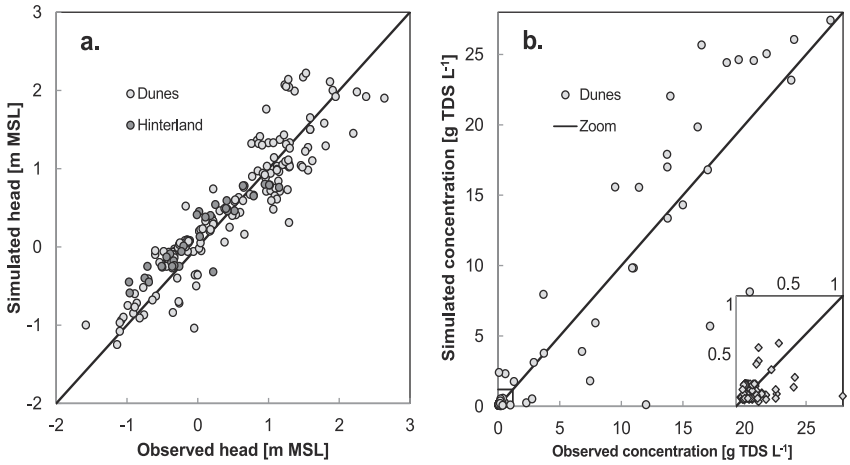

Figure 2.7 Comparison of observed and simulated heads (a) and concentration (b).

2.4 Results

2.4.1 Model calibration

For the calibration of the variable-density groundwater model, we compared the simulated pre-development groundwater head and TDS concentration with recent observations of groundwater heads and chloride concentrations (Figure 2.7). The calibration was performed with averaged values of recent observations, and therefore transient model was strictly speaking not calibrated. We think this is acceptable, because of: the long-term scope of this study, the conservative value of 0.15 that was used for the specific yield in the simulations, and the deficiency in long-term time-series of head and especially salinity. The absolute mean error between observed and simulated heads was 0.27 m (RMSE of 0.33 m), and between observed and simulated TDS concentrations was 1.17 g TDS L^{-1} (RMSE of 2.75 g TDS L^{-1}). The largest deviations in head occur at observation points that are situated near infiltration basins or pumping wells, whereas the deviations in TDS concentration appear to be well-distributed. These deviations are probably primarily caused by heterogeneity in the phreatic aquifer and spatial variations in the abstraction rates of pumping wells.

The groundwater heads of 137 observations points and the chloride concentrations of 55 observations points were used to quantify the error and calibrate the model. Despite this relatively large number of observations points, it is important to note that all observations of chloride and 72% of observations of groundwater heads – that were used in the model calibration – originate from the monitoring system in Solleveld. The simulation of the groundwater head and especially the TDS concentration are therefore most reliable in Solleveld and the immediate surrounding system. The phreatic groundwater level and depth of the fresh-brackish interface of the calibrated model are shown in Figure 2.8.

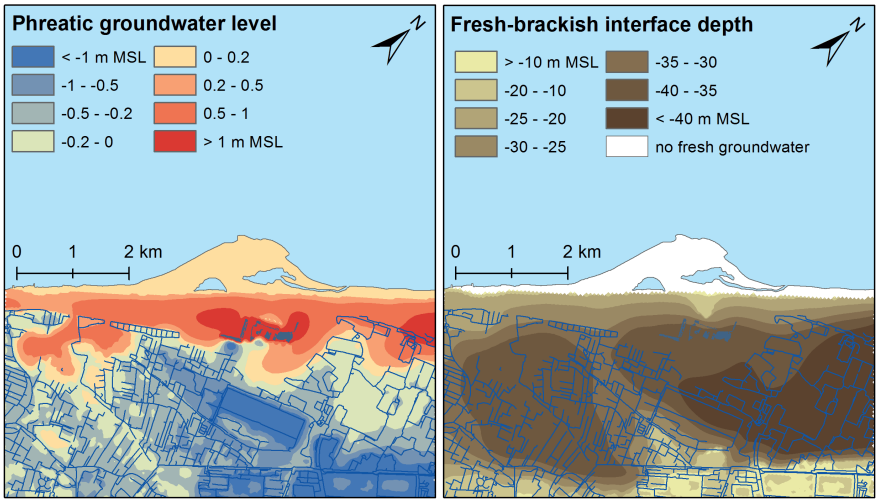

Figure 2.8 Phreatic groundwater level (left) and freshbrackish interface depth (right) after calibration, before the construction of the Sand Engine (2010–2011).

Phreatic groundwater flows from the coastal dunes toward the sea, pumping wells, and low-lying drained polders. The aquitard beneath the phreatic aquifer (between -16 and -20 m MSL) limits the interaction with the underlying confined aquifer, leading to a substantial head difference across the aquitard (ranging between 0.3 to 1.4 m in multilevel monitoring wells). The fresh groundwater lens below the coastal dunes extents to approximately -30 and -40 m MSL and the interface between brackish and saline groundwater lies between -40 and -50 m MSL, corresponding with the observed depth of the interfaces (Figure 2.13). Drainage in low-lying polders leads to the seepage of brackish or saline groundwater, which results in a reduction of the fresh groundwater lens thickness (Figure 2.8).

In order to assess the performance of the calibrated groundwater model, we have compared simulated groundwater heads and TDS concentrations with recent observations at 8 monitoring locations on the Sand Engine (Figure 2.9). The absolute mean error between observed and simulated groundwater heads was 0.36 m, and between observed and simulated TDS concentrations was 6.5 g TDS L^{-1}. The model appears to underestimate the hydraulic gradient – in particular in the higher regions of the Sand Engine – and groundwater salinities with a concentration higher than 15 g TDS L^{-1} (between 6 and 20 m below surface). Probable causes of these discrepancies lie in the initial groundwater level and salinity (strongly influenced by the construction), the underestimation of the vertical anisotropy as a result of small mud drapes in the Sand Engine and varying weather conditions (e.g. recharge, overwash). In addition, the measured TDS concentrations are single point measurements that may not represent the average TDS concentration in the Sand Engine.

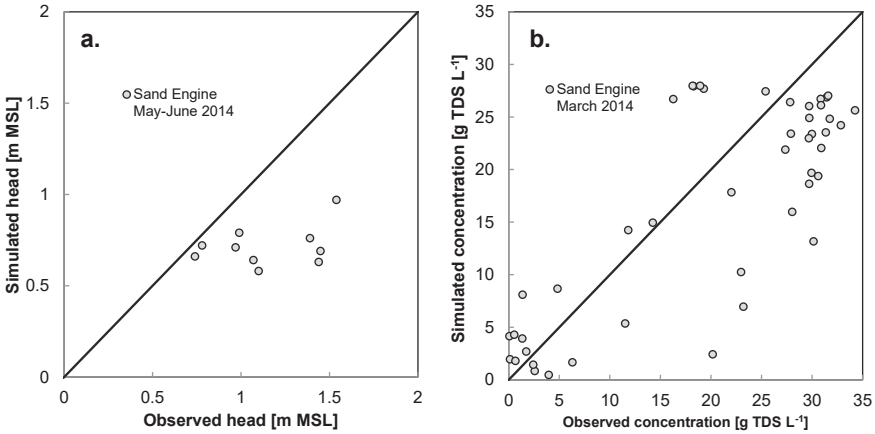

Figure 2.9 Comparison of (a) average groundwater head in May – June 2014 and (b) (single) TDS concentrations of soil samples taken between 10 and 14 March 2014 with model simulations in the Sand Engine.

2.4.2 Grid convergence test

In order to justify that the chosen spatial discretization was adequate for reliable numerical quantifications of the potential effect of the Sand Engine on fresh groundwater resources, we have executed a grid convergence test for the period 2011 to 2050 (with and without Sand Engine). The numerical simulations that are described in this paper were performed with a horizontal grid size of 50 m, and 50 layers with a variable thickness from 1 (upper layers) to 10 m (lower layers). This spatial discretization was tested with three additional simulations with higher and lower spatial resolutions (Table 2.4): one with a finer horizontal grid size of 25 m (model simulation S1), one with a coarser horizontal grid size of 100 m (S2), and one with an equal horizontal grid size of 50 m and an increased vertical resolution of the upper layers (S3). In the upper part of the model, up to a depth of -50 m a.m.s.l., the layer thicknesses were lowered by 50% (30 layers were added, up to a total of 80 layers).

Table 2.4 Grid convergence index (GCI) of the simulated increase in the volume of fresh groundwater in 2050 (situation with Sand Engine), for three simulations that contain different spatial grid refinements (S1 to S3). See Roache (1994) for more information

Sim.	Grid size	Layers	Refinement Ratio	Relative Error	Order of accuracy	GCI
S1	25 m	50	1.585	0.0224	3.36	0.76 %
S2	100 m	50	1.585	0.1074	3.36	3.63 %
S3	50 m	80	1.286	0.1487	3.36	14.0 %

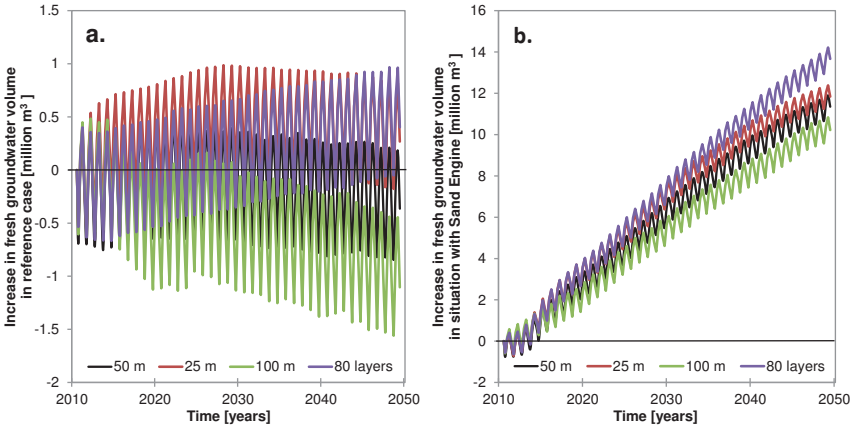

Figure 2.10 Increase of the volume of fresh groundwater in the situation without Sand Engine (a) and situation with Sand Engine (b) in the period 2011 to 2050, where the legend refers to the four grid discretization simulations.

Stability constraints and accuracy requirements were used for the temporal discretization of the simulations, and therefore the convergence of the solutions with regard to the temporal discretization was not tested. However, we have performed an additional test with respect to the coupling of the flow and solute-transport equations. The simulations were conducted with the "explicit coupling" approach. In order to test this coupling approach, an additional simulation was conducted with the "implicit coupling" approach (density criterion of 0.2 kg m^{-3}). For more information on these coupling approaches, we refer to the reports that describe the model code SEAWAT (Guo and Langevin, 2002; Langevin et al., 2003). All the additional numerical simulations include no climate change scenario, and were compared to the current numerical simulations that contained a horizontal resolution of 50 m and 50 layers. The initial conditions of all additional numerical simulations were equal to the calibrated predevelopment groundwater heads and TDS concentrations.

The comparison of the numerical simulations with varying spatial resolutions (Figure 2.10) shows a similar increase of the volume of fresh groundwater during the simulation period of 2011 to 2050. In the situation with the Sand Engine (Figure 2.10b), a coarser spatial resolution lowered the projected volume of fresh groundwater (–10% in 2050), and a finer horizontal and vertical spatial resolution raised the projected volume of groundwater (respectively +4 and +20% in 2050). However, when taking into account the deviations in the volume of fresh groundwater in the reference case (Figure 2.10a), the total change in the volume of fresh groundwater becomes smaller; respectively –2, +0 and +14% in 2050. The additional simulation with the "implicit approach" to coupling shows a small to negligible difference (smaller than 2% during the entire simulation period) with the simulations with the "explicit approach" to coupling of flow and transport equations (Figure 2.11).

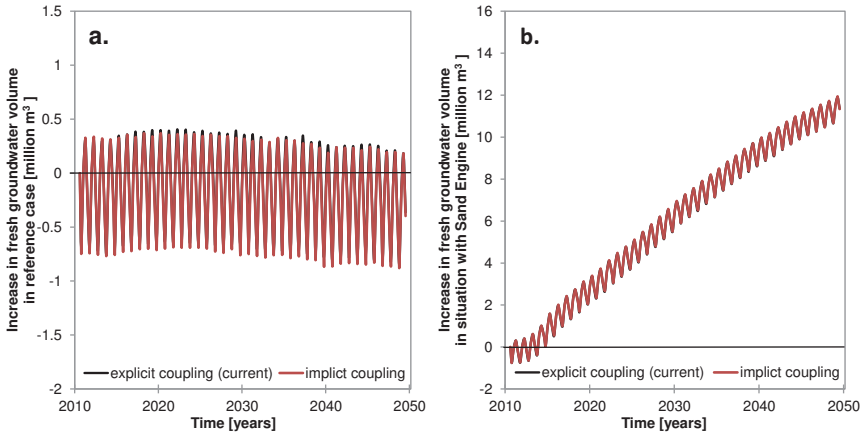

Figure 2.11 Increase of the volume of fresh groundwater in the situation without Sand Engine (a) and situation with Sand Engine (b) in the period 2011 to 2050, where the legend refers to the coupling of flow and transport equations.

In order to provide a uniform measure and error analysis of the spatial grid convergence, the Grid Convergence Index (GCI) was applied to the simulated increase of the volume of fresh groundwater in the model domain in 2050. The GCI indicates to what extent the simulated increase in the volume of fresh groundwater differs from the asymptotic volume, which would be reached with further spatial refinements of the model grid. For more information on the GCI we refer to Roache (1994). The GCI of the additional model simulations S1 to S3 (Table 2.4) was calculated with a safety factor of 1.25. The ratio in the GCI of simulation S1 and S2 showed that the simulation was within the asymptotic range of convergence (ratio approaches 1), which suggests that the grid was sufficiently refined. The GCI of model simulations S1 to S3 confirms that a horizontal refinement leads to small reductions in the numerical error in the volume of fresh groundwater, and that an increase in the vertical resolution could lead to a larger reduction of the numerical error. However, the refined model simulations (Figures 2.10 and 2.11) suggest that the increase in the volume of fresh groundwater would increase with a higher spatial resolution. Therefore, we think that the chosen spatial discretization was adequate for reliable numerical estimations of the effect of the Sand Engine on the volume of fresh groundwater.

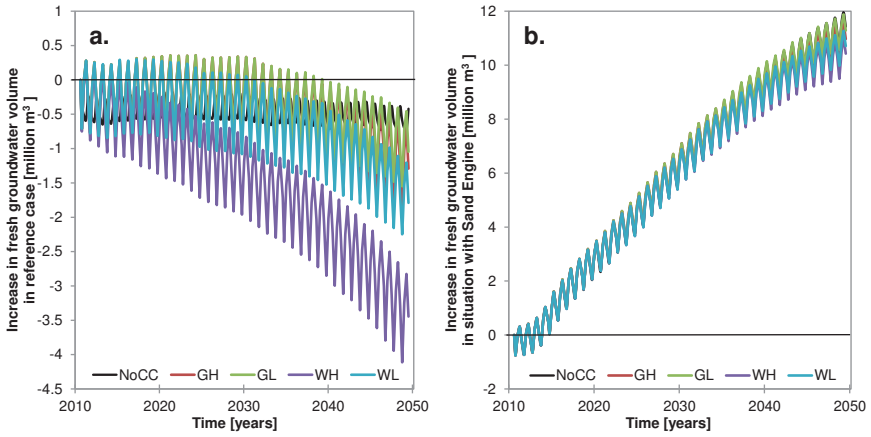

Figure 2.12 Increase of the volume of fresh groundwater in the situation without Sand Engine (a) and situation with Sand Engine (b) in the period 2011 to 2050, where the legend refers to (climate) scenarios (as mentioned in Table 2.3).

2.4.3 Fresh groundwater resources

The effect of the construction and long-term morphological evolution of the Sand Engine on the volume of fresh groundwater is initially small and similar to the situation without the Sand Engine (Figure 2.12). In all model scenarios the volume of fresh groundwater slightly declines in the first years, because of the small size of the freshwater lens in the Sand Engine with respect to the cell resolution and the instability of the initial conditions. However, the gradual growth of the freshwater lens in the Sand Engine and adjacent areas eventually leads to an increase of the volume of fresh groundwater in the model domain of 0.3 to 0.5 million m^3 per year. This increase of the volume of fresh groundwater manifests itself mainly as an outward extension of the fresh groundwater lens in the phreatic aquifer. Underlying aquifers and aquitards may even become more saline, primarily as a result of transient boundary conditions (i.e. historical coastal erosion and on-going sea level rise) leading to continuing historical seawater intrusion. In addition, rising groundwater levels in and around Sand Engine can lead to increases in the infiltration of saline groundwater through the thin aquitard (Figures 2.13 and 2.14).

The sea-level rise (in total) of 0.15 m in climate scenarios G_L and G_H and 0.25 m in climate scenarios W_L and W_H lead to a decline in the volume of fresh groundwater, because of the increase of seawater intrusion and inundation of the coastal area. However, the effect of sea-level rise is relatively small in respect to the total increase of fresh groundwater (Figure 2.12). The long-term predictions in precipitation and evapotranspiration within the four climate scenarios (Table 2.3) have a limited effect on the total volume of fresh groundwater.

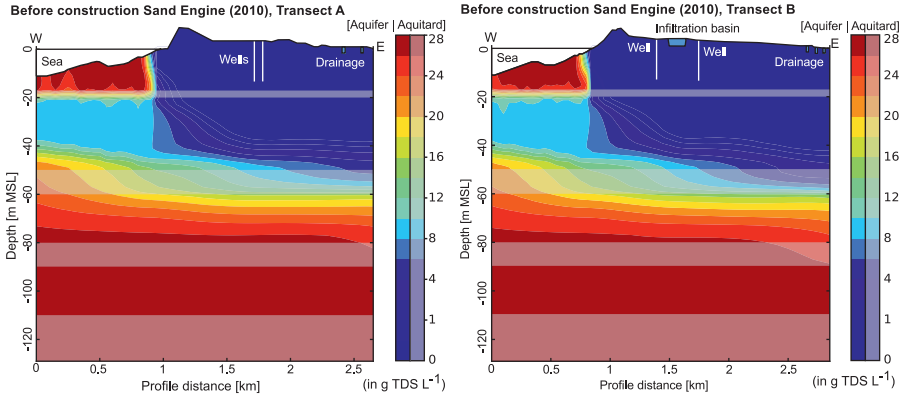

Figure 2.13 Transects with the simulated groundwater salinity (in g TDS L^{-1}) in 2010 (pre-development Sand Engine), for transect A and B (see Figures 2.2 and 2.3).

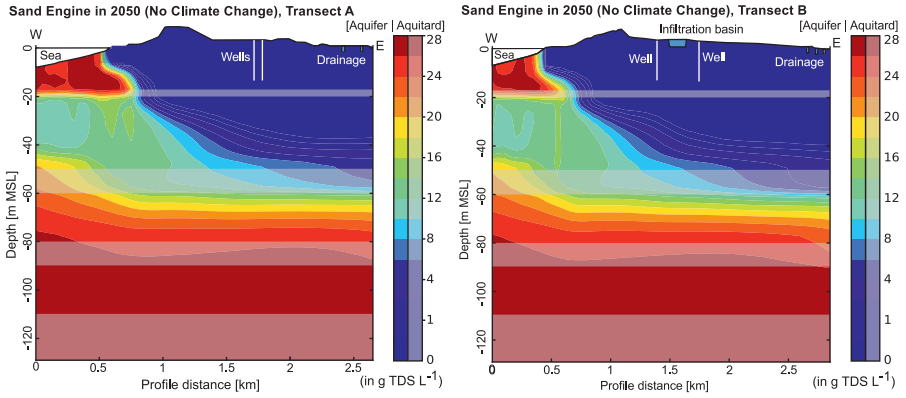

Figure 2.14 Transects with the simulated groundwater salinity (in g TDS L^{-1}) in 2050 (with Sand Engine, No Climate Change), for transect A and B (see Figures 2.2 and 2.3).

The climate scenarios with a strong response (G_H and W_H) lead to a smaller volume of fresh groundwater, when compared with the climate scenarios with a weak response (G_L and W_L). This is primarily a result of the difference in the net groundwater recharge in the climate scenarios, and the overall (yearly) volume of groundwater recharge is larger in the milder climate scenarios (G_L and W_L). The larger increase in precipitation in winter seasons of climate scenario G_H and W_H, coincides with a stronger increase in evaporation and a smaller increase in precipitation in the summer seasons (Table 2.3). However, the contrast between these climate scenarios only becomes apparent after 2030, because the precipitation and evapotranspiration patterns are equal until 2030 and diverge after 2030.

In addition to the change in fresh groundwater resources in the beach-dune system, the simulations with the long-term morphological evolution of the Sand Engine show small to negligible increases (smaller than 1 m in 2050) in the freshwater lens thickness in low-lying polders. However, changes in the total salt load in drains, canals and ditches are small in the situation with and without the Sand Engine. As a result the construction and morphological evolution of the Sand Engine may lead to small decrease of seawater intrusion, but this effect will probably be small to negligible and limited to small low-lying polders in a short distance from the Sand Engine (Figure 2.15).

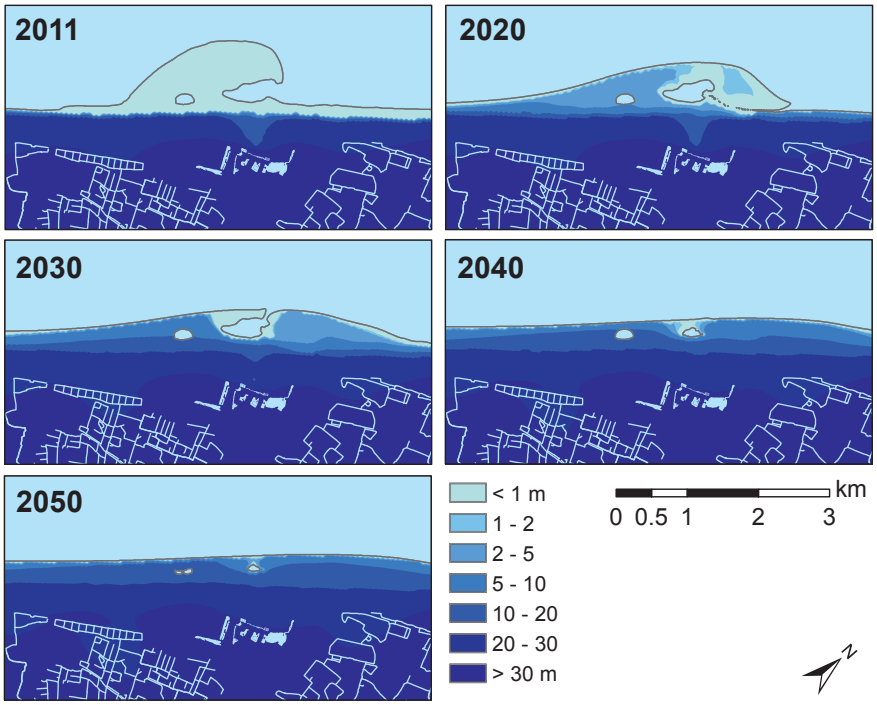

Figure 2.15 Thickness of fresh groundwater [m] in reference scenario near the Sand Engine from 2011 to 2050.

2.5 Discussion

The model simulations show that the construction of the Sand Engine may result in the growth of the volume of fresh groundwater by several million m^3. Despite the gradual erosion of the nourished sand – leading to a slow return to the previous state – the volume of fresh groundwater may continue to rise for decades after the construction of the mega-nourishment. However, tidal fluctuations and in particular storm surges will lead to land-surface inundations and consequently to a salinization of fresh groundwater. In addition, the increase in the volume of fresh groundwater is dependent on the rate of sea-level rise and the extent to which precipitation and evapotranspiration patterns will diverge from present conditions. This steady increase of the volume of fresh groundwater is in contrast with the reference case (without the construction of the Sand Engine) where historical and future sea-level rise lead to a decrease of the volume of fresh groundwater. Our results also suggest that the construction of the Sand Engine may abate the salinization of neighbouring polders, by reducing upward seepage of saline groundwater. Even though the reduction of the salinization is probably slight and limited to a small area, it might constitute an important mitigation in other applications of mega-nourishments.

Comparisons of observed and simulated groundwater heads and salinities show a good correspondence before and after the construction of the Sand Engine, despite large variations between observed and simulated groundwater salinities at individual locations. To some extent these discrepancies can be accounted for by the relatively sharp transition between fresh and salt groundwater, through which small variations in depth can result in large differences in groundwater salinities. Other factors that were not included in the simulations and that probably led to discrepancies in observed and simulated groundwater heads and salinities are: historical events (e.g. changes in groundwater level and salinity during the construction of the Sand Engine), large inundations of the Sand Engine due to storm-surges (e.g. two major storms in 2011 – 2016 inundated approximately 56% of the Sand Engine), variations in abstraction rates of pumping wells, fluctuations in sea salinity and unaccounted vertical layering of the Sand Engine deposits. These factors were not included in the model simulations because of the absence or shortage of data, and the long-term scope of this study. However, the overall similarity between observations and simulations, in combination with the absence of systematic errors in the model calibration, confirms the reliability of the model. Most of the observations – in particular groundwater salinity – emanate from the monitoring system in the adjacent dune area Solleveld and to a lesser extent the Sand Engine. The simulated groundwater heads and salinities are therefore most reliable in our area of interest, and the reliability is less in other areas in the model domain. However, the most substantial changes in groundwater salinity will take place in the area close to the Sand Engine, and variations in groundwater head and salinity in other areas will probably have a small to negligible impact on the potential effects of the Sand Engine.

Considering the scale and nature of our research objective, we neglected small and local variations in hydraulic parameters (e.g. hydraulic conductivity, layer thickness, porosity, and storage coefficient) in the model simulations. Supported by geological data and models, each aquifer and aquitard was defined homogeneous and anisotropic, with the exception of the phreatic aquifer. This reduction of the model complexity enhances the ability to differentiate and to understand the simulated processes, and leads to a smaller computation time of the model. However, small or local variations in groundwater head or salinity that are caused by heterogeneity will not be accurately reproduced in the model simulations.

One of the largest uncertainties in the study is the long-term morphological evolution of the Sand Engine, despite extensive calibration and validation and the large number of processes that are included in Delft3D (e.g. wind shear, wave forces, tidal forces, density-driven flows). The highly dynamic nature of the coastal zone, the absence of aeolian transport in the Delft3D simulations, and the lack of understanding of some processes, can lead to incremental differences with reality. Even though measurements of the last four years show a reasonable fit with the projections of the sediment volume changes and erosion patterns (de Schipper et al., 2014), future morphological change can turn out to be significantly different from the morphological model. For example, the growth of dune grasses and the exposure of shell deposits may prove to reduce erosion and decelerate the morphological evolution of the Sand Engine, or an accumulation of sand in the lagoon might lead to earlier silt up, and therefore a reduction of seawater intrusion in comparison with the projections. The implementation of one simulation of morphological change in the model calculations is therefore a significant limitation in the estimation of the potential fresh groundwater resources. For a more extensive analysis of the uncertainties in the prediction of the effects on fresh groundwater resources, it is recommended to simulate more morphological scenarios in future studies.

In addition to the long-term morphological evolution of the Sand Engine, large uncertainties also exist in the climatological predictions of sea-level rise, precipitation and evaporation in future decades. Predictions of sea-level rise for the North Sea in 2050 range between 15 to 40 cm above MSL, and model simulations have shown that substantial changes in the growth or volume of fresh groundwater resources can occur within this range. Changes in sea-level rise and the intensity or frequency of storm surges will not only significantly influence fresh groundwater, but will also contribute to coastal erosion and alter the morphological development of the Sand Engine.

2.6 Conclusions

Local mega-nourishments such as the Sand Engine might become an effective solution for the threats that many low-lying coastal regions face, and with this study we have shown that fresh groundwater resources can substantially grow within the lifespan of the nourishment. The results in this study show that for the Sand Engine, the construction of a mega-nourishment can lead to increase of fresh groundwater of approximately 0.3 to 0.5 million m^3 per year. However, the increase in fresh groundwater resources in a mega-nourishment is highly dependent on the shape and location of the mega-nourishment, the precipitation surplus, the frequency and intensity of storm surges, and local hydrogeological conditions. Therefore dependent on the design and location of the mega-nourishment this may provide an opportunity to combine coastal protection with the protection of fresh groundwater resources. This study also demonstrated that, with relatively simple modifications, a changing morphology can easily be modelled with a variable-density groundwater model such as SEAWAT.

Acknowledgements

We thank Arjen Luijendijk and Pieter Koen Tonnon for providing Delft3D data, and performing additional Delft3D simulations. This research is supported by the Dutch Technology Foundation STW, which is part of the Netherlands Organisation for Scientific Research (NWO), and which is partly funded by the Ministry of Economic Affairs. This work was carried out within the Nature-driven nourishment of coastal systems (NatureCoast) program.

3 Monitoring and simulation of salinity changes in response to tide and storm surges in a sandy coastal aquifer system

Based on: Huizer, S., Karaoulis, M. C., Oude Essink, G. H. P., and Bierkens, M. F. P. (2017), Monitoring and simulation of salinity changes in response to tide and storm surges in a sandy coastal aquifer system, Water Resources Research 53, 6487–6509, doi:10.1002/2016WR020339.

Abstract

Tidal dynamics and especially storm surges can have an extensive impact on coastal fresh groundwater resources. Combined with the prospect of sea-level rise and the reliance of many people on these resources, this demonstrates the need to assess the vulnerability of coastal areas to these threats. In this study, we investigated the impact of tides and storm surges on coastal groundwater at a pilot location on the Dutch coast (viz., the Sand Engine). To monitor changes in groundwater salinity under a variety of conditions, we performed automated measurements with electrical resistivity tomography for a period of two months between November 2014 and January 2015. The obtained resistivity images were converted to salinity images, and these images served effectively as observations of the impact of tidal fluctuations, salt water overwash during storm surges, and the recovery of the freshwater lens after land-surface inundations. Most of the observed changes in groundwater head and salinity could be reproduced with a two-dimensional variable-density groundwater flow and salt transport model. This shows that groundwater models can be used to make accurate predictions of the impact of tides and storm surges on fresh groundwater resources, given a thorough understanding of the (local) system. Comparisons of measurements and model simulations also showed that morphological changes and wave run-up can have a strong impact on the extent of land-surface inundations in (low-elevation) dynamic coastal environments, and can therefore substantially affect coastal fresh groundwater resources.

3.1 Introduction

Most coastal regions in the world rely on groundwater as their main source of fresh water for agricultural, domestic, and industrial sectors. However, in many coastal regions, the availability of fresh groundwater is threatened by unsustainable levels of groundwater abstraction and rising sea-levels (Ferguson and Gleeson, 2012). Combined with the likely continuation of sea-level rise (SLR) and increase in the frequency and intensity of storm surges (Nicholls, 2010; Wong et al., 2014), this will

lead to more seawater intrusion (SWI) in coastal aquifers. One important driver of the increase in SWI will consist of more extensive and frequent land-surface inundations (LSI) (Ketabchi et al., 2016). Low-elevation coastal systems with shallow groundwater levels are particularly vulnerable in this respect, because these systems are most susceptible to LSI and SWI (McGranahan et al., 2007), and an increase of the groundwater level in response to SLR is restricted (Michael et al., 2013).

These threats and the reliance of many coastal communities on fresh groundwater raise the importance of an optimal management of fresh groundwater in coastal aquifers to control or mitigate salinization (Khan et al., 2015). However, the management of coastal groundwater can be complex, because the extent of LSI and SWI depends on many factors: e.g. groundwater abstractions, aquifer hydraulic properties, and coastal hydrodynamics and morphodynamics (Ferguson and Gleeson, 2012; Vallejos et al., 2014). Several studies have therefore stressed the importance of intensive monitoring, to acquire more data in different hydrogeological conditions and in real-world coastal aquifers (Werner et al., 2013; Ketabchi et al., 2016).

A promising monitoring technique for LSI and SWI in coastal aquifers is (time-lapse) electrical resistivity tomography (ERT) (de Franco et al., 2009; Ogilvy et al., 2009; Henderson et al., 2010; Morrow et al., 2010; Hermans et al., 2012). In ERT, the non-invasive direct current (DC) resistivity method is used to visualize the subsurface resistivity distribution in two or three-dimensional images (Revil et al., 2012). One of the main advantages of this method is the ability to conduct automated time-lapse measurements along multidimensional arrays, and therefore to provide images of the evolution of the fresh-salt groundwater distributions over time (Ogilvy et al., 2009). Additionally this technique can help to constrain or validate parameters in groundwater models (Comte and Banton, 2007; Nguyen et al., 2009; Beaujean et al., 2014).

Many studies have addressed the possible effects of climate change and in particular SLR on coastal groundwater resources (Oude Essink et al., 2010; Watson et al., 2010; Chang et al., 2011; Webb and Howard, 2011; Michael et al., 2013). Most of these studies have neglected LSI (Ataie-Ashtiani et al., 2013), and recent studies have shown that LSI can have a significant impact on SWI in coastal aquifers (Ketabchi et al., 2014; Morgan and Werner, 2014). LSI is primarily driven by coastal forcing (Figure 3.1), ranging from tidal fluctuations with a small to negligible impact on the mixing zone, to episodic events such as storm surges that can lead to significant SWI (Ataie-Ashtiani et al., 1999; Wilson et al., 2011). Many laboratory and modelling studies have examined the impact of coastal hydrodynamics and morphodynamics on aquifers (Robinson et al., 2007a; Kuan et al., 2012; Liu et al., 2012; Yang et al., 2013; Holding and Allen, 2015a; Levanon et al., 2016). However, only a few studies have compared model simulations with real-world measurements over an entire lunar cycle (Abarca et al., 2013; Heiss and Michael, 2014). These studies have demonstrated that tides create complex flow patterns.

Coastal forcing can also lead to significant changes in coastal geomorphology, e.g. migration of sandbars or coastal erosion (Anthony, 2013). Complex fluid and sediment interactions, such as interactions between breaking waves, wave run-up and run-down, and groundwater flow in the swash zone, strongly determine the accretion or erosion rate of a coastal beach (Bakhtyar et al., 2009). The resulting cross-shore and alongshore morphological evolution of a coast can have large influences on the extent of SWI and LSI (Ataie-Ashtiani et al., 2013; Zhang et al., 2016).

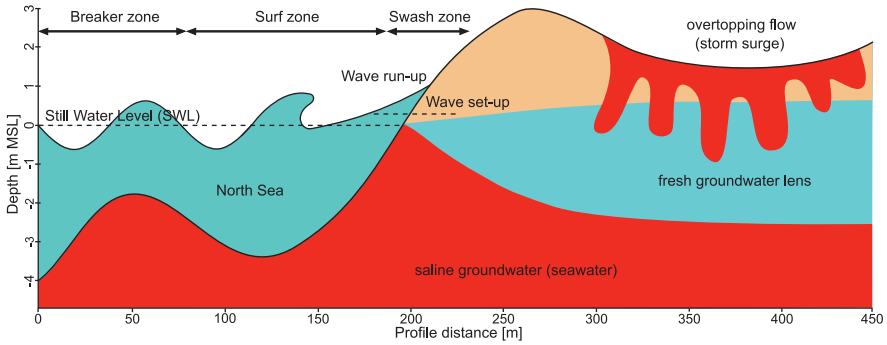

Figure 3.1 Illustration of coastal flow processes at the measurement site.

In this study, we investigated the impact of coastal hydrodynamics and morphodynamics on coastal groundwater with geophysical measurements and model simulations during the winter of 2014 - 2015. We have used time-lapse ERT to perform automated measurements of changes in the fresh-salt groundwater distribution in a mega-nourishment pilot called the Sand Engine, located in the Netherlands (Mulder and Tonnon, 2011). The aim of this study is to examine the impact of coastal forcing on the fresh-salt groundwater distribution, to evaluate the quality of time-lapse ERT as a monitoring method of LSI and SWI in coastal aquifers, and to assess the ability of a variable-density groundwater and coupled salt transport model to simulate the observed variability and change. For the evaluation of time-lapse ERT as a monitoring method, we have performed sensitivity analysis and synthetic modelling as described in Henderson et al. (2010).

The most innovative aspect of this study is that we combined intensive monitoring of SWI and LSI with detailed model simulations over a period of several months. The morphodynamic environment of the measurement area resulted in the measurement of the impact of tides, storm surges, and coastal geomorphological changes on the fresh-salt groundwater distribution in a real-world coastal aquifer. The paper first briefly describes the study site and monitoring set-up, and then provides an overview of the key results from time-lapse ERT measurement. Next, the model set-up, calibration, and results are described, evaluated, and discussed, emphasizing on the quality of ERT measurements for the monitoring of SWI processes.

3.2 Data and Methods

3.2.1 Study Site: The Sand Engine

The Sand Engine (also called Sand Motor) is a pilot project that consists of the construction of a concentrated (mega) beach nourishment of 21.5 million m^3 sand at the Dutch coast in 2011 (Figure 3.2), and the evaluation of this new type of nourishment with respect to current practices in the Netherlands (i.e., large-scale distribution of sand). The postulated theory is that natural forces (wind, waves and currents) will gradually distribute the replenished sand along the retreating coast, support natural dune growth, and simultaneously limit the disturbance of local ecosystems. First results confirm that the mega-nourishment led to a growth of adjacent coastal sections and dunes (de Schipper et al., 2016). In addition, recent research showed that concentrated mega-nourishments can lead to an increase of local fresh groundwater resources (Huizer et al., 2016).

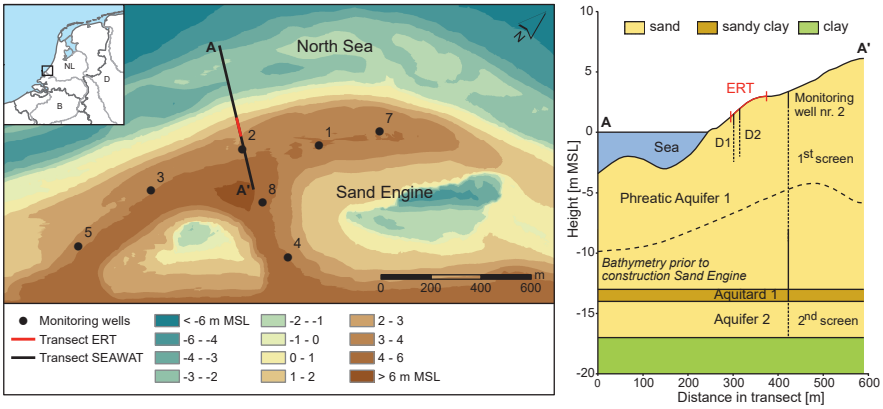

Figure 3.2 Contour map and hydrogeological cross section of the Sand Engine between 27 October and 1 November 2014, with the location of the monitoring wells, ERT measurement transect (red line), and the groundwater model transect (black line, A - A'). The dashed line in the cross section marks the bathymetry prior to the construction of the Sand Engine.

In the study area, the primary source of fresh groundwater is precipitation, which was on average 938 mm per year in the period June 2011 until May 2016. Another important source of fresh groundwater is the inflow of groundwater from the adjacent dune area Solleveld through the unconfined coastal aquifer. In general this coastal aquifer consists of 15 - 25 m fine to coarse sand (median grain size of 150 - 400 mm), with a few thin discontinuous clay layers, and is separated from underlying aquifers by a layer of clay and peat (Figure 3.2). Groundwater head measurements in the dunes and previous model simulations of the area (Huizer et al., 2016) indicate that groundwater flows downward through this aquitard. Groundwater level measurements in monitoring wells 1 - 8 (Figure 3.2) on the Sand Engine show no long-term trend, which suggests that the initial effect of the nourishment on groundwater heads is

currently small or absent. However, the volume of fresh groundwater resources seems to be gradually increasing in the study area, and in the remainder of this paper we have investigated the impact of tides and storm surges on these resources.

3.2.2 Resistivity Imaging (ERT)

Most applications of ERT are based on the analysis of contrasts in the electrical resistivity of sediments or fluids to monitor processes in porous media (Kuras et al., 2009). In this case, the contrasts in the electrical resistivity are primarily caused by differences in water content, and groundwater salinity. The measurement of the DC resistivity is based on the injection of an electrical current in the ground with multi-electrode arrays and measurement of the potential differences in the other electrodes. An increase in the distance between electrodes reduces the spatial resolution and enlarges the depth of investigation, while different pairs of injection electrodes along the profile line allow imaging of the resistivity distribution of the subsurface.

Measurement set-up

We conducted automated time-lapse ERT measurements from 14 November 2014 10:58 until 20 January 2015 10:23, along an 80 m transect at the outer perimeter of the Sand Engine (Figure 3.2), situated perpendicular to the shoreline (i.e., cross-shore direction). The surface elevation along the transect varied from 11 to 13 m MSL, encompassing the local mean high water (MHW) height of 11.09 m MSL at the site (Figure 3.3). Alongside this transect two monitoring wells (D1 and D2) were installed for the measurement of groundwater heads and groundwater conductivity (Figure 3.2). The location was selected because the 2-D measurement set-up requires a (predominantly) parallel direction of groundwater flow and LSI, to avoid a misinterpretation of observed changes in the resistivity images. This specific section of the Sand Engine was the optimal site for the measurements:

1. The local topography was relatively simple and similar along the shoreline.
2. The field data and model simulations indicate that the dominant groundwater flow direction was cross-shore, and therefore parallel to the transect.
3. This section of the Sand Engine was most vulnerable to LSI.

For all ERT measurements, the dipole-dipole configuration was implemented, which is a conventional and frequently used configuration in surveys since it is sensitive to lateral changes while the acquisition time is fast, something of importance in time-lapse studies. The measurement set-up consisted of 160 electrodes with a constant spacing of 0.5 m between each electrode. Each electrode was connected to an iron pinlocated at the same position and depth as the electrodewith a stainless steel wire. All electrodes were buried in a trench with a depth of 0.3 – 0.5 m below surface, for public health and safety and to protect the electrodes from coastal forcing and vandalism. The measurements were carried out and controlled with the MPT

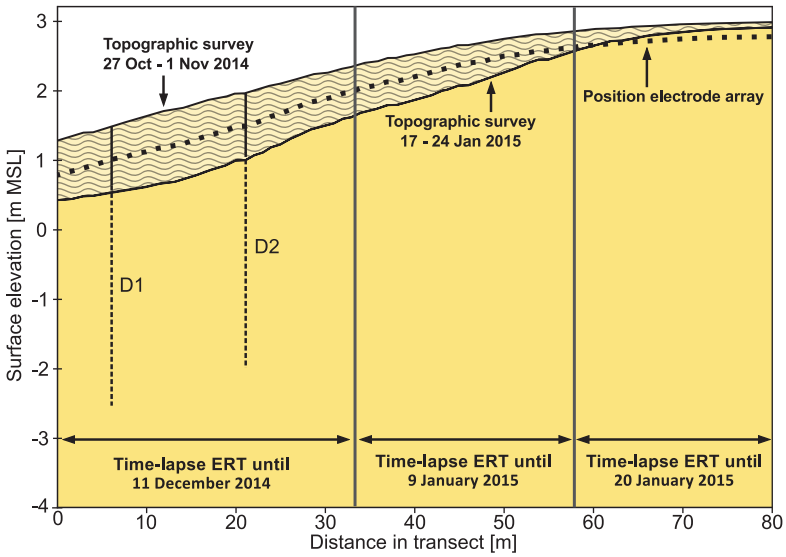

Figure 3.3 Cross section of the ERT measurement transect containing the implemented consecutive model surface elevations, where the wave-shading pattern indicates the erosion of sand in the measurement period. The horizontal arrows and vertical black lines mark the reduction of the ERT measurement transect on 12 December 2014 and 10 January 2015.

DAS-1 Electrical Impedance Tomography System, which was placed (with all related equipment) in an elevated and locked container to protect the instruments. The system was connected with another buried electrical cable to the electricity network in the Argus (video sampling) station, which is located in the centre of the Sand Engine (Rutten et al., 2017). In addition, the system was connected to the Internet with the MRD–350 industrial mobile broadband (3G router), to be able to remotely monitor and control the measurements.

However, substantial coastal erosion during the measurement period (Figure 3.3) led to the exposure segments of the electrode array, and consequently broken electrode connections. This rendered lower sections of the electrode array unusable, and therefore the number of available electrodes dropped during the measurements (Figure 3.3): all 160 electrodes were employed until 11 December 2014, 96 electrodes until 9 January 2015, and 47 electrodes until 20 January 2015. In order to maximize the number of measurements, the time interval between measurements was reduced in accordance with the decline in electrodes. Until 23 December 2014, the measurements were conducted with an interval of 30 min, from 24 December 2014 to 13 January 2015 19:00 with an interval of 15 min, from 13 January 2015 19:00 to 20 January 2015 with an interval of 10 min. This coastal erosion also affected the measurements in monitoring well D1 and D2, and reliable groundwater level and groundwater conductivity measurements could only be obtained until 19 December 2014.

Resistivity Inversion

All resistivity measurements were inverted with the four-dimensional (4-D) inversion algorithm as described by Kim et al. (2009, 2013), and Karaoulis et al. (2011), where inversion is the procedure to go from the measured data to an inverted resistivity image, also called a tomogram. In this algorithm both data and model are defined in space-time coordinates, and regularizations in both space and time domains are adopted to reduce inversion artefacts and to stabilize the inversion. The objective function consists of three terms that are minimized in a trade-off manner: data misfit, model roughness in the space domain, and model roughness in the time domain (Kim et al., 2009). The minimization is expressed either in terms of the L1 norm or the L2 norm, and the selection of the norm is dependent on the behaviour of the data and the inverse model parameters (Kim et al., 2013).

The inversion was conducted sequentially with five monitoring surveys or reference time steps in each inversion, and every inversion used homogeneous half-space as the starting model. The inversion model consisted of 159 columns with a constant spacing of 0.5 m, and 9 layers with a variable thickness of 0.167 - 0.833 m. All minimizations were expressed in terms of the L2 norm (i.e., full least-squares minimization), and the inversion of the model roughness in the space domain was conducted with a constant Lagrangian multiplier of 0.1. In addition, negative apparent resistivities and one electrode (and related electrode combinations) with a continuously high contact resistance where excluded from the inversion. All resulting unweighted and weighted RMS errors in the inversion process remained below 1%.

Salinity-Conductivity Relationship

For the comparison of the inverted electrical resistivities with model simulated salinities, we estimated the salinity (expressed in total dissolved solids – TDS) from the inverted bulk electrical resistivities (q in Ohm m) using a similar procedure as described in Post (2012) and Hermans et al. (2012). First the groundwater resistivity (qw in Ohm m), and inversely the groundwater conductivity (rw in S m^{-1}) was estimated from the bulk resistivity with a variant of the classical Waxman and Smits (1968) model. The cation exchange capacity in this model was ignored, because the clay fraction in the upper part of the sand nourishment is negligible (Figure 3.2).

This reduces the model to a simple linear relation:

$$\rho = \rho_w \frac{F}{{s_w}^{\mathrm{n}}}, \quad \sigma = \sigma_w \frac{{s_w}^{\mathrm{n}}}{F} \tag{3.1}$$

where F is the electrical formation factor of the sediment, sw is the relative water saturation, and n is the saturation exponent.

The focus of this research was limited to the saturated zone, and thus sw was constrained to a value of 1. Estimated salinities in the unsaturated zone were therefore excluded from the analysis of the effect of tides and storm surges.

The formation factor was also estimated with Equation 3.1, i.e., equal to the ratio between the groundwater conductivity and the bulk conductivity (σ in S m^{-1}): on-site measurements of the groundwater conductivity between 14 November 2014 10:58 and 11 December 2014 03:57 in monitoring well D1 (Figure 3.3) at a depth of 20.5 m MSL were divided by the inverted bulk conductivity at the same approximate position. Ignoring anomalous conductivities, this resulted in an average formation factor of 4.2 in this period with a standard deviation of 0.3, which is similar to literature values for coarse sand (Friedman, 2005; Goes et al., 2009). The variability in the formation factor was mainly a result of fluctuations in the on-site measured groundwater conductivity, and a gradual decline in only the inverted bulk conductivity. Possibly the water inside monitoring well D1 was more sensitive to LSI, which led to a larger response in conductivity and the absence of a (clear) falling trend.

Groundwater salinities were estimated with the salinity-conductivity relationship as defined in the algorithm of the Practical Salinity Scale (PSS) 1978 (Fofonoff and Millard Jr., 1983). This so-called Practical Salinity S_p is a dimensionless measure of salinity, which is defined in terms of the ratio with the conductivity of standard seawater ($S_p = 35$) at a temperature of 15°C, and at atmospheric pressure. The calculation of S_p is dependent on the electrical conductivity, the temperature, and (water) pressure at depth of the measurement (IOC et al., 2010). Temperatures were estimated with measurements in monitoring well 2 at a depth of 20.2 m MSL (Figure 3.2), which dropped from 13.8°C on 14 November 2014 to 10.6°C on 20 January 2015. Deviations from atmospheric pressure were ignored in the calculations, because the observed variations in atmospheric pressure have negligible effects on the S_p. The PSS 1978 is only defined for salinities in the range $2<S_p<42$. Consequently, for salinities between 0 and 2 the extension of the PSS 1978 as defined by Hill et al. (1986) was adopted. The dimensionless values for S_p were converted to salinities in g TDS L^{-1}, with the relationship between the chloride concentration and the Practical Salinity as described in Millero et al. (2008).

3.2.3 Variable-Density Groundwater Flow Model

For the analysis of the observed changes in groundwater head and salinity in the fresh-salt groundwater mixing zone, we developed a 2-D variable-density groundwater model with a horizontal spacing of 0.2 m and vertical spacing of 0.2 m. Variable-density saturated groundwater flow and coupled salinity transport were simulated with the computer code SEAWAT (Langevin et al., 2008). The governing flow and solute transport equations in SEAWAT are coupled and solved with a cell-centred finite difference approximation. Numerous studies have used this model code to simulate variably-density, transient groundwater flow in coastal environments (Mao et al., 2006; Robinson et al., 2007b; Heiss and Michael, 2014; Pauw et al., 2014). Pressure heads and saturation levels in the unsaturated zone will have an important impact on infiltration rates, however in this research we have focused on processes in the saturated zone.

In the simulations we have assumed that the infiltration of freshwater by precipitation and seawater by LSI occur instantaneously. We believe this choice is justified because of the high infiltration rates of the coarse sand, and the relatively shallow unsaturated zone along the measurement transect (maximum 2 m).
The groundwater flow model was situated perpendicular to the shoreline, alongside the ERT measurement transect (Figure 3.2). Based on four boreholes with a depth of 20 m below surface, situated 7 - 400 m from the model transect, we modelled two aquifers and one aquitard (see cross section in Figure 3.2). The aquifers contain fine-grained to medium coarse-grained sand and occasionally shells, and the aquitard consist of sandy clay to clay.

Initial Conditions
The groundwater head and salinity distribution at the start of the time-lapse ERT measurement were reconstructed with model simulations from the completion of the Sand Engine in June 2011 until the start of the measurements in November 2014. The initial distribution of the groundwater salinity in the model was defined completely saline, i.e., equal to the average seawater salinity at the site of approximately 28 g TDS L^{-1} (Rijkswaterstaat, 2012). In the intervening period, the Sand Engine experienced substantial geomorphological changes, in particular along the outer perimeter of the peninsula, where the shoreline retreated approximately 200 m (de Schipper et al., 2016). These geomorphological changes of the Sand Engine were monitored with monthly to bimonthly topographic surveys (including bathymetry) as part of an intensive monitoring program. Dependent on the monitoring frequency and the extent of morphological change, we have updated the surface elevation every 1 - 3 months in the model by sequential grid regenerations. For the extent of the morphological change, we used this criterion for the exclusion of topographic surveys: the maximum (horizontal) shift in the topography, above the mean neap tide height (+0.86 m MSL) and below the maximum run-up height (in the concerning period), should be smaller than 10 m. The excluded surveys (8 out of a total of 30 surveys) where either conducted in the summer season (fewer storm surges), or surveys that were conducted quickly after another (e.g. twice in 1 month).

Boundary Conditions
Sea-level fluctuations were based on high frequency (10 min time interval) tide gauge measurements (also called Still Water Level: SWL) in the harbours of Scheveningen and Hoek van Holland, which are located 7.5 km north and 9.3 km south from the study site. Based on the position of the study site, we used an averaged time series of both measurement sites as an estimate of the local sea-level fluctuations. This approximation was corroborated with a comparison to short-term on-site sea-level measurements between 17 September and 23 October 2014, which revealed an absolute mean error of 0.06 m and a RMSE of 0.075 m. In the model simulations, only sea-level fluctuations larger than 2 cm were incorporated, which resulted in stress periods with a variable duration of 10 - 190 min.

Based on the sea-level and the topography, the inundation extent was determined for every stress period, and modelled as "General Head (head-dependent) Boundaries and Drains" as described in Mulligan et al. (2011). All model layers in the phreatic aquifer (Figure 3.2) were defined convertible (saturated thickness) and rewettable with a wetting threshold of 0.01 m (McDonald et al., 1992). Despite this relatively small wetting threshold, and detail in the simulation of the sea-level fluctuations, not all model cells were reactivated in every stress period unless an additional infiltration rate was added to the simulations. This deficiency was only observed for sea levels that were larger than the MHW height. Therefore, to ensure a reactivation of all inundated model cells, an additional infiltration of 0.008 m per minute of seawater was added to the area of inundation for sea-levels larger than the MHW height. The adopted infiltration rate was the lowest rate that led to a reactivation of all inundated model cells, and this rate equalled the drainable volume of two model layers over a 10 min period.

Besides this simulation of the SWL (model scenario S1), two additional model scenarios (S2 and S3) with estimations of, respectively, the wave set-up height and the wave run-up height at the site were implemented to study and improve the resemblance of the simulations with reality (Figure 3.1). Wave set-up is defined as the local rise of the mean seawater level (with respect to SWL), caused by wave breaking. Wave run-up is defined as the maximum level of wave up-rush on the beach (with respect to SWL), which is only exceeded by 2% of run-up events. The wave set-up height ¡g¿ and wave run-up height R_2 in every stress period were estimated with general empirical expressions (Stockdon et al., 2006):

$$< \eta >= 0.35\,\beta_f\,(H_0 L_0)^{1/2} \tag{3.2}$$

$$R_2 = 1.1\left(0.35\,\beta_f (H_0 L_0)^{1/2} + \frac{[H_0 L_0 (0.563\,\beta_f^2 + 0.004)]^{1/2}}{2}\right) \tag{3.3}$$

where H_0 is the deep water significant wave height, L_0 is the deep water wave length, and β_f is the foreshore beach slope. The significant wave height and wave length were estimated with measurements at the "Euro platform" of the Ministry of Infrastructure and the Environment (Rijkswaterstaat), which is located 50 km southwest from the study site (Figure 3.4).

Wave set-up (S2) was modelled similarly to the observed sea-level fluctuations (SWL), and wave run-up (S3) as the combination of wave set-up and wave up-rush (Figure 3.1). Nonlinear effects of wave set-up on the surface water level were not included, because possible seawater circulations through the aquifer will probably have a small to negligible effect on the fresh-salt groundwater distribution. Wave up-rush was modelled as an infiltration of seawater, between the wave set-up height $< g >$ and the wave run-up height R_2.

The infiltrated volume of seawater at the wave set-up height $< g >$ was estimatedin every stress periodas the drainable storage (determined by specific yield) between SWL and $< g >$. Above the wave set-up height $< g >$; this infiltration volume was reduced linearly to a value of 10% at the wave run-up height R_2. The value of 10% is a best guess that was based on the number of run-up events that reach the run-up height R_2 (generally between 1 and 3 events in 10 min), the average infiltrated volume at the wave set-up height $< g >$ (0.013 m between June 2011 and 20 January 2015), and the assumption that at least 0.001 m infiltrates during every run-up event.

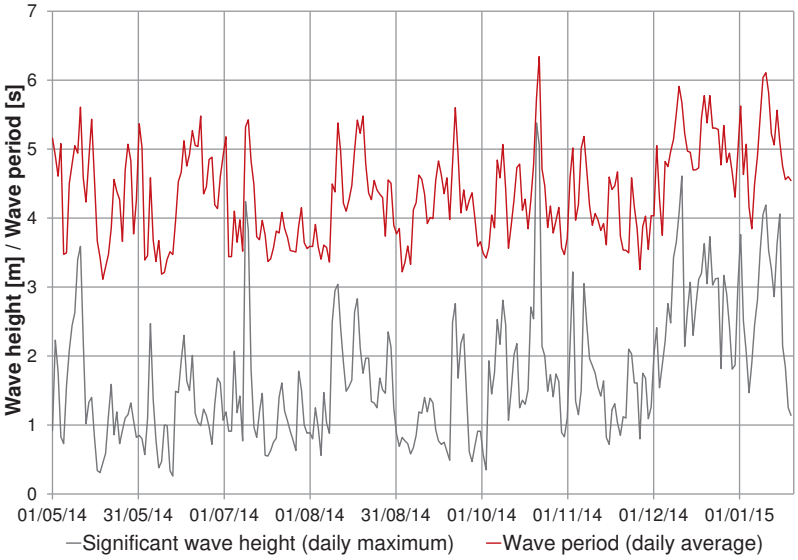

Figure 3.4 Measured deep water significant wave height H_0 (daily maximum) and deep water wave period (daily average) at the "Euro platform" (50 km SW from the study site).

The inland boundary of the model was simulated as a constant groundwater head and constant concentration boundary, where the vertical distribution and change of the groundwater head and salinity in the boundary were estimated with a separate 1-D groundwater flow model. This 1-D model consisted of the same hydrogeological properties as the calibrated 2-D model (Table 3.1), groundwater recharge, and the local saline groundwater head (monitoring well 8). Based on groundwater level measurements in monitoring wells 2, 4, and 8 and the local topography, we assumed that the change in groundwater salinity was predominantly determined by groundwater recharge. The local groundwater head was assigned to the bottommost model layer and defined as a variable head, equal to the daily moving average of the measured groundwater head in monitoring well 8 for the period 1 June 2014 to 20 January 2015 (Figure 3.2). In the preceding period, we have implemented the average groundwater head. The salinity in this bottommost layer was set equal to average seawater salinity.

Table 3.1 Calibrated parameter values implemented in the model simulations.

Layer Type	**Parameter**	**Value**
All model layers	Longitudinal dispersivity	0.02 m
	Transverse dispersivity	0.002 m
Phreatic aquifer	Horizontal hydraulic conductivity	36 m d^{-1}
1: [above –9 m MSL]	Vertical hydraulic conductivity	18 m d^{-1}
	Specific yield	0.20
Aquitard	Horizontal hydraulic conductivity	0.115 m d^{-1}
1: [-13 to –14 m MSL]	Vertical hydraulic conductivity	0.0115 m d^{-1}
	Specific storage	0.0002
Aquifer	Horizontal hydraulic conductivity	36 m d^{-1}
1: [-9 to –13 m MSL]	Vertical hydraulic conductivity	7.2 m d^{-1}
2: [-14 to –17 m MSL]	Specific storage	0.0002

Hourly measurements of precipitation and reference crop evapotranspiration at a measurement station in Hoek van Holland were used to estimate groundwater recharge. The hourly groundwater recharge was linearly distributed over smaller-sized stress periods. For the estimation of the potential soil evaporation, we used crop coefficients for bare or sandy soil (De Bruin and Stricker, 2000; Meinardi, 1994): 0.6 for the summer (April - September), and 0.9 for the winter (October - March). Monthly precipitation and potential soil evaporation were subtracted, in order to generate monthly estimates of the fraction of the hourly precipitation that reaches the groundwater level. It is important to note that this approach might lead to an overestimation of soil evaporation in months with prolonged dry periods, which will mainly affect the summer season and to a lesser extent the winter season.

Model Calibration

The groundwater model was calibrated with measurements of the groundwater head in multilevel monitoring well 2, which is situated alongside the 2-D model (Figure 3.2). This monitoring well contained two well screens, situated in separate aquifers (see cross section in Figure 3.2). The calibration was performed with model scenarios S1, S2, and S3 (respectively SWL, wave set-up, and, wave run-up), for measurements from 1 May 2014 until the start of the scenario simulations on 21 October 2014. The calibration strategy consisted of extensive sensitivity analyses, manual model parameter calibration, and comparisons of measured and simulated groundwater heads for the calibration period. In this strategy, we have adopted two calibration criteria: the error between the measured and simulated groundwater head should be smaller than the observed variation in groundwater level (average standard deviation is 0.1 m in the calibration period), and the simulated groundwater head should correlate with the observed fluctuation pattern.

The parameter calibration comprised of the manual adjustment of a selection of the most sensitive model parameters: (horizontal and vertical) hydraulic conductivity, storage coefficients, and (longitudinal and transverse) dispersivity. These adjustments consisted of small incremental changes from an initial best guess, which was based on previous model simulations in the same area (Huizer et al., 2016). Other parameters such as groundwater recharge were based on measurements, and were excluded from the calibration. The longitudinal and transversal dispersivity were adapted in agreement with the observed mixing zone thickness. The calibrated set of model parameters is shown in Table 3.1.

Model Scenarios

As described in section 3.2.3, the observed SWL, estimated wave set-up, and estimated wave run-up were implemented in three separate model scenarios (S1, S2, and S3), to analyse the reproducibility of the observed LSI and SWI processes in the ERT measurements. These model scenarios S1, S2, and S3 were executed for the initialization period of 1 June 2011 (completion Sand Engine) to 21 October 2014, and the study period of the 21 October 2014 to the end of the ERT measurements on 20 January 2015. The simulations were started before the ERT measurements to incorporate the storm surge that occurred between 21 October 2014 16:00 until 22 October 09:00 (significant offshore wave height of 4 - 5.4 m, and offshore wave period of 6.3 - 7.2 s). This storm surge led to the inundation of the entire measurement transect, as indicated with the highest measured SWL on the 22 October 2014 in Figure 3.5. This was the most intensive storm at the Sand Engine since 6 December 2013, which led to the highest seawater level and consequently the most extensive LSI of the measurement period. Other storms that occurred during the measurement period were on 11 December 2014 (significant offshore wave height of 3 - 4 m, and offshore wave period of 5.5 - 6.5 s) and on 11 January 2015 (significant offshore wave height of 3.5 - 4.2 m, and offshore wave period of 5.8 - 6.7 s), and the highest measured seawater levels during these storms are also indicated in Figure 3.5.

Coastal forcing – and the earlier mentioned storm surges in particular – led to substantial morphological changes at the Sand Engine in the measurement period, as illustrated in Figure 3.5. This morphological change is based on two extensive topographic (including bathymetry) surveys that were conducted on the Sand Engine between 27 October 2014 and 1 November 2014, and between 17 and 24 January 2015. Each survey produced a large collection of height measurements that were spatially interpolated to obtain an estimation of the surface elevation along the model transect (Figure 3.5). The disparity between these surface elevations shows the retreat of the shoreline at the site during the surveys. In order to obtain an optimal correspondence in the actual and the modelled topography, the horizontal average of both surface elevations was used as an estimation of the intermediate elevation along the model transect from 12 to 31 December 2015. Before and after this period, we have adopted interpolations of the two topographic measurements (see dashed line in Figure 3.5).

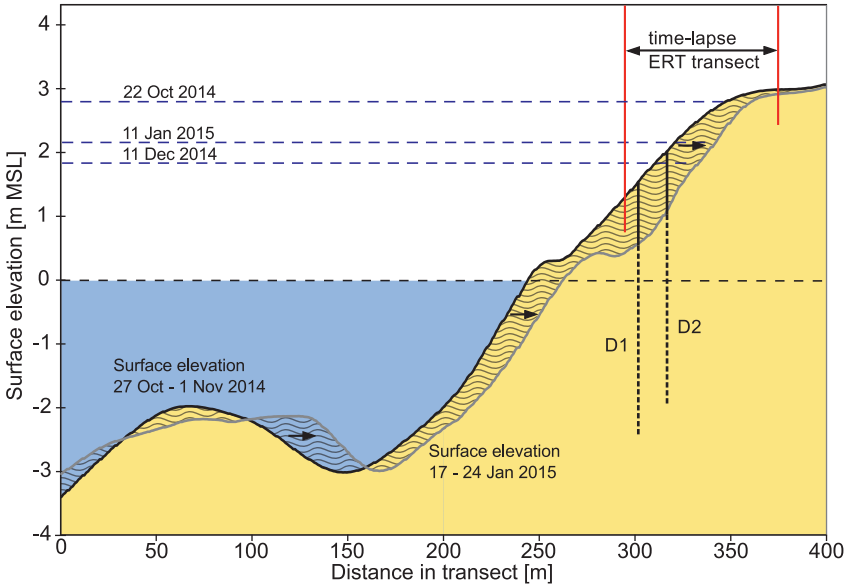

Figure 3.5 Cross section with the observed surface elevations at the measurement site: 27 October to 1 November 2014 (black line), and 17 to 24 January 2015 (grey line). The wave-shading pattern between the lines marks the erosion or accretion of sand in the intervening period. The red lines mark the ERT transect and the blue dashed lines mark the three highest SWL in the measurement period.

In order to study the effect of groundwater recharge on the salinity distribution in more detail, model scenario S3 was also simulated without groundwater recharge. This simulation was only executed for the study period after the calibration (21 October 2014 to 20 January 2015), and preceding simulations of model scenario S3 were used as initial conditions.

3.3 Results

3.3.1 Groundwater Head

In most of the calibration period, the simulated groundwater head in the model scenarios closely resemble the observed fluctuation pattern, substantiating that the groundwater model accurately describes the course of the groundwater level and groundwater flow in the study site (Figure 3.6). The absolute mean error between the measured and simulated groundwater head of model scenario S1, S2, and S3 is, respectively, 0.06, 0.05, and 0.05 m in the phreatic aquifer (RMSE 0.07, 0.06, and 0.05 m), and respectively 0.13, 0.12, and 0.10 m in the bottom aquifer (RMSE 0.17, 0.15, and 0.13 m). Wave set-up (S2) and in particular wave run-up (S3) results in larger LSI and consequently higher groundwater levels.

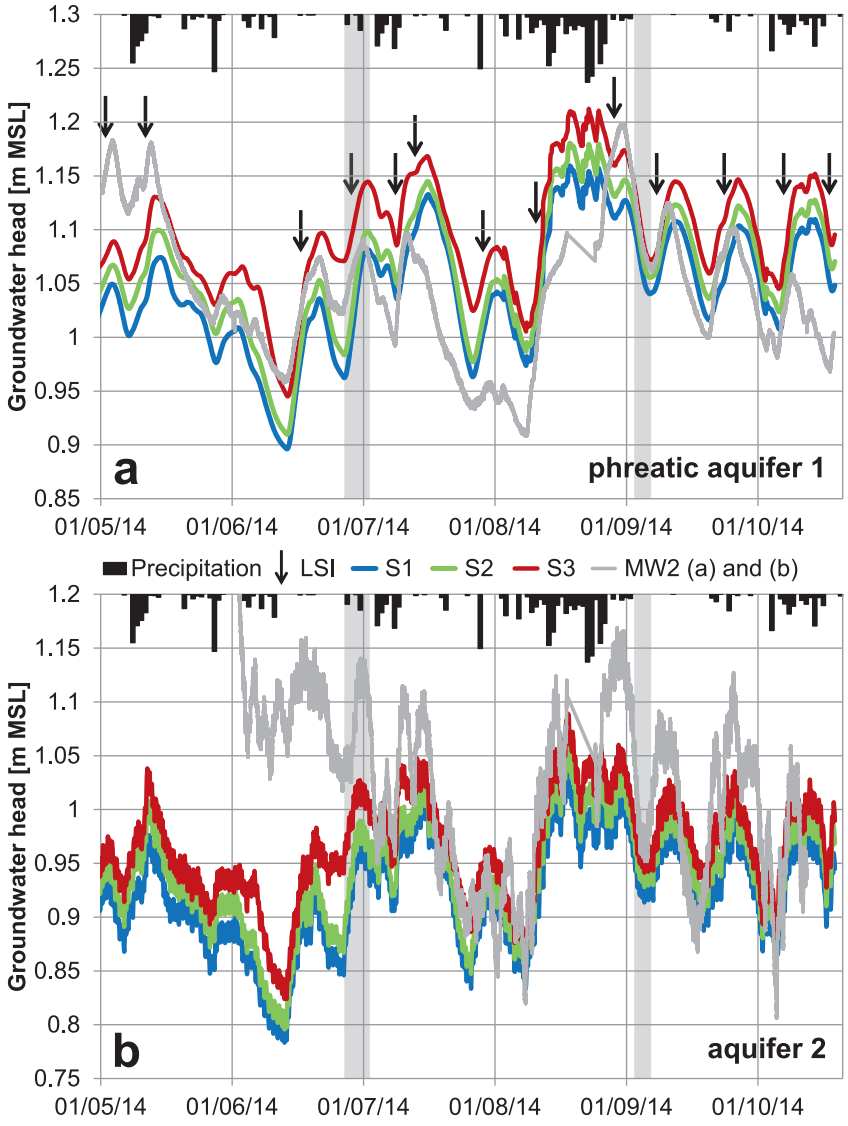

Figure 3.6 (a) Measured groundwater head (grey line) in the upper well screen of monitoring well 2 and (b) the lower well screen of monitoring well 2, with the simulated groundwater head of model scenario S1 (SWL, blue line), S2 (wave set-up, green line), and S3 (wave run-up, red line). The vertical grey bars mark topographic surveys on the Sand Engine, the arrows mark LSI instances where the sea-level was higher than the Mean High Water Spring (MHWS) height of +1.28 m MSL, and the black bars indicate the daily precipitation (in mm d^{-1}) with a maximum of 21 mm on 22 August 2014.

Overall, the observed fluctuation in groundwater head can to a large extent be explained by variations in sea-level (spring tide-neap tide cycle), coastal geomorphology, groundwater recharge, and groundwater flow across the inland model boundary. The initial deviation of the groundwater head of approximately 0.20 in the bottommost aquifer – in contrast with the resemblance in the upper aquifer – is probably caused by underestimations in the inflow of groundwater across the inland model boundary in the previous period, possibly in combination with geologic differences.

Focusing on the effect of tides and storm surges, Figure 3.6 shows that for most LSI instances (indicated with black arrows) the simulated increase in groundwater head is similar to the measurements (e.g. on 9 and 24 September), while in some instances the model overestimates the increase in groundwater head (e.g. on 14 and 30 July). Probably the primary cause for this contrast are mismatches between the actual and modelled topography, which is a consequence of continued morphological changes between the bimonthly topographic surveys. For example, photographs of the Sand Engine from the Argus (video sampling) station indicate that a sand bar developed in the intertidal zone, after the storm surge on 9 July 2014 (Figure 3.4), and this sand bar could have dampened the extent of the LSI on 14 and 30 July.

As for precipitation, Figure 3.6 shows that precipitation led to negligible to small rises – often in the order of centimetres – in the measured groundwater level, as for example during relatively high rainfall events on 27 May (17.7 mm in 15 h) and 28 July (16.8 mm in 11 h). Because the measured precipitation was probably generally close to reality, this indicates that the volume of groundwater recharge was substantially reduced due to evaporation and storage. In most instances, the simulated response to precipitation was similar to the measured response, however in some instances (e.g. the period of high rainfall between 13 and 25 August) the simulated change in groundwater head appeared to large when compared with measurements. This suggests that either the simulated evaporation in this period was underestimated, or that the volume of precipitation stored in the unsaturated zone was larger than anticipated.

The performance of the calibrated model was examined with observations of the groundwater level from 7 November to 19 December 2014, taken in monitoring well D1 and D2 (Figure 3.7). These observations were situated near the local MHW height of 11.09 m MSL and were therefore more exposed to sea-level fluctuations in comparison with monitoring well 2. The similarity in the observed and simulated groundwater head in this period confirms the reliability of the calibrated model at different distances from the local MHW height. The absolute mean error between the measured and simulated groundwater head of model scenario S1, S2, and S3 is respectively 0.142, 0.138, and 0.135 m for monitoring well D1 (RMSE 0.19, 0.18, and 0.17 m), and respectively 0.14, 0.13, and 0.11 m for monitoring well D2 (RMSE 0.20, 0.18, and 0.15 m).

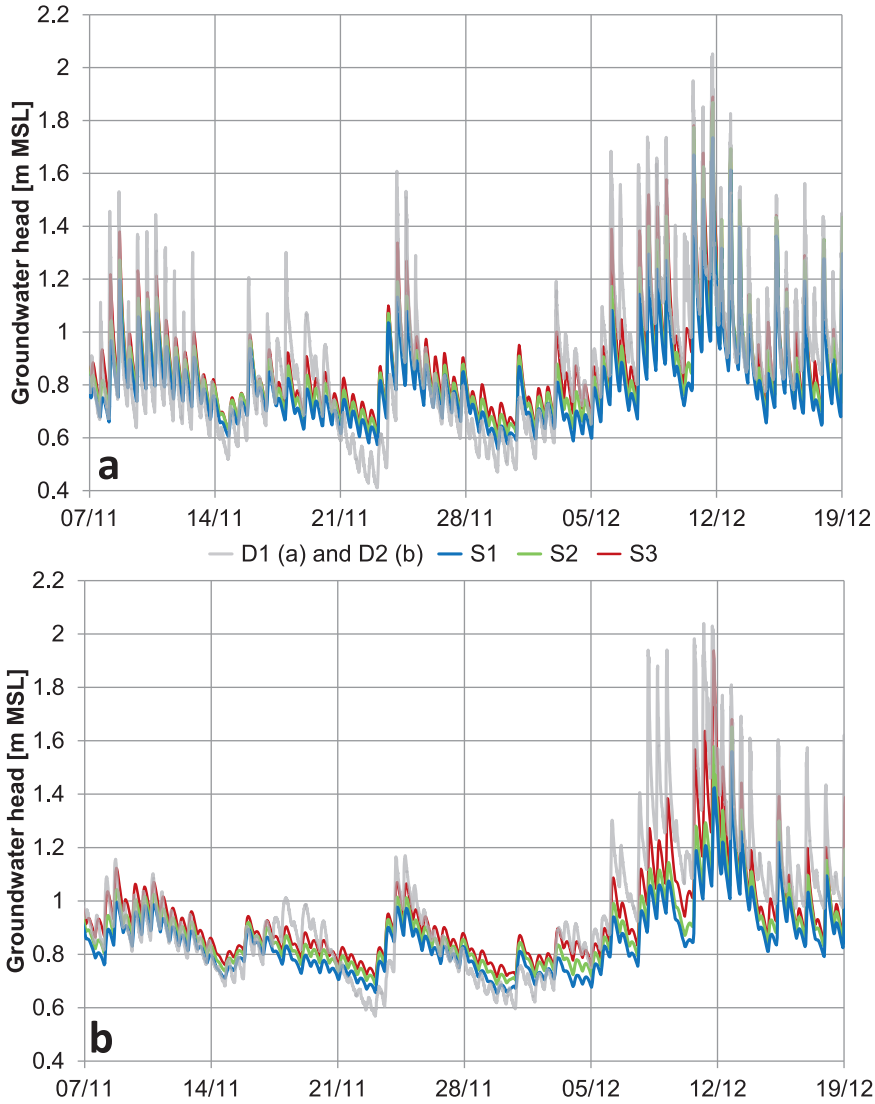

Figure 3.7 Measured groundwater head in monitoring well (a) D1 and (b) D2, and simulated groundwater head in model scenario S1 (SWL, blue line), S2 (wave set-up, green line), and S3 (wave run-up, red line).

During the first 4 weeks (7 November to 5 December), the weather conditions were generally calm with low wave heights (Figure 3.4), in contrast with the stormy conditions in the last 2 weeks (5 - 19 December). This resulted in fewer and less extensive inundations in the period before 5 December, and consequently smaller variations in groundwater head, and this contrast is captured in both the measured and simulated groundwater head. However, in some periods the simulated and measured groundwater head diverge, as for example between 17 and 22 November. Photographs of the site from the Argus (video sampling) station indicate that this mismatch is probably caused by a sand bar, which (slowly) developed in the intertidal zone in this period, and this shortened or dampened the extent of inundations.

In addition, in many instances the response of the groundwater head to LSI is underestimated. However, comparisons of the model scenarios (Figure 3.7) suggest that the incorporation of wave run-up led to a small improvement in the simulation of the response of the groundwater level to coastal hydrodynamics and morphodynamics. In particular in scenario S1 (SWL), the model seems to underestimate short-term fluctuations in groundwater level, but the incorporation of wave run-up in scenario S3 led to additional inundation height of 0.1 - 0.7 m.

For the analysis of the frequency and extent of LSI during the measurement period, observed instances of LSI along the ERT measurement transect were compared with the simulated LSI in model scenario S1 (SWL) and S3 (wave run-up; Figure 3.8). In both measurements and model simulations, we have defined the maximum extent of LSI (defined with respect to the seaward boundary of the electrode array) on the basis of the first substantial deviation in the resistivity or salinity (at least 100%) in the upper layers of the phreatic aquifer.

Variations in the extent of LSI (Figure 3.8) show that LSI are not only dependent on the sea-level, but also on the storm intensity, and (changes in) the local topography (i.e., surface elevation and morphology). Changes in the storm intensity can lead to substantial variations in wave run-up, and therefore to an extension of LSI in instances with equal sea-levels. The simulations confirm the importance of wave run-up by showing that the incorporation of wave run-up reduces the underestimation in the level of LSI and lowers the error between the measured and simulated extent of LSI in all instances. However, variations in the local topography, due to the continued retreat of the shoreline (Figure 3.5), can also lead to substantial shifts in the area of inundation.

3.3.2 Groundwater Salinity

The inverted time series of resistivity images of 14 November 2014 to 20 January 2015 were converted to salinity with the procedure that was described in section 3.2.2. In the presentation and discussion of the results, we have concentrated on these salinities to be able to differentiate between fresh, brackish, and salt groundwater, to improve the connection of changes in salinity with LSI or other processes, and to perform side-by-side comparisons with the model simulated salinities.

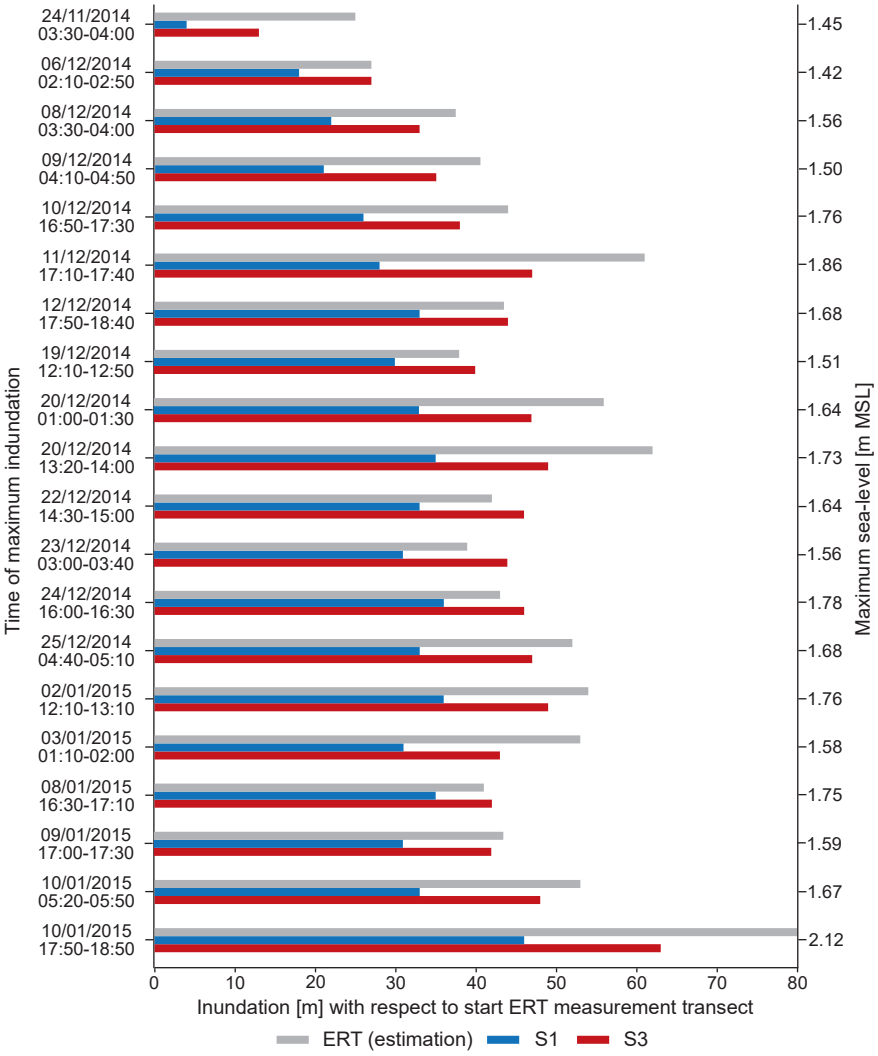

Figure 3.8 Maximum extent of LSI (m) along transect with respect to seaward boundary of the ERT measurement, for model scenario S1 (SWL, blue line), and S3 (wave run-up, red line).

But first this time series of interpreted groundwater salinities was used to investigate the effect of coastal hydrodynamics and morphodynamics on the fresh-salt groundwater distribution. In this study, we have focused on the change in groundwater salinity between the groundwater level and a depth of 21 m MSL, because the aim of this study lied on fresh groundwater resources and this depth range encompasses most of the observed changes in the fresh-salt groundwater mixing zone, and because the ERT data were most sensitive and therefore reliable near the surface (see Section 3.3.3).

The observed changes in groundwater salinity in the measurement period show that in most instances an increase in salinity coincides with tides and storm surges, and that the impact varies with the extent of the inundation. This is illustrated in Figure 3.9, with the (average) maximum increase in salinity and the (average) total increase in salinity during LSI between 14 November and 11 December, for LSI with sea-levels larger or equal to 10.86 m MSL (Mean High Water Neap: MHWN), 11.09 m MSL (MHW), and 11.28 m MSL (MHWS). Decreases in salinity along the measurement transect are predominantly caused by falling groundwater levels (frequently as a consequence of LSI), and to a lesser extent by (high) rainfall events (Figure 3.10). However some of the (small) changes in the measured salinity cannot be explained by LSI and recharge. Possible causes for these are small fluctuations in the electrical resistivity, measurement errors (related to disconnection of electrodes or rapid changes in resistivity), and changes in moisture content in the unsaturated zone.

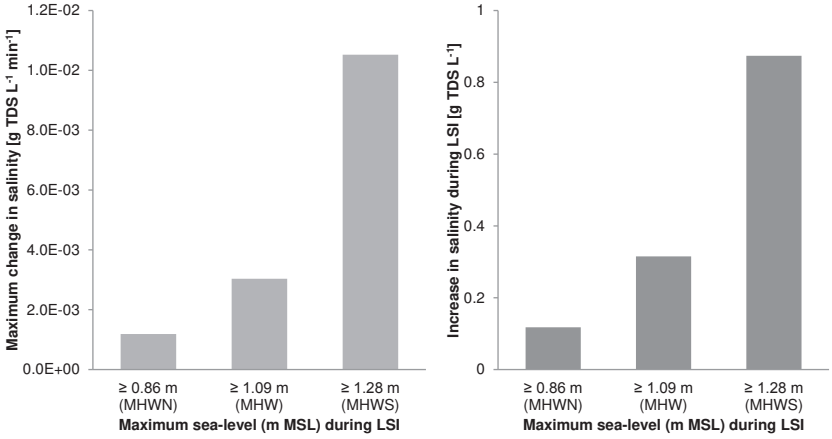

Figure 3.9 Average maximum increase in salinity (in g TDS L^{-1} min^{-1}) and average total increase in salinity during LSI (in g TDS L^{-1}), as observed in the ERT measurements between 14 November and 11 December 2014, grouped for LSI with sea-levels larger or equal to the MHWN, the MHW, and the MHWS.

For the examination of particular effects of LSI (e.g. wave run-up and recharge) on the fresh-salt groundwater distribution, we compared measured and simulated changes in groundwater salinity. The comparison of the change in salinity was conducted in two respects: first in relation to the change in groundwater salinity (Figure 3.10), and second in time (Figures 3.11 and 3.12) with respect to the salinity distribution on the 14 November 2014 11:00 (start of measurements). Changes in the length of the electrode array (Figure 3.3) were adopted in the comparison with model simulations, and only sections with reliable measurements were compared.

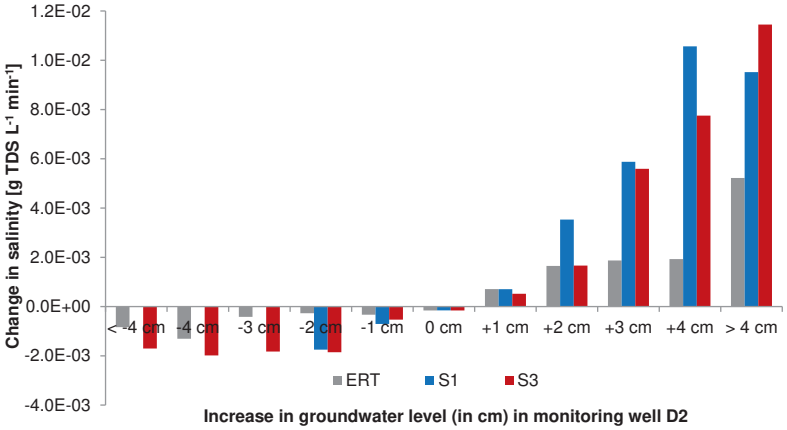

Figure 3.10 Average increase in groundwater salinity (in g TDS L^{-1} min^{-1}) between 14 November and 11 December 2014, as observed in the ERT measurements (grey), model scenario S1 (SWL, blue), and model scenario S3 (wave run-up, red), grouped by the change in groundwater head (in cm) at monitoring well D2 and sampled with a 30 min interval.

The overall resemblance between the measured and simulated change in groundwater salinity demonstrates – in particular for model scenario S3 – that the changes in groundwater salinity along the measurement transect are primarily determined by sea-level fluctuations and associated groundwater flow (Figures 3.10 and 3.11). In addition, the contrast in the reproducibility of the observed phenomena between model scenario S1 (SWL), S2 (wave set-up), and S3 (wave run-up) substantiates the importance of a reliable estimation of LSI, and in particular wave run-up.

Groundwater recharge has a small effect on the groundwater salinity in the measurement period (see Figure 3.12). Many differences in the measured and simulated salinity are probably caused by underestimations in the extent of LSI, e.g. the effect of inundations between 14 and 20 November, and between 20 and 24 December is underestimated (Figure 3.8). Other possible causes for differences between measured and simulated salinities are related to errors in the conversion of the electrical resistivity to groundwater salinity, underestimations in the fluctuation of the groundwater level (see Figure 3.7), or changes in measured electrical resistivity that are related to moisture content.

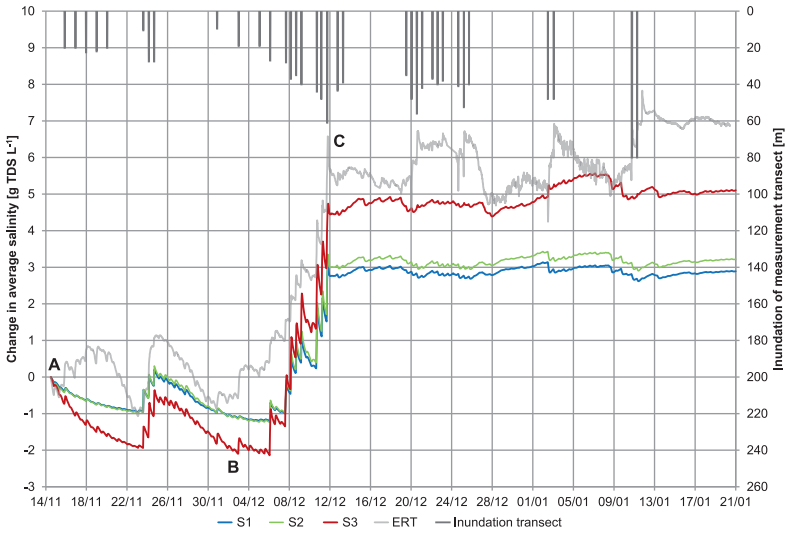

Figure 3.11 Change in salinity (g TDS L^{-1}) with respect to the initial salinity distribution, for the observed salinity (grey line), model scenario S1 (SWL, blue line), S2 (wave set-up, green line), and S3 (wave run-up, red line). Instances of LSI (m) of (sections of) the transect are shown with dark grey bars. The letters A, B, and C mark the time of the three images shown in Figure 3.13.

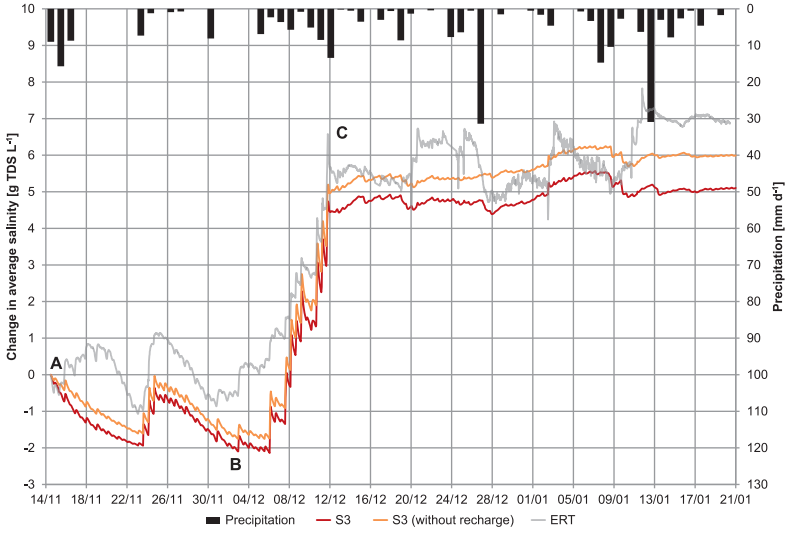

Figure 3.12 Change in salinity (g TDS L^{-1}) with respect to the initial salinity distribution, for the observed salinity (grey line), and model scenario S3 (wave run-up) with recharge (red line) and without recharge (orange line). The precipitation is given in mm d^{-1} with black bars. The letters A, B, and C mark the time of the three images shown in Figure 3.13.

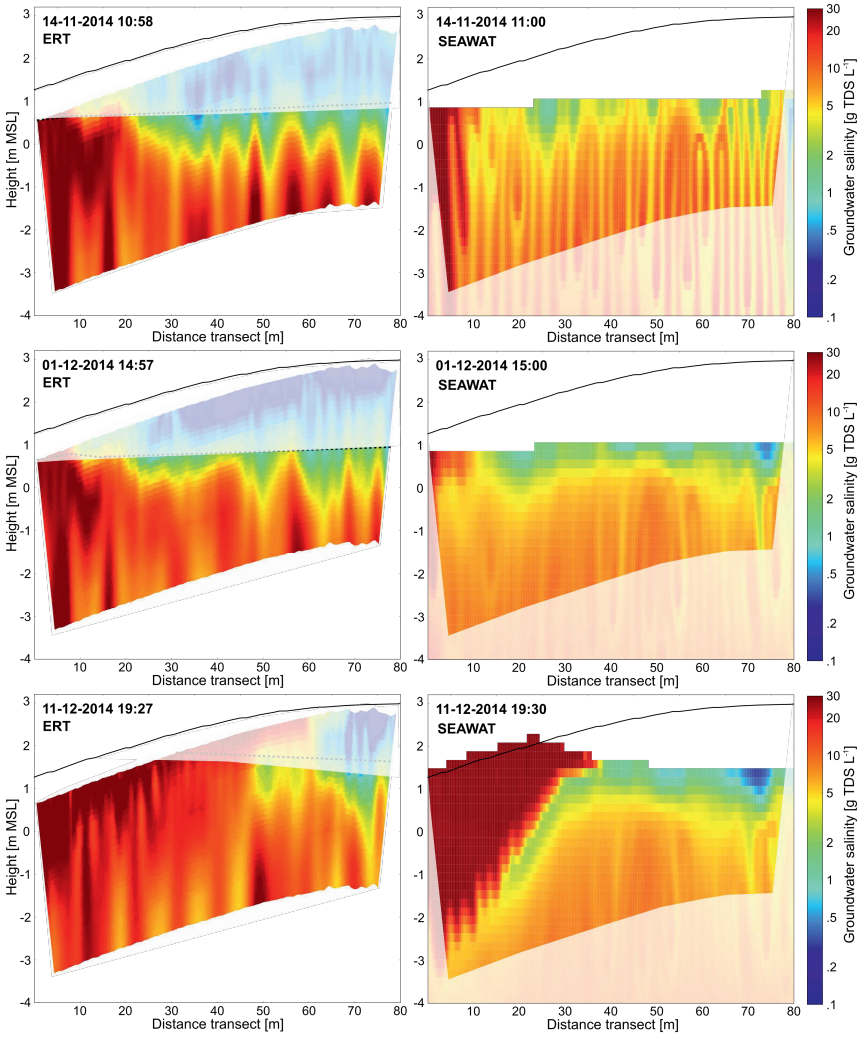

Figure 3.13 2-D images of the (left) measured and the (right) simulated groundwater salinity (S3, wave run-up) for three instances: 14 November 11:00 (start of measurements); 1 December 15:00 (after a calm weather period); and 11 December 19:30 (after substantial inundations). These instances are also indicated in Figures 3.11 and 3.12 with letters A, B, and C.

Comparisons of the absolute groundwater salinity in measurements and simulations shows that the general pattern matches, with increases in salinity due to inundations and a small fresh to brackish groundwater lens on the landward side (Figure 3.13). The complete time-series of the measurements and simulations is included as supporting information. But some groundwater salinities appear to be underestimated in the model simulations or overestimated in the converted salinities. Conversely, the groundwater salinity at the seaward side appears to be higher in the simulations. These differences are probably caused by the inversion (smoothing and artefacts, see Section 3.3.3), errors in the conversion of the resistivity to groundwater salinity, errors in the initial salinity distribution, or mismatches in the salinization of the coastal aquifer during LSI.

3.3.3 Synthetic Modeling

The resolution of the inverted resistivity images and potential inversion artefacts was evaluated with a synthetic modelling exercise, consisting of the inversion of simplified hypothetical resistivity images (Henderson et al., 2010). In this study, two hypothetical cases with a shallow fresh groundwater lens – representative of the conditions at the study site – were created with a 2-D groundwater model: case 1 with a sea-level height equal to MHW (1.09 m MSL), and case 2 with an LSI (1.1 - 2.2 m MSL) of the fresh groundwater lens (Table 3.2).

This 2-D model contained the same hydrogeological properties and model parameters as the calibrated model, as described in section 3.2.3. The implemented model grid was identical to the tomogram: 159 columns with a constant spacing of 0.5 m, 28 layers with a constant thickness of 0.167 m, and a surface elevation that consists of the 160 measured electrode elevations (incorporated as model nodes). The groundwater salinities in unsaturated model cells were set to 0.1 g TDS L^{-1}. Figure 3.14 shows the simulated groundwater salinity in case 1 and 2.

Table 3.2 Model parameters in case 1 "MHW" and case 2 "LSI".

Model Parameter	**Case 1 "MHW"**	**Case 2 "LSI"**
Groundwater recharge	1.4 mm d^{-1} + 0.2 g TDS L^{-1}	0.97 μm min^{-1} + 0.2 g TDS L^{-1}
Initial conditions	1.2 m MSL + 28 g TDS L^{-1}	Output of case 1
Inland boundary	1.1 m MSL + fresh/salt interface at 0.45 m MSL	1.1 m MSL + fresh/salt interface at 0.45 m MSL
Model period	180 days	360 min/6 h
Sea-level	1.09 m MSL + 28 g TDS L^{-1}	1.1-2.2 m MSL + 28 g TDS L^{-1}

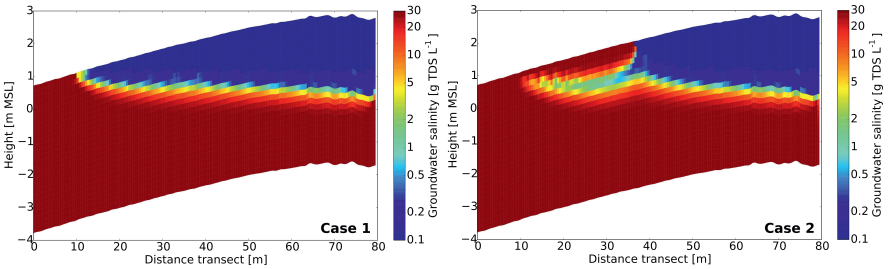

Figure 3.14 Simulated groundwater salinity of case 1 and 2.

The generated salinity distributions were converted to resistivities with Equation 3.1, using the same formation factor as described in section 3.2.2 and the assumption that the groundwater conductivity and groundwater salinity are similar. The resulting resistivities were averaged from 27 to 9 model layers, in accordance with the inverse model used in the time-lapse measurements: 159 columns with a constant spacing of 0.5 m, 9 layers with a variable thickness of 0.167 - 0.833 m. In addition, we added random electrical noise of 1 mV V^{-1} to the inverse models of case 1 and 2 to simulate the field data.

In order to assess the effect of the chosen minimization norm, both cases were inverted with the full least-squares inversion (minimizing in L2 norm) and the full L1 norm inversion (minimizing L1 in norm). In addition, to assess the effect of Lagrangian multipliers, both cases were also inverted with the constant multiplier of 0.1, and the automatic calculation of the multiplier that is based on the Active Constraint Balancing (ACB) technique (Yi et al., 2003).

The inverted distributions of the groundwater salinity (Figures 3.15 and 3.16) closely resemble the simulated distributions (Figure 3.14) for both cases; the overall pattern is captured with all chosen minimization norms and with both the automatic (ACB) and constant Lagrangian multiplier. All inversions also seem to result in an over smoothing of the simulated fresh-salt groundwater mixing zone, and this effect increases with depth, parallel with the decrease in resolution.

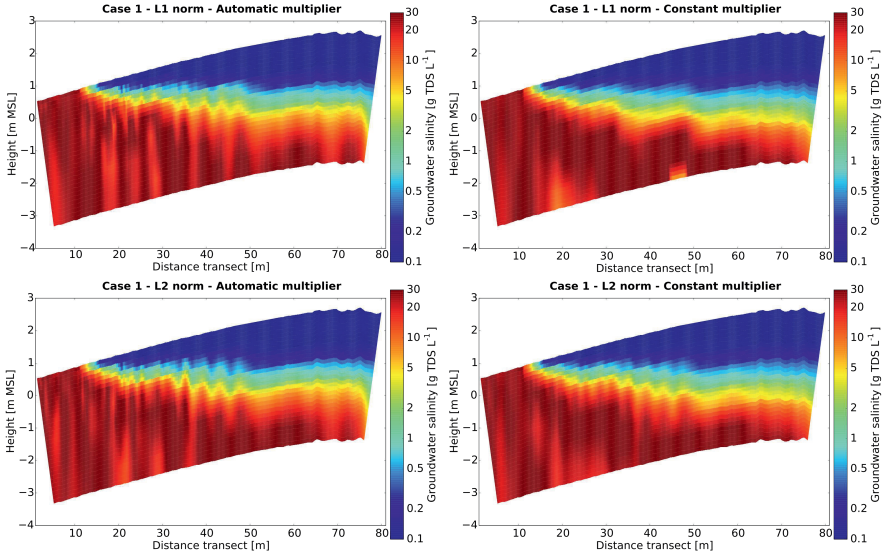

Figure 3.15 Inverted groundwater salinity of case 1 "MHW", with (top) L1 or (bottom) L2 minimization norms and an (left) automatic or (right) constant Lagrangian multiplier.

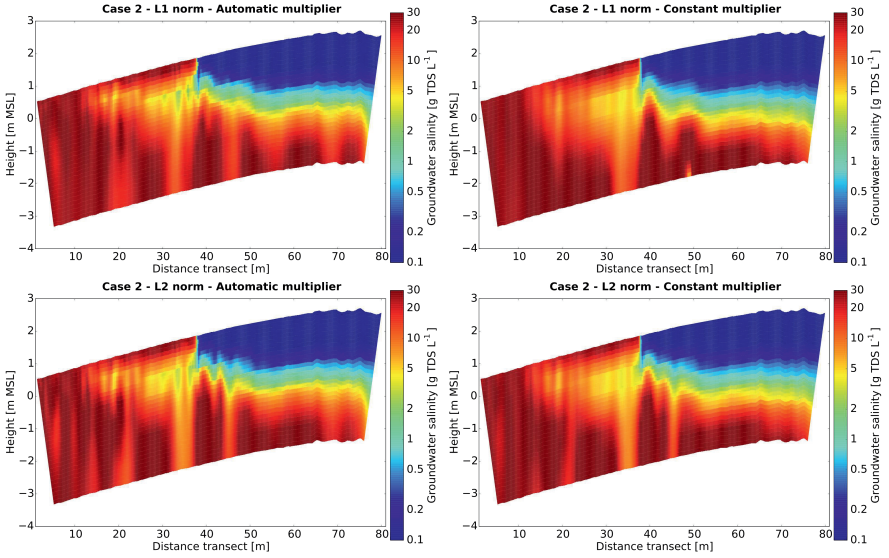

Figure 3.16 Inverted groundwater salinity of case 2 "LSI", with (top) L1 or (bottom) L2 minimization norms and an (left) automatic or (right) constant Lagrangian multiplier.

Table 3.3 RMS error of the inverse model for case 1 "MHW" and case 2 "LSI"

	Case 1 "MHW"		Case 2 "LSI"	
Model RMS Error	Inversion	Salinity	Inversion	Salinity
L1 norm minimization Automatic multiplier	5.8%	5.7 g TDS L^{-1}	5.9%	6.4 g TDS L^{-1}
L1 norm minimization Constant multiplier	7.4%	6.5 g TDS L^{-1}	7.0%	6.4 g TDS L^{-1}
L2 norm minimization Automatic multiplier	5.5%	5.7 g TDS L^{-1}	5.6%	6.4 g TDS L^{-1}
L2 norm minimization Constant multiplier	5.7%	5.7 g TDS L^{-1}	5.9%	7.3 g TDS L^{-1}

In addition, Figures 3.15 and 3.16 show that most vertical features in groundwater salinity near the bottom of images are not present in the simulations, and are probably caused by the decrease in resolution with depth. These inversion artefacts occur with both the L1 and L2 minimization norms, and with the automatic and constant Lagrangian multiplier. However, the images suggest that the automatically calculated Lagrangian multiplier is more vulnerable to these inversion artefacts. For an exact comparison of the inversion methods, we have added the weighted RMS error of the inverse model and the RMS error of the groundwater salinity (inversion compared with simulation) in Table 3.3. The RMS error is lowest for the L2 norm minimization and the automatic Lagrangian multiplier, but the differences between the inversion methods are small.

3.4 Discussion

3.4.1 Imaging Groundwater Salinity With ERT

The time-lapse ERT measurement yielded a time series of 2-D images of electrical resistivities. For the visualization of changes in the fresh-salt groundwater distribution, and for the comparison with model simulations, these resistivities (inverse is conductivity) were converted to groundwater salinities with the Practical Salinity Scale (PSS) of 1978. The salinity-conductivity relationship in the PSS-1978 is determined by laboratory experiments on (diluted) standard seawater, and is therefore only applicable to water with a similar composition of major ions (viz., Na^+, K^+, Mg^{2+}, Ca^{2+}, Cl, HCO_3^-, SO_4^{2-}) as standard seawater. Groundwater salinities at the study site are predominantly a result of the mixing of seawater and rainwater, and will satisfy this requirement to a large extent. However, variations in the chemical composition will probably occur at low salinities (smaller than 2 g TDS L^{-1}), because of the (relatively small) inflow of coastal groundwater and the formation of ions – in particular bicarbonate (HCO_3^-) – by chemical processes. In addition, small errors or variations in the electrical formation factor can result in substantial deviations in the determination of the groundwater conductivities.

This time series of estimated groundwater salinities, and accordingly time-lapse ERT, provided us the instruments to effectively investigate the impact of coastal hydrodynamics and morphodynamics and precipitation on coastal groundwater. The 2-D images contained detailed information on the extent of LSI, and on the change in the fresh-salt groundwater distribution over time. In particular the ability to perform (automated) measurements in multiple dimensions for a period of 2 months was a benefit of the time-lapse ERT. For example, with this method we were able to delineate the extent of multiple inundations with relative accuracy, and coincidentally observe the (2-D) impact on the fresh-salt groundwater distribution. However, an aspect that occasionally led to small anomalies is related to the duration of each individual measurement, which varied between 10 and 30 min. Rapid changes in groundwater salinity and saturation levels during individual measurements caused local anomalies in the electrical resistivity.

It should be noted that inversion of resistivity images often results in non-unique solutions of the electrical resistivity, and that the resolution of inverted images decreases with depth. Generally a decrease in resolution leads to a larger deviation from the actual or earth resistivity and a stronger effect of the starting model and chosen regularization criteria on the acquired data. Inundations of the electrode array can also lead to a reduction in the resolution, because the highly conductive surface-water layer causes a preferential flow of the electrical current (Henderson et al., 2010). This was anticipated in this study and therefore we have focused on data that was acquired close to surface, between the groundwater level and a depth of 21 m MSL as described in section 3.3.2. Potential poor resolutions in inundated segments of the electrode would only be temporary, and the shallow fresh or brackish groundwater lens in these segments would probably become completely saline. In addition, the reliability of the inversion process was substantiated by low RMS errors (smaller than 1%).

3.4.2 SWI Processes Due to Tides and Storm Surges

The similarity of the measured and simulated groundwater head, extent of LSI, and change in groundwater salinity proves that reliable simulations of the fluctuation of the groundwater head in complex dynamic coastal environments can be conducted with the adopted simulation methodology. With detailed information on fluctuations in sea-level, topography, and precipitation, it was possible to relatively accurately reproduce short and long-term variations in LSI and groundwater salinity with the calibrated variable-density groundwater model. Here, the incorporation of wave set-up and especially wave run-up in the simulations led to a substantial improvement in the estimation of the extent of LSI and SWI. This suggests that in areas with gently sloping beach profiles the extent of inundation could be underestimated when wave run-up is neglected, especially during storm surges.

An important cause of the observed differences between measurement and simulations is probably related to the morphological evolutionbetween the monthly to bimonthly topographic surveysthat was not incorporated in the simulations. This morphological evolution resulted in a gradual retreat of the shoreline (often exacerbated by storm surges) and the formation of sandbars along the outer perimeter of the Sand Engine, which resulted in shifts of the inundated area. These sandbars could have led to a shift in the location where waves break and reduced wave run-up, and (partially) blocked the flow of seawater, especially when sandbars were connected along the shoreline. Thus, small morphological changes can lead to substantial changes in the area of inundation and wave run-up, and therefore have a strong impact on fresh groundwater in coastal aquifers. For the improvement of simulations of groundwater salinity in such dynamic coastal conditions, it is necessary to incorporate more information on the morphological change during storm surges. Thus, for accurate and detailed delineations of the groundwater head and salinity in local dynamic coastal environments, it is recommended to monitor the local topography frequently or to perform accurate morphological simulations.

In general the simulated fresh-salt groundwater distribution matches the observed patterns in the time-lapse ERT images. These are patterns such as the observed development of a small fresh to brackish groundwater lens after the intensive storm in the night of 21 - 22 October 2014, and the gradual salinization of the aquifer due to repeated LSI. Deviations in absolute groundwater salinities are probably primarily caused by a combination of errors in the inversion (e.g. over smoothing and inversion artefacts, see Section 3.3.3), errors in the conversion of electrical conductivities to groundwater salinities, errors in the wave set-up and wave run-up height and related LSI and SWI during storm surges, and errors in the simulated fresh-salt groundwater distribution in the period previous to the measurements. To differentiate the contribution of each of these factors and to improve simulations in these local dynamic coastal environments, it is recommended to perform more extensive measurements of the groundwater salinity. In addition, wave set-up and wave run-up height was estimated with empirical run-up formulas, where the infiltration of seawater by wave run-up was roughly estimated. This approach generally improves the simulation of SWI processes in these environments, but refinements in the prediction of the extent of LSI and the infiltrated volume of seawater can lead to further substantial advances. For example, the incorporation of unsaturated zone processes in the approach could improve the estimation of the volume of seawater that infiltrates during wave run-up, because the infiltration is probably very sensitive to the saturation level.

3.5 Conclusions

The measurements show that time-lapse ERT can be a valuable and promising technique for the measurement of temporal and spatial changes in groundwater salinity in dynamic coastal environments. ERT can especially be effective in the measurement of rapid processes such as the effects of salt water overwash and intrusion during and after storm surges. The observed changes in salinity due to groundwater recharge, tidal dynamics, and storm surges could to a large extent be simulated by a variable-density groundwater model, suggesting that given a thorough understanding of the (local) system, groundwater models can be used to make predictions of the effects of tides and storm surges. However, an accurate numerical simulation of the effect of LSI in (topography-limited) dynamic coastal environments, and especially during storm surges, requires detailed information about morphological changes along the coastline and reliable estimates of the extent of wave run-up.

Acknowledgements

We thank Mike van der Werf, Marco de Kleine, and Andre Cinjee for their extensive support in the planning, set-up, and upkeep of the ERT measurement. This research is supported by the Dutch Technology Foundation STW, which is part of the Netherlands Organization for Scientific Research (NWO), and which is partly funded by the Ministry of Economic Affairs. This work was carried out within the Nature-driven nourishment of coastal systems (NatureCoast) program. The data used to produce the results of this paper may be obtained by contacting the corresponding author.

4 Impact of coastal forcing and groundwater recharge on the growth of a fresh groundwater lens in a mega-scale beach nourishment

Based on: Huizer, S., Radermacher, M., de Vries, S., Oude Essink, G. H. P., and Bierkens, M. F. P. (2018), Impact of coastal forcing and groundwater recharge on the growth of a fresh groundwater lens in a mega-scale beach nourishment, Hydrology and Earth System Sciences 22, 1065–1080, doi:10.5194/hess-22-1065-2018.

Abstract

For a large beach nourishment called the Sand Engine – constructed in 2011 at the Dutch coast – we have examined the impact of coastal forcing (i.e. natural processes that drive coastal hydro- and morphodynamics) and groundwater recharge on the growth of a fresh groundwater lens between 2011 and 2016. Measurements of the morphological change and the tidal dynamics at the study site were incorporated in a calibrated three-dimensional and variable-density groundwater model of the study area. Simulations with this model showed that the detailed incorporation of both the local hydro- and morphodynamics and the actual recharge rate can result in a reliable reconstruction of the growth in fresh groundwater resources. The neglect of tidal dynamics, land-surface inundations, and morphological changes in model simulations can result in considerable overestimations of the volume of fresh groundwater. In particular, wave run-up and coinciding coastal erosion during storm surges limit the growth in fresh groundwater resources in dynamic coastal environments, and should be considered at potential nourishment sites to delineate the area that is vulnerable to salinization.

4.1 Introduction

Groundwater is an important – in many situations vital – source of high-quality fresh water for most coastal communities in the world. However, these coastal fresh groundwater resources are to an increasing degree affected by seawater intrusion, primarily caused by (excessive) groundwater abstraction and sea-level rise (Ferguson and Gleeson, 2012; Taylor et al., 2013). Global population growth in the coming decades will lead to a rising demand for fresh water, and combined with the projected sea-level rise this will likely result in a gradual decline of fresh groundwater resources (Famiglietti, 2014; Wong et al., 2014).

In addition, sea-level rise can also increase coastal flooding – caused by storm surges – and may lead to an increase in coastal erosion, which in turn will induce seawater intrusion and may cause a loss of wetland and biodiversity (FitzGerald et al., 2008; Passeri et al., 2015; Wong et al., 2014). Coastal lowlands with low topographic gradients and small islands are particularly vulnerable, because these areas are the most susceptible to coastal flooding and seawater intrusion (FitzGerald et al., 2008; McGranahan et al., 2007; Michael et al., 2013; Rotzoll and Fletcher, 2012).

There are two potential responses to these rising threats to coastal communities, especially in relation to sea-level rise: (global) mitigation and (local) adaptation (Nicholls, 2011; Wong et al., 2014). With the progression of our knowledge and expectations on sea-level rise, the international perspective has shifted to adaptation (Brown et al., 2014). Some countries, such as the Netherlands, Germany and the United States, have implemented coastal protection measures, which is the only adaptation approach that additionally might help to preserve fresh groundwater resources (van Koningsveld and Mulder, 2004; Rosenzweig and Solecki, 2010; Sterr, 2008).

In the Netherlands – a vulnerable low-lying country with a long history of coastal flood management – sandy shorelines have been successfully maintained and reinforced with an extensive sand nourishment programme in the last decades (Giardino et al., 2011; Keijsers et al., 2015). The anticipation of sea-level rise has led to new adaptation measures (Kabat et al., 2009), where the construction of a large concentrated beach nourishment called the Sand Engine (also called Sand Motor) is one notable example (Figure 4.1). This large beach nourishment was created on the Dutch coast as part of an effort to attain a more sustainable coastal protection approach (Slobbe et al., 2013). Contrary to regular nourishments, the Sand Engine is deemed advantageous because it only causes a disturbance at a concentrated part of the coastline during a short time, after which the excess sand nourishes the larger length of the coastline gradually by natural along-shore sand transport (Stive et al., 2013).

In previous studies, we showed that large beach nourishments such as the Sand Engine can potentially lead to substantial increases in fresh groundwater resources (Huizer et al., 2016) and that the impact of tides and storm surges on these resources can be simulated accurately when the system is thoroughly understood (Huizer et al., 2017). This raised questions concerning the potential growth of fresh groundwater resources in the Sand Engine following its construction in 2011, and how important the impact of coastal forcing (i.e. natural processes that drive coastal hydro- and morphodynamics such as wind, waves, and tides) precipitation and evaporation was on the observed growth in fresh groundwater resources. In other words, did the freshwater lens grow substantially following the construction of the Sand Engine, is it possible to reproduce this growth reliably with a numerical model, and how important is detailed information on land-surface inundations, geomorphological changes, and groundwater recharge for the replication of this growth?

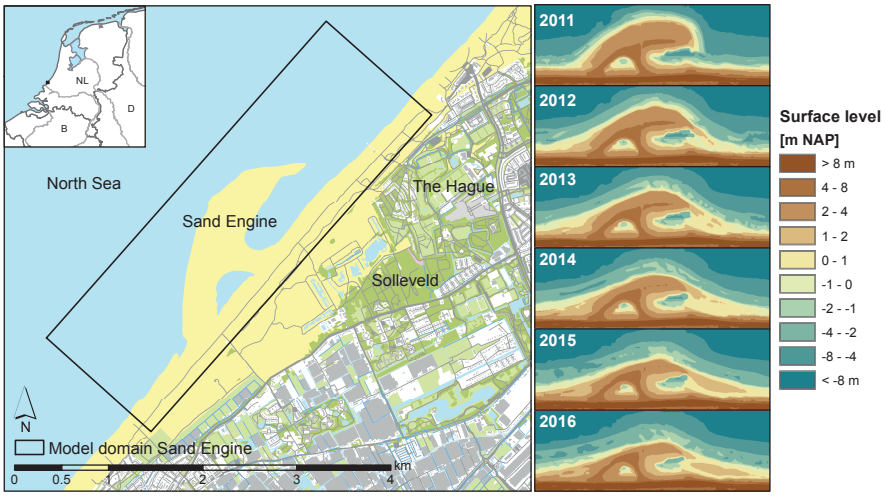

Figure 4.1 Map of the study area with the model domain (left), and the change of the surface level in the study area (morphological development) between 2011 and 2016 (right) in metres with respect to the NAP datum, which is approximately equal to mean sea level.

To answer these questions this study aims to reconstruct the development of the freshwater lens and mixing zone between 2011 and 2016, and evaluate the importance of an accurate description of (1) land-surface inundations, (2) geomorphological changes and (3) groundwater recharge for the prediction of the growth of fresh groundwater resources. Both the reconstruction and evaluation were conducted with a three-dimensional (3-D) variable-density groundwater model, where the model simulations were calibrated and evaluated with (transient) groundwater head and groundwater salinity measurements. Considering the aims of this study, it is important to note that both the spatial and temporal changes of fresh groundwater resources in the Sand Engine are simulated, calibrated and evaluated.

4.2 Data and methods

4.2.1 Site description: Sand Engine

The Sand Engine (also called Sand Motor) is a large concentrated beach nourishment of approximately 17 million m^3 sand, which was placed on the Dutch coast in 2011 as a hook-shaped peninsula (Figure 4.1). This nourishment is part of an innovative pilot project in which this nourishment method is evaluated with respect to the current practice of large-scale distribution of smaller volumes of sand. One appealing hallmark of the Sand Engine is that natural forces (i.e. wind, waves and currents) gradually transport the replenished sand along the retreating coast, and simultaneously support natural dune growth (Slobbe et al., 2013).

Coastal forcing storm surges in particular led to substantial geomorphological changes at the Sand Engine in the measurement period. Between 2011 and 2016 the shoreline along the outer perimeter of the peninsula retreated approximately 200 m (de Schipper et al., 2016). The geomorphological changes of the Sand Engine were monitored every 1 – 3 months with topographic surveys, as part of an intensive monitoring programme. Spatial interpolations of all topographic surveys were used to update the surface elevation in the groundwater model, and these were implemented as sequential grid regenerations.

4.2.2 Variable-density groundwater flow model

Spatial and temporal changes in fresh and salt groundwater in the Sand Engine were simulated with a 3-D groundwater model, in which the computer code SEAWAT was used to simulate variable-density saturated groundwater flow and salinity transport (Langevin et al., 2008). In SEAWAT the governing flow and solute transport equations are coupled and solved with a cell-centred finite difference approximation. Numerous studies have applied this code to simulate variably-density, transient groundwater flow in coastal environments (Colombani et al., 2016; Holding and Allen, 2015a; Pauw et al., 2014; Rasmussen et al., 2013; Webb and Howard, 2011).

The model domain had a length of 4500 m and width of 1500 m (Figure 4.1), and was discretized into 75 rows and 225 columns with horizontal cell sizes of 20 m, and 28 layers with a thickness of 0.5 m in the upper layers and 1 m in layers below -7 m NAP (Amsterdam Ordnance Datum, which is approximately equal to MSL). Boreholes from the Sand Engine and adjacent dunes show that the subsoil of the study area consists of sandy aquifers with fine to coarse-grained sand, which are (partially) interrupted by two thin aquitards consisting of sandy clay, and are separated from underlying aquifers by an aquitard consisting of clay and peat (Figure 4.2). The replenished sand and upper aquifers (Aquifer 1a and 1b) are mainly composed of medium coarse-grained sand, while the sand in the dunes and below -9 m NAP (Aquifer 2) is mainly composed of fine-grained sand (Figure 4.2). The underlying aquitard – situated between -17 and -20 m NAP – was defined as the local hydrogeological base of the model.

The boundaries of the model domain were defined either as a no-flow boundary (boundaries perpendicular to shoreline, and hydrogeological base) or as a specified head and concentration boundary (boundaries parallel to the shoreline). Specific head and concentration boundaries within the North Sea equalled tide gauge measurements in the harbours of Scheveningen and Hoek van Holland and seawater salinity of 28 g TDS L^{-1} (i.e. equal to the observed average seawater salinity at the site: Rijkswaterstaat (2012)). The inland specified head and concentration boundary, situated in the Solleveld dune area, was determined with an extra simulation with the calibrated groundwater model as described in Huizer et al. (2016).

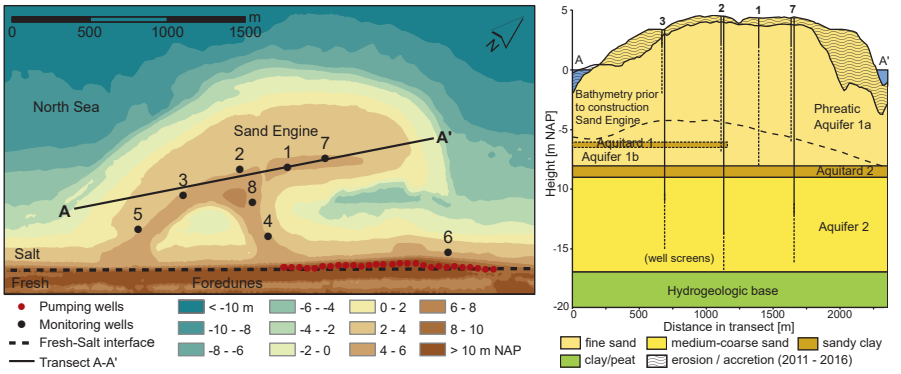

Figure 4.2 Contour map of topographic height (in metres with respect to the NAP datum) and hydrogeological cross section (along black line, A - A') of the Sand Engine between 1 and 3 August 2011, with the location of monitoring wells (black points) and pumping wells (red points). The dashed line in the cross section marks the bathymetry prior to the construction of the Sand Engine, and the wave-shading pattern marks the erosion or accretion of sand between 3 August 2011 and 3 June 2016.

In this calibrated model the groundwater recharge was adapted according to the model scenarios (Section 4.2.5). The groundwater head distribution at the start of the model simulations – before the completion of the Sand Engine in June 2011 – were set equal to the calibrated conditions of the same previously mentioned model Huizer et al. (2016). The initial groundwater salinity distribution was approximated with a sharp (vertical) fresh-salt groundwater interface in the foredunes (see Figure 4.2), because the former model underestimated the salinization close to the dunes and because previous nourishments led to seawater intrusion in the (newly constructed) foredunes. The interface was positioned in the foredunes with fresh groundwater salinities of 0.1 g TDS L^{-1} in the Solleveld dune area, and completely saline groundwater in the foredunes, beach and Sand Engine (28 g TDS L^{-1}). Model cells close to this interface and in the Solleveld dune area were excluded from evaluations.

In the adjacent dune area Solleveld a drinking-water company extracts groundwater, and in order to prevent any undesirable or unexpected effects of the construction of the Sand Engine to the groundwater quality (e.g. flow of saline groundwater towards pumping wells), 29 pumping wells were installed in 2012 on the first dune ridge (see red points in Figure 4.2). These pumping wells keep the groundwater level at +0.8 to +1 m NAP with the aim to control the direction of the groundwater flow, and were included as such in the model simulations (Stuurman, 2010).

4.2.3 Model calibration

The groundwater model was calibrated with groundwater head measurements in monitoring wells 1 to 8 (Figure 4.2), from 1 May 2014 until the end of the scenario simulations on 31 May 2016. These monitoring wells all contain one well screen in Aquifer 1a (phreatic), and monitoring wells 2, 3, 7, and 8 contain a second well screen in Aquifer 2 (see cross section in Figure 4.2). Simulated groundwater salinities were compared with chloride measurements, which were obtained from soil samples that were taken during the construction of the monitoring wells between 10 and 14 March 2014. For the conversion of the measured chloride concentrations to salinity (TDS), we have adopted the relation between chloride and TDS as found in the North Sea; 0.553 g Cl L^{-1} in 1 g TDS L^{-1} (Millero, 2003). In this study freshwater was classified as 0 – 1 g TDS L^{-1}.

The calibration comprised of manual model parameter adjustments and comparisons of measured and simulated (transient) groundwater heads and groundwater salinities. For the evaluation of the fit to the measured groundwater heads, the subsequent calibration criteria were adopted: the error between the measured and simulated transient groundwater head should be smaller than the observed variation in groundwater level (average standard deviation is 0.1 m in the calibration period), where the variation in the simulated groundwater head should be similar to the observed fluctuation pattern. For the calibration of the groundwater salinities equivalent criteria were adopted: the depth of the fresh-to-salt groundwater interface and mixing zone thickness should be smaller than the observed mixing zone thickness (in our case approximately 2 m), where the error between the measured and simulated groundwater salinity should be small or explicable. The calibration concentrated on a selection of model parameters: hydraulic conductivity, storage coefficients, and dispersivity. These model parameters were adjusted with small incremental changes from an initial estimate, which was identical to a previous model calibration of the same area (Huizer et al., 2016). The dispersivity was adapted in accordance with the observed mixing zone thickness.

Ideally, we would have liked to split the data into a calibration and a validation dataset (split sample approach). However, the number of observation locations and the length of the time series made such an approach unachievable, and therefore all available information was used for the calibration. This meant that only the lack of fit of the model could be verified, not the predictive uncertainty. The calibrated set of model parameters is shown in Table 4.1.

Table 4.1 Calibrated parameter values implemented in the model simulations.

Layer Type	Parameter	Sand Engine	Dunes
All model layers	Longitudinal dispersivity	0.1 m	
	Transverse dispersivity	0.01 m	
	Effective porosity	0.30	
	Specific storage	0.0002 m	
Phreatic aquifers	Horizontal hydraulic conductivity	28.8 m d^{-1}	10 m d^{-1}
1a: [above –6 m NAP]	Vertical hydraulic conductivity	14.4 m d^{-1}	5 m d^{-1}
1b: [–6.5 to –8 m NAP]	Specific yield	0.20	
Aquitards	Horizontal hydraulic conductivity	0.0576 m d^{-1}	
1: [–6 to –6.5 m NAP]	Vertical hydraulic conductivity	0.00576 m d^{-1}	
2: [–8 to –9 m NAP]			
Aquifer	Horizontal hydraulic conductivity	10 m d^{-1}	
2: [–9 to –17 m NAP]	Vertical hydraulic conductivity	5 m d^{-1}	

4.2.4 Model convergence

To test whether the adopted spatial model discretization returned reliable quantifications of the volume of fresh groundwater in the study site, a grid convergence or refinement test was conducted. As described in Section 4.2.2, the reference model discretization consisted of a horizontal grid size of 20 m, and 28 layers with a variable thickness of 0.5 (upper layers) to 1 m (lower layers). This discretization was tested with three additional simulations with higher and lower spatial resolutions: one with an increased vertical resolution of 0.25 to 0.5 m over 56 layers (S1), one with a decreased vertical resolution of 1 to 2 m over 14 layers (S2), and one with a coarser horizontal grid size of 30 m (S3). All the model parameters, initial conditions, and boundary conditions of the simulations were equal to the calibrated model. The convergence in regard to the temporal model discretization was not tested, because stability constraints were used to calculate the length of transport time steps.

4.2.5 Model scenarios

The importance of detailed information on (1) land-surface inundations (2) geomorphological changes, and (3) groundwater recharge for reliable reconstructions of the growth of the freshwater lens in the Sand Engine was evaluated with model simulations for the period of 1 June 2011 (completion Sand Engine) to 31 May 2016. Using the calibrated model as a representation of the actual growth in fresh groundwater resources, the importance of each factor was evaluated with model scenarios that consist of simplifications to this detailed reference model. The simplifications were based on assumptions that are often made in model simulations. The adopted methodology in the calibrated model and the model scenarios are summarized in Table 4.2, and described in detail in Section 4.2.5.

Table 4.2 Summary of model scenarios (grey items are equal to reference case).

Model scenario	**North Sea (water level)**	**Lagoon (water level)**	**Topography**	**Extinction Depth**
Reference	Tide gauge + waves	Model hindcast	Surveys	0.5 m
A	A1: MSL	A1: MSL	Surveys	0.5 m
Inundation	A2: Tide gauge	Model hindcast	Surveys	0.5 m
B	Tide gauge + waves	Model hindcast	B1: Constant	0.5 m
Morphology	Tide gauge + waves	B2: Tide gauge	Surveys	0.5 m
C	Tide gauge + waves	Model hindcast	Surveys	C1: 0.25 m
Recharge	Tide gauge + waves	Model hindcast	Surveys	C2: 0.75 m

Land-surface inundations

For the simulation of the land-surface inundations we used the same method as in Huizer et al. (2017). In this paper the method is described briefly, and for a more extensive description and evaluation of this method we refer to Huizer et al. (2017). Tide gauge measurements with a 10-minute time interval in the harbours of Scheveningen and Hoek van Holland were used to estimate the seawater level near the Sand Engine (i.e. still water level: SWL). The average seawater level of both measurement sites was used as an estimate of the local seawater level, and the tidal North Sea boundary was modelled as 'General Head (head-dependent) Boundaries and Drains' (Mulligan et al., 2011). All model layers above -2 m NAP were defined convertible (saturated thickness) and rewettable with a wetting threshold of 0.05 m (McDonald et al., 1992). To ensure a reactivation of all inundated model cells, an additional seawater infiltration of 0.01 m per minute (equal to the vertical hydraulic conductivity) was added to the area of inundation during rising tides. In addition, to analyse the impact of tidal dynamics on fresh groundwater resources, a simulation (scenario A1) with a constant seawater level of 0.065 m NAP (MSL simulation period) was executed (Table 4.2).

Wave set-up (i.e. local rise of the MSL) and wave run-up (i.e. maximum level of wave up-rush on the beach) will result in an increase in the extent of land-surface inundations, and hence to an increase of seawater intrusion. To assess the impact of wave set-up and wave run-up on fresh groundwater resources both processes were included in the reference model, and excluded in model scenario A2 (Table 4.2). Wave set-up was modelled with an identical approach as the observed seawater level fluctuations, and wave run-up as an infiltration of seawater between the wave set-up height and the wave run-up height. The infiltration rate at the wave set-up height was estimated as the drainable storage (determined by specific yield) between SWL and the wave set-up height, and above the wave set-up height this infiltration rate was reduced linearly to a value of 10% at the wave run-up height.

The wave set-up and wave run-up height in every model period was estimated with the parametrization for set-up on dissipative sites (Stockdon et al., 2006), which is dependent on the deep water significant wave height, and the deep-water wave length. The deep-water significant wave height and deep-water wave length were estimated with offshore measurements at the measurement location called "Euro platform", located 50 km southwest from the study site.

Geomorphology

The morphological evolution of the Sand Engine in the period 2011-2016 has led to significant decreases in the dimensions of the tidal channel (hereafter referred to as lagoon), which gradually choked the tidal system in the lagoon (de Vries et al., 2015). As a result the tidal amplitude decreased over time and the mean water level inside the lagoon increased (Figure 4.3).

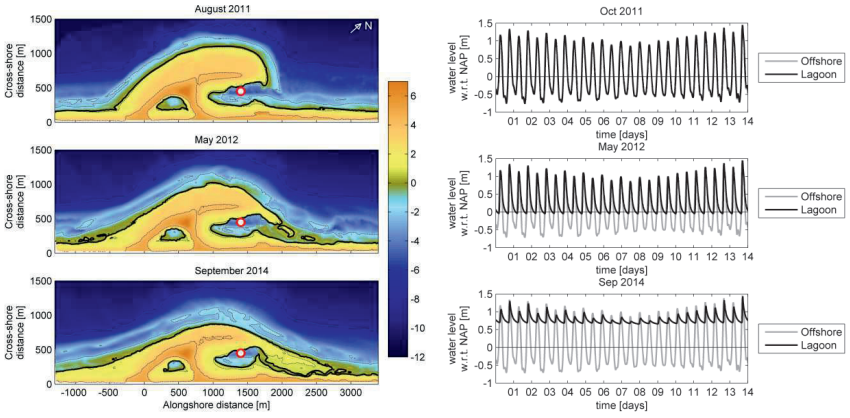

Figure 4.3 The images show three measurements of distinct morphologies of the Sand Engine domain in 2011, 2012, and 2014. The red circle represents the location where tides inside the lagoon are calculated with the Delft3D flow model in de Vries et al. (2015). The graphs show the simulated tides inside and outside the lagoon as obtained with the three successive morphologies.

In an effort to produce a hindcast of tidal water levels inside the lagoon for the period of 3 August 2011 to 4 January 2016, the numerical flow model by de de Vries et al. (2015) was extended Figure 4.4. This depth-averaged flow model was constructed with the modelling package Delft3D (Lesser et al., 2004), which numerically integrates the shallow water equations. Measurements of morphology and boundary conditions (wind and water levels) were included in the simulation:

1. Prescribed water levels along the offshore boundary were based on tidal stations north (Scheveningen) and south (Hoek van Holland) of the Sand Engine.

2. The lateral boundaries were forced with Neumann conditions, which represent the alongshore water level gradient.

3. The bottom friction was specified with a spatially uniform Chézy coefficient of 65 $m^{1/2}$ s^{-1}.

4. A constant eddy viscosity of 0.01 m^2 s^{-1} was applied.

5. The influence of wind was taken into account as a wind shear stress at the free surface.

The model bathymetry and associated nourishment geometry was constructed from a set of 34 bathymetric field surveys at the Sand Engine and the adjacent coastal cell. These surveys were conducted using a jetski-mounted single-beam echo sounder for the submerged part of the domain and a real-time kinematic differential GPS mounted on an all-terrain vehicle for the dry beach (de Schipper et al., 2016).

The hindcast of tidal water levels inside the lagoon was implemented in the reference model, where we assumed that the lagoon water level sustains over the whole channel. Before and after the hindcasted period we assumed that the water levels inside the lagoon were identical to the offshore seawater levels. Note that after 4 January 2016 the choking of the tidal system in the lagoon was (temporarily) lifted, because the continued erosion of the outer perimeter of the Sand Engine and the increasing hydraulic gradient between the lagoon and the North Sea led to breach of the sand barrier that separated the two systems.

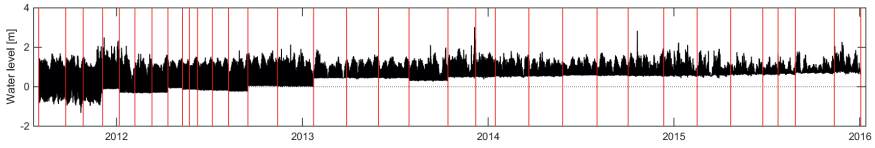

Figure 4.4 Simulated water level (in m NAP) inside the lagoon from 3 August 2011 to 4 January 2016, where the vertical red lines signify topographic surveys.

To determine the impact of the observed morphological changes and the increase of the mean water level inside the lagoon on fresh groundwater resources, two additional model scenarios (B1 and B2) were implemented (Table 4.2). In model scenario B1 all morphological changes between 2011 and 2016 were excluded and hence the topography of the Sand Engine remained constant (equal to the situation in August 2011). In model scenario B2 the choking of the tidal system in the lagoon was ignored and thus the water level in the lagoon remained equal to the North Sea throughout the simulation period (model scenario B2).

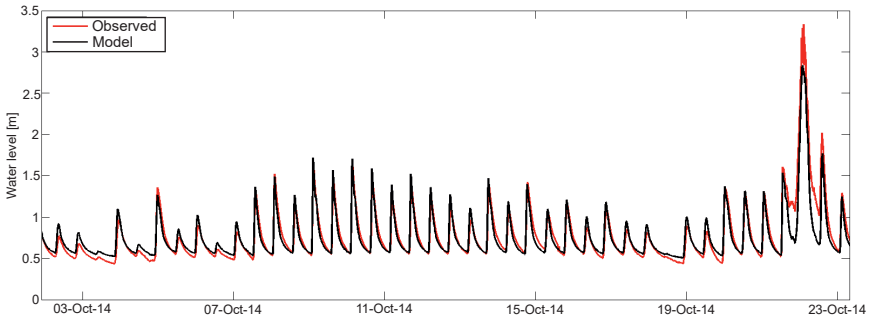

Figure 4.5 Observed and simulated water levels in the lagoon from 2–23 October 2014, which contains a fortnightly spring-neap tidal cycle and a storm surge around 22 October.

Groundwater recharge

Hourly measurements of the precipitation at a measurement station in Hoek van Holland – located 9 km south-southwest from the measurement site – were used as an estimate of the precipitation on the Sand Engine. Potential soil evaporation was calculated with the FAO Penman-Monteith method for hourly time steps, where the mean wind speed, air temperature, global radiation, and relative atmospheric humidity were also based on hourly measurements in Hoek van Holland (Allen et al., 1998). The FAO Penman-Monteith equation was adapted with estimations of the aerodynamic resistance and surface resistance for bare sand (Voortman et al., 2015). Similar to Voortman et al. (2015) the ratio between the incoming solar radiation and the clear sky solar radiation between sunset and sunrise was linearly interpolated between the 4 to 6 h average before sunset and after sunrise (Gubler et al., 2012).

The actual soil evaporation was estimated with the average moisture content between surface elevation and the extinction depth, where the evaporation was set equal to the potential evaporation for moisture contents equal and larger to field capacity. For moisture contents smaller than field capacity, the soil evaporation drops linearly to zero, parallel with the decrease in moisture. For coarse sand, field capacity was estimated as 0.042 cm^3/cm^3 (Wösten et al., 2001). The moisture content was calculated with a water budget method of precipitation and evaporation, where we assumed that percolation only occurs when the moisture content equals field capacity. At that point the groundwater recharge equals the (positive) difference between precipitation and evaporation. This method for the estimation of the actual evaporation and percolation to the groundwater is comparable to the approach used in Falkland and Woodroffe (2004) and Post and Houben (2017). Based on literature data the extinction depth was estimated as 0.5 m (Shah et al., 2007; Wösten et al., 2001). However, because of uncertainties in this estimation, we have also conducted model scenarios C1 and C2 with extinction depths of 0.25 and 0.75 m (50%; Table 4.2).

The effects of sea spray deposition were estimated with semi-empirical equations (Stuyfzand, 2014) with wind speed and wind direction measurements in Hoek van Holland. For the angle of the coastal high water line we used the angle of the shoreline of 228, as existed prior to the construction of the Sand Engine. Between June 2011 and May 2016 the resulting annual mean TDS concentration – caused by sea spray deposition – was respectively 0.11, 0.08, 0.06, and 0.04 g TDS L^{-1} at 100, 200, 500, and 1000 m from the local mean high water (MHW) height of +1.09 m NAP. These TDS concentrations were linearly interpolated based on the distance from the MHW height, with a maximum concentration of 0.11 g TDS L^{-1}.

4.3 Results

The calibrated groundwater model (i.e. reference case) contained all elements of the previously described model scenarios that were deemed important for the growth of the fresh groundwater resources (Section 4.2.5): estimates of wave set-up and wave run-up, hindcast of tidal water levels inside the lagoon, and a groundwater recharge that was based on an extinction depth of 0.5 m below surface. The simulated (transient) groundwater head and groundwater salinity of this model were compared with measurements at the study site. In addition, the reliability of the adopted spatial discretization was tested with a grid convergence test, consisting of simulations with lower and higher spatial resolutions. In the subsequent model scenarios, the effects of coastal forcing, geomorphology, and groundwater recharge on the growth of fresh groundwater resources were examined with respect to this calibrated model.

4.3.1 Model evaluation

Figure 4.6 and 4.7 show that the simulated groundwater head closely resemble the observed fluctuation pattern at the eight monitoring wells (MWs) on the Sand Engine. This demonstrates that the calibrated model can reproduce the observations with plausible model parameters (Table 4.1) and indicates that the groundwater dynamics are described satisfactorily. The similarity between the observed and simulated groundwater head is strongest near the shoreline (MW 1, 2, 5, 7) and in the centre of the Sand Engine (MW 8), with RMS errors varying between 0.08 and 0.15 m. Closer to the dunes (MW 4 and 6) the RMS error increases slightly due to temporary underestimations in the simulated groundwater head. The only exception to this overall pattern is MW 3, which has a larger RMS error in comparison with the other MWs. However, the simulated fluctuation of the groundwater head in MW 3 is similar to the measurements, and the larger RMS error is primarily a result of a systemic underestimation. This underestimation of the groundwater head at MW 3 is probably caused by mismatches in the local geology (e.g. finer sand, or variations in the position, thickness or conductivity of aquitards) that reduces the decline in groundwater head. This possibility is corroborated by the contrast in the observed and simulated groundwater head in the bottom aquifer at MW 2 and 3 (Figure 4.7).

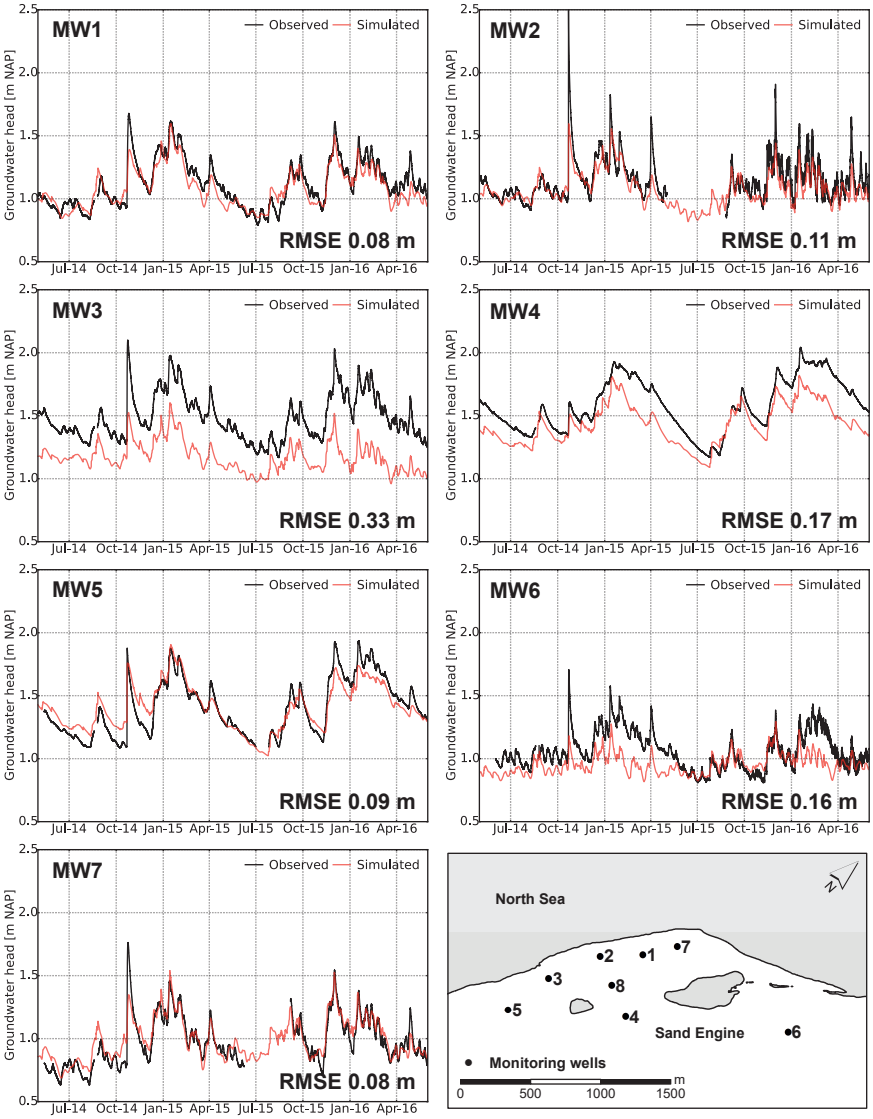

Figure 4.6 Observed and simulated groundwater level in MW 17 (phreatic aquifer 1: see Figure 4.2), from May 2014 to June 2016.

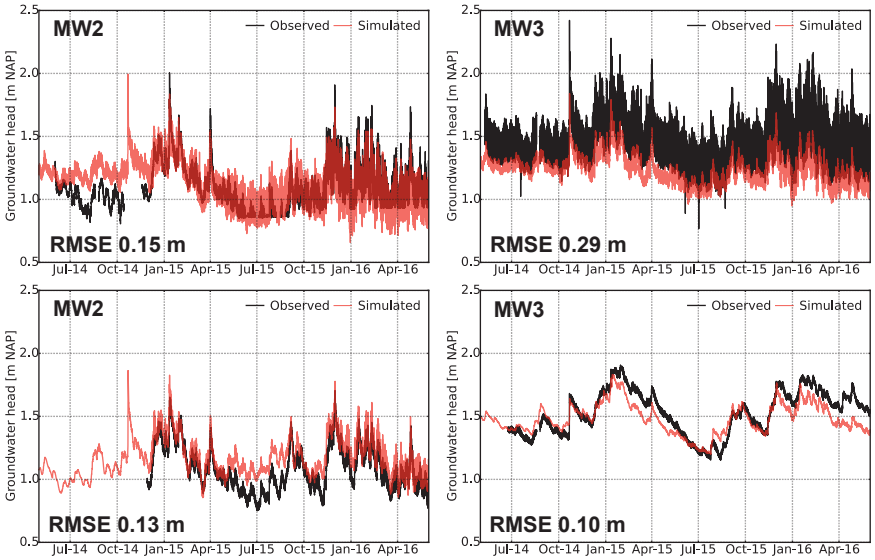

Figure 4.7 Observed and simulated groundwater head in MW 2, 3, 7 and 8 (in aquifer 2: see Figure 4.2), from May 2014 to June 2016.

The measurements indicate that the attenuation of the tidal signal is stronger at MW 2 and weaker at MW 3, while MW 2 is situated closer to the shoreline than MW 3. Thus, this suggests a stronger variability in the thickness, hydraulic conductivity or spatial distribution of aquitard(s) near these MWs.

One of the likely causes of the temporary underestimations of the groundwater head in MW 4, 6, and 8 and to a lesser extent MW 3 is (temporary) deviations of the groundwater head at the inland model boundary, as for example between February and July 2015 and February and June 2016. In these periods the deviation is largest for MW 4, 6 and 8. The mismatches on the inland model boundary are most likely caused by overestimations of groundwater abstractions in the dunes (i.e. changes in abstraction rate throughout the year) or underestimations in the groundwater recharge rates in the dunes.

Another notable deviation in the observed and simulated groundwater head is the rapid rise of the groundwater level in MW 1, 2, 3, 5, 6, and 7, during a storm surge on 22 October 2014 (see also Figure 4.5). The rise of the groundwater level is smaller in the model simulations – especially in the monitoring wells that lie closest to the shoreline – and this is probably caused by an underestimation of the wave run-up height or seawater infiltration during this storm surge.

The depth profiles of the groundwater salinity (Figure 4.8) confirm the presence of a fresh groundwater lens on top of an otherwise saline aquifer. Only in MW 4 the measurements show a decrease in the groundwater salinity at depth, but it is uncertain whether this is the result of a single measurement error or an actual deviation from the overall observed pattern. In addition, Figure 8 shows that the reference simulation closely resembles the observed groundwater salinity in most monitoring wells. However, the deviations suggest that the average North Sea salinity may be higher (MW 1, 2, 3, and 7), and indicate that the thickness of the fresh groundwater lens is slightly overestimated in the reference case. The cause of this slight overestimation will likely either lie in an overestimation of the volume of groundwater recharge or an underestimation of the salinization of fresh groundwater by coastal flooding (in particular during storm surges). The only exception is MW 6, where the depth of the freshsalt groundwater interface is underestimated, and the likely cause for this deviation is a mismatch in the initial groundwater salinity near the dunes (e.g. overestimation of the salinization by nourishments).

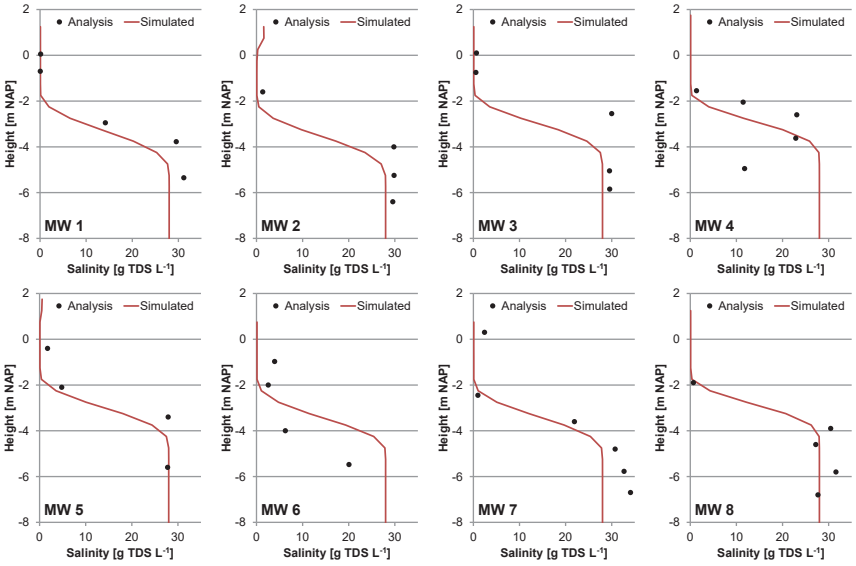

Figure 4.8 Depth profiles with the observed (black points) and simulated (red line) groundwater salinity in MW 1 – 8, obtained between 10 and 14 March 2014.

4.3.2 Grid convergence

Simulations with finer and coarser grid resolutions (S1, S2, and S3) show increases of the volume of fresh groundwater similar to the reference model (Figure 4.9). Coarser spatial resolution (S2 and S3) resulted in lower volumes of fresh groundwater, and a finer vertical spatial resolution (S1) resulted in a nearly identical growth of the fresh groundwater volume. However, at the end of the simulation period (May 2016) the overall deviation in the simulated change in fresh groundwater is small (1.1 – 1.16 million m^3). This convergence is probably mainly caused by aquitard 1 (Figure 4.2), which hampers the growth of fresh groundwater resources in a large section of the study area. Thus, the additional simulations show that subsequent increases of the spatial resolution would lead to similar growth curves, which suggests that the model grid was sufficiently refined.

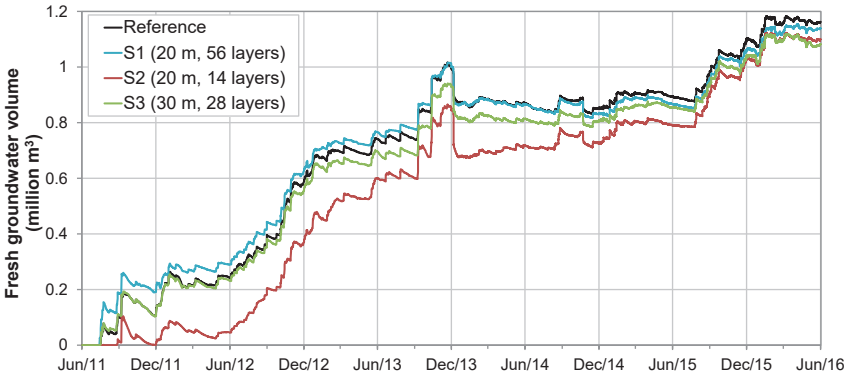

Figure 4.9 Change in the volume of fresh groundwater from June 2011 to May 2016 for the calibrated model (reference case) and model convergence simulations S1, S2 and S3.

4.3.3 Scenario A: land-surface inundations

One of the processes that can inhibit the growth of fresh groundwater resources in large beach nourishments is coastal forcing, which is the driving force of land-surface inundations. Tides will lead to frequent land-surface inundations near the shoreline (i.e. intertidal area), and storm surges to occasional and more extensive inundations (intertidal to supratidal area). In both cases the inundations will lead to a periodic infiltration of seawater in the intertidal and supratidal area, where the extent and duration of the inundations will depend on the intensity of wind and wave forces, and local morphology.

The model simulations confirm that coastal forcing limits the growth of fresh groundwater resources in the Sand Engine, as illustrated in the divergence in growth of the fresh groundwater volume in the reference model and model scenario A1 (approximately 1,700,000 m^3: Figure 4.10). This contrast in growth over the simulated period is primarily caused by the periodic salinization of fresh groundwater in the intertidal and supratidal area, where simultaneously geomorphological changes between 2011 and 2016 led to substantial increases in the intertidal and supratidal area (Figure 4.11).

The in- and exclusion of wave set-up and wave run-up in respectively the reference model and model scenario A2 has a similar – but smaller – effect on the growth of the fresh groundwater volume (Figure 4.10). The neglect of wave set-up and wave run-up leads to an underestimation of the extent of land-surface inundations and the infiltrated volume of seawater, especially during storm surges (Figure 4.11). In addition, it is important to note that the model calibration suggests the wave run-up height or seawater infiltration rate during storm surges was underestimated (Section 4.3.1).

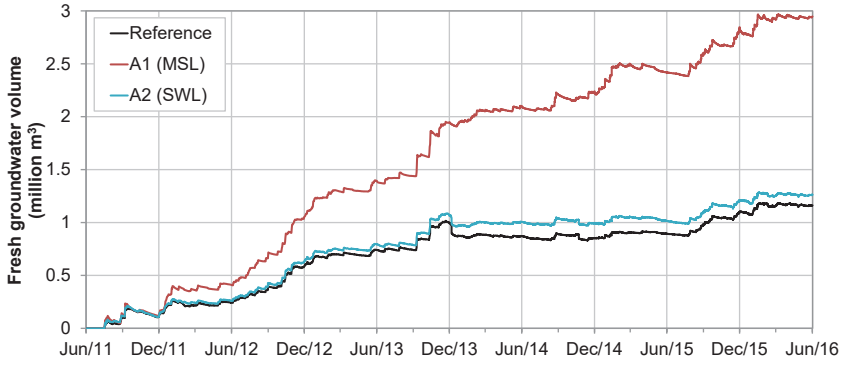

Figure 4.10 Simulated increase in the volume of fresh groundwater in the model domain from June 2011 to May 2016, for the reference model (incl. wave set-up and wave run-up), model scenario A1 (constant MSL), and model scenario A2 (SWL).

Another important variable that reflects the divergence in the model scenarios is the groundwater table. The omission of tides and storm surges leads to an underestimation of seawater intrusion, and therefore an underestimation in the groundwater levels. In model scenario A1 the groundwater level on 1 June 2016 is 0.4 – 0.6 m lower than the reference case – and observed groundwater levels. In turn, this leads to a reduction of submarine fresh groundwater discharge and a larger inflow of fresh groundwater from the adjacent dune area, which also contributes to the overestimation of the growth of fresh groundwater resources in the study area.

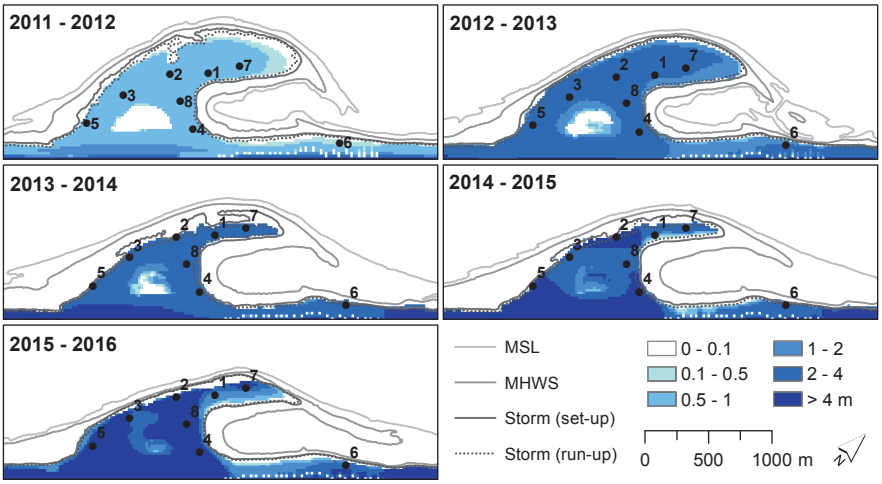

Figure 4.11 Thickness of fresh groundwater lens (in metres) 1, 2, 3, 4, and 5 years after the construction of the Sand Engine, with contour lines of the MSL, MHWS, and (estimated) maximum wave set-up and wave run-up height of every yearly period.

4.3.4 Scenario B: geomorphology

Besides hydrodynamics, coastal forcing also drives morphodynamics. Geomorphological changes in the study area from June 2011 until May 2016 consisted of a substantial retreat of the shoreline along the outer perimeter of the Sand Engine (Figure 4.1) and a gradual decline in surface elevations (Luijendijk et al., 2017; de Schipper et al., 2016). These morphological changes led to a direct loss of fresh groundwater due to coastal erosion, and to more substantial indirect losses because of a shift and in some situations extension of the intertidal and supratidal area (Figure 4.11). The simulation with a constant surface elevation and bathymetry (B1) shows that the absence of morphodynamics would have led to substantially higher fresh groundwater volumes (approximately 600,000 m^3 in June 2016) in the study area (Figure 4.12).

Another result of the morphological changes was the development of a lagoon, which led to a gradual decrease of the tidal amplitude and increase of the mean water level in the lagoon from 2011 to 2016, as described in Section 4.2.5. The model simulations show that this led to a small decrease in the growth of the fresh groundwater volume (70,000 m^3 on 1 June 2016) in comparison with model scenario B2 where the water level in the lagoon remained equal to the offshore sea level (Figure 4.12).

The effect of the morphological evolution of the lagoon on the overall growth in the volume of fresh groundwater is relatively small in comparison with model scenario A2 (Section 4.3.3), and C1 and C2 (Section 4.3.5), because the inundation extent during storm surges (e.g. high seawater levels) is similar in both situations. The smaller growth of the fresh groundwater lens is primarily caused by a rise of the local groundwater level (around the lagoon), which led to a reduced inflow of fresh groundwater from the adjacent dune area and an increase in seawater intrusion.

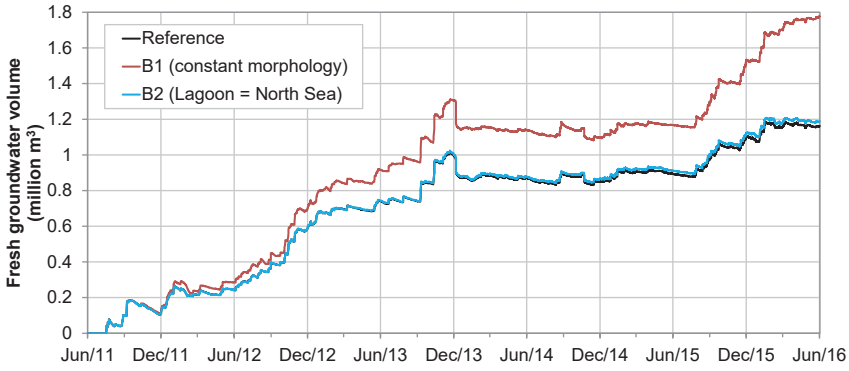

Figure 4.12 Increase in the volume of fresh groundwater from June 2011 to May 2016, for the reference case (with hindcast of the lagoon water level), model scenario B1 (constant morphology), and model scenario B2 (lagoon water level equal to North Sea).

4.3.5 Scenario C: groundwater recharge

On average the yearly precipitation from June 2011 until May 2016 was 938 mm, of which 421 mm fell in March – August (spring – summer) and 517 mm in September – February (autumn – winter). The average yearly potential soil evaporation was 990 mm, of which 695 mm evaporated in March – August and 295 mm in September - February. Thus, the net surplus based on the potential soil evaporation was -52 mm per year. However, moisture levels in the upper part of the unsaturated zone on the Sand Engine were often (especially in spring and summer) too low to attain this potential evaporation rate. The actual evaporation rate was therefore important for the net groundwater recharge in the study area.

Based on the available soil moisture between the surface and the extinction depth (see Section 4.2.5), the actual evaporation rate was determined. The resulting groundwater recharge for the respective extinction depths of 0.25, 0.5 and 0.75 m, as shown in Figure 4.13, varied between 595 mm (+78 mm relative to the reference case), 516 mm, and 470 (-46 mm relative to the reference case) mm per year. Most of the groundwater recharge (30 to 34%) occurred in autumn and winter, and least (9 to 12%) in spring. Therefore, as to be expected, larger extinction depths led to more evaporation and less groundwater recharge, in particular in the spring and summer.

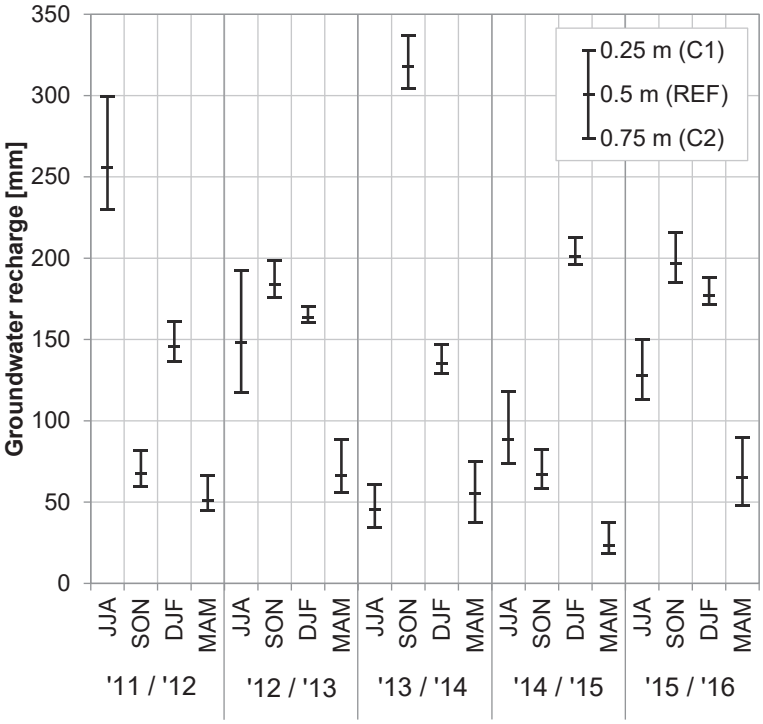

Figure 4.13 Simulated groundwater recharge per season (JJA: summer, SON: autumn, DJF: winter, MAM: spring) from June 2011 until May 2016, for the reference model (extinction depth 0.5 m), model scenario C1 (extinction depth 0.25 m: less evaporation), and model scenario C2 (extinction depth 0.75 m: more evaporation).

The simulated change in the fresh groundwater volume (Figure 4.14) shows that groundwater recharge is one of the primary driving mechanisms, with increases in periods with relatively high percolation rates and a stabilization or decrease in periods with relatively low percolation rates. Parallel to groundwater recharge, most of the overall growth in the fresh groundwater lens occurs in the autumn and winter seasons. In periods with low recharge rates, the loss of fresh groundwater – primarily due to submarine groundwater discharge and coastal erosion – leads to a stabilization or decrease in the overall fresh groundwater volume in the study area. One notable example is the change in the fresh groundwater volume over the period March 2014 to November 2015, which coincides with a substantially lower than average groundwater recharge (Figure 4.13).

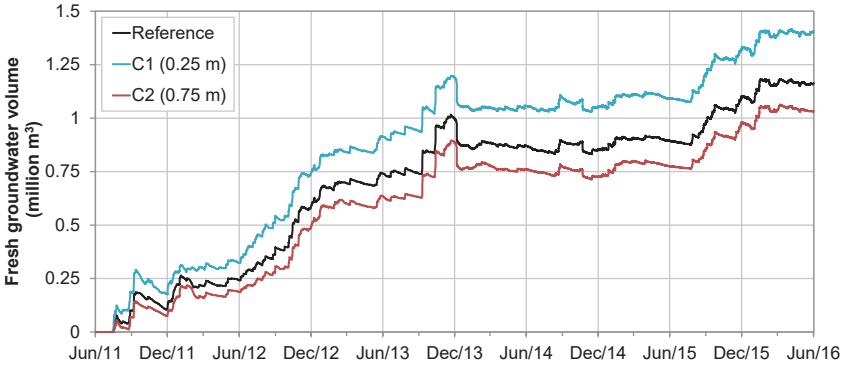

Figure 4.14 Increase in the fresh groundwater volume from June 2011 until May 2016, with the calibrated model with an extinction depth of 0.5 m (Section 4.2.5), a 50% decreased extinction depth of 0.25 m (C1), and a 50% increased extinction depth of 0.75 m (C2).

4.4 Discussion

The measurements and model simulations showed a substantial growth of fresh groundwater resources in the Sand Engine between 2011 and 2016, and demonstrated the importance of both coastal forcing and groundwater recharge for an accurate reproduction of the growth of the freshwater lens. Periods with high rainfall (autumn and winter) led to sharp increases in the fresh groundwater volume, while periods with little or no rainfall (spring and summer) led to a net loss of fresh groundwater. Coastal forcing led to land-surface inundations and considerable geomorphological changes in the study area, where inundation events resulted in the salinization of the intertidal and supra-tidal areas and morphodynamics led to a shift or in some instances extension of these areas. Storm surges in particular were important for the determination of the growth of the freshwater lens, because these were the primary drivers of coastal erosion and led to the most extensive land-surface inundations.

Comparisons of the calibrated reference model with simulations that excluded coastal hydro- and morphodynamics (scenario A1 and B1) showed that the incorporation of these processes was essential for a good calibration result and a reliable estimate of the intertidal and supratidal area, and thus essential for the estimation of the growth of the fresh groundwater resources. Besides the impact of land-surface inundations on the freshwater lens, tidal dynamics also played an important role in the height and variability of the groundwater head. For example, the exclusion of these tidal dynamics in model scenario A1 led to an underestimation of the groundwater heads between 0.4 and 0.6 m at MW1 to 8. In addition, where model scenario A1 indicates a continued growth in fresh groundwater resources between June 2011 and May 2016, the model scenarios with tidal dynamics (reference and scenario A2) only indicate a clear (net) growth in fresh groundwater resources between June 2011 and December 2013, and a slight (net) growth or stabilization in the period thereafter.

For most MWs the simulated transient groundwater head and groundwater salinity corresponded well with measurements. This demonstrates that the hydro- and morphodynamic conditions of the study area could be reproduced with the adopted methodology. Most of the discrepancies between measurements and simulations could be explained by unmapped geological heterogeneity (near MW3), and mismatches in the initial groundwater salinity distribution (near the coastal dunes). It is important to note that the simulated groundwater salinity could only be compared with groundwater salinity measurements that were conducted in March 2014. Therefore, it is uncertain to what extent the simulated change in groundwater salinity corresponds with the salinity distributions of the period thereafter.

While the close similarity between the measured and simulated groundwater head time series under realistic hydrogeological parameter settings indicates that the tidal dynamics and extent of land-surface inundations are well represented in the model, the modelled wave set-up height and wave run-up height (and related infiltration of seawater) probably differed strongly with reality at times. Small variations in surface elevation, bathymetry, wave height, and wave period could have led to substantial variations in wave set-up and wave run-up. Underestimations of the increase of the groundwater level during some of the storm surges (see Figure 4.6) also indicate an underestimation of wave set-up height, wave run-up height, or the infiltration of seawater. However, these differences could also be caused by deviations in the modelled and actual morphology at the study site. Despite the frequent topographical measurements, interim morphological changes were not observed. This especially affects periods with rapid and extensive morphological changes, e.g. periods with frequent or intensive storm surges. However, based on the calibration results and comparisons with on-site observations we believe that the adopted approach attained realistic but rough estimates of the effects of wave set-up and wave run-up on the coastal aquifer.

Being the main source of fresh groundwater, groundwater recharge is another important control on the development of the fresh groundwater resources of the Sand Engine. Vegetation was virtually absent on the Sand Engine, with the exception of a few pockets of dune grass in the last years of the simulated period, and therefore the processes that determine the groundwater recharge rates could be limited to precipitation and soil evaporation. Because the depth to the groundwater table was relatively large (generally larger than 1.5 m below surface) in relation to the expected extinction depth, capillary rise will be limited or non-existent and was therefore neglected. Given these simplifications and the aims of this paper, we opted to estimate recharge rates with the described water budget method and analyse the uncertainty with the alterations to the extinction depth.

For future studies on the (potential) growth of fresh groundwater resources in coastal areas, it is recommended to monitor wave set-up, wave run-up, and seawater infiltration and evaluate the accuracy of the adopted approach in this research under various conditions. However, this will require frequent topographic measurements to monitor morphological changes in the coastal area, as for example the periodic topographic surveys (every 1 – 3 months) that were executed on the Sand Engine. In addition, simulations with unsaturated groundwater flow could provide more detailed estimates of the growth in fresh groundwater resources in these areas, because of a potential improvement in the simulation of groundwater recharge and seawater infiltration.

4.5 Conclusions

Between 2011 and 2016 the growth of the freshwater lens in a mega-scale beach nourishment (the Sand Engine) was primarily determined by the groundwater recharge, (maximum) land-surface inundations due to storm surges, groundwater in- and outflow, and to a lesser extent by geomorphological changes:

1. Groundwater recharge was the primary contributor to the growth of fresh groundwater in the large concentrated beach nourishment. An accurate estimation of the actual soil evaporation – besides meteorological measurements – will likely be important for the determination of the net input of fresh groundwater in any coastal area.

2. Storm surges produced the most extensive land-surface inundations, and the coinciding infiltration of seawater resulted in a salinization of most of the fresh groundwater volume within this inundation area. The model simulations showed that (accurate) estimates of the maximum wave set-up and wave run-up height are important to delineate the area that is vulnerable to seawater intrusion and reconstruct the growth of fresh groundwater resources.

3. The groundwater level, or better, the hydraulic gradients within the study area, determined the inflow of fresh groundwater from adjacent dunes and outflow of (fresh) groundwater via submarine groundwater discharge. Model simulations that underestimate the height of the groundwater level, e.g. by the neglect of tidal dynamics, can therefore lead to considerable overestimation of the fresh groundwater volume.

4. Finally, the geomorphological changes led to a gradual decline of the area that was not affected by seawater intrusion. Together with the increase of the mean water level inside the lagoon, this led to a small restriction of the potential growth in fresh groundwater resources.

In conclusion, the incorporation of hydro- and morphodynamics and accurate estimation of groundwater recharge rate are essential for a reliable estimate of the growth of fresh groundwater resources in dynamic coastal environments.

Acknowledgements

This research is supported by the Dutch Technology Foundation STW, which is part of the Netherlands Organization for Scientific Research (NWO), and which is partly funded by the Ministry of Economic Affairs. This work was carried out within the Nature-driven nourishment of coastal systems (NatureCoast) program. Most of the raw data collected in this programme are available at the 4TU.Centre for Research: (`https://doi.org/10.4121/collection:zandmotor`). Other data sets that were used to produce the results of this paper may be obtained by contacting the corresponding author.

5 Global potential for the growth of fresh groundwater resources with large beach nourishments

Based on: Huizer, S., Luijendijk, A. P., Bierkens, M. F. P., and Oude Essink, G. H. P., (under review) Global potential for the growth of fresh groundwater resources with large beach nourishments, submitted to Scientific Reports.

Abstract

Large-scale beach nourishments may provide vulnerable sandy shores worldwide a means of coastal protection, while simultaneously increasing fresh groundwater resources. This hypothesis has been demonstrated for a concentrated mega-scale beach nourishment called the Sand Engine at the Dutch coastline. Whether a coastal area is suitable for beach nourishments and can subsequently induce a growth in fresh groundwater resources depends on the appropriateness of the intended site for beach nourishments, and the attainable growth in fresh groundwater resources. In this study we presume that all eroding sandy beaches are suitable for large beach nourishments, and focus on the impact of these nourishments on (stored) fresh groundwater in various coastal settings. The growth in fresh groundwater resources – as a consequence of the construction of a beach nourishment – was quantified with 2-D variable-density groundwater models, for a global range in geological parameters and hydrological processes. Our simulation results suggest that large beach nourishments will likely lead to a (temporary) increase of fresh groundwater resources in most settings, and therefore potentially for most erosive sandy shores. However, for a substantial growth in fresh groundwater, the coastal site should receive sufficient groundwater recharge, consist of sediment with a low to medium hydraulic conductivity, and be subject to a limited number of land-surface inundations. Our global analysis shows that 17% of the shorelines – excluding Arctic regions – may consist of such erosive sandy beaches, and of these sites 50% have a high potential suitability. This suggests an opportunity worldwide to combine coastal protection with an increase in fresh groundwater resources.

5.1 Introduction

Millions of people reside in coastal areas that are vulnerable to coastal flooding, and projections show that the (global) population in these areas will increase significantly in the coming decades (Neumann et al., 2015). Sea-level rise will likely lead to an increase in the frequency and severity of coastal flooding, in particular in tropical areas, and therefore exacerbate flood risk (Nicholls and Cazenave, 2010; Vitousek et al., 2017). Other effects of sea-level rise are deteriorating coastal wetlands,

beach erosion, seawater intrusion, and impeded drainage (Nicholls, 2011). Without adaptation this will lead to large losses of habitable and agricultural land, as well as increases in saltwater intrusion in surface waters and coastal aquifers especially in combination with the human-induced subsidence that occurs in many coastal areas (FitzGerald et al., 2008; Syvitski et al., 2009; Wong et al., 2014). Thus, these vulnerable coastal areas require appropriate adaptation responses to manage the flood risk and reduce negative flood consequences (Giosan et al., 2014; Hallegatte et al., 2013; Nicholls, 2011).

For open (sand, gravel or mixed) beaches one of the potential adaptation responses are beach nourishments (also called replenishments), which have been widely and successfully applied as a counter measure for coastal recession (Cooke et al., 2012; Habel et al., 2016; Hanson et al., 2002; Keijsers et al., 2015; Luo et al., 2015; Shibutani et al., 2016; Valverde et al., 1999). Until recently, these nourishments have primarily been applied in relatively small volumes, often on a regular basis, and close to the shoreline (Charlier et al., 2005). However, in 2011 a pilot project with a large concentrated beach nourishment of ca. 21 million m^3 of sand, called the Sand Engine (also named Sand Motor), was realized in the Netherlands (Mulder and Tonnon, 2011). The replenished sand was designed to be largely distributed along the coast and into the dunes by natural forces (e.g. waves, currents, and wind). This "Building with Nature" approach is anticipated to provide a more ecologically sustainable alternative than other coastal protection approaches, in particular with regard to the current practice of frequent small-scale shoreface and beach nourishments (Slobbe et al., 2013). When proven that this pilot project is successful, it may become a more widespread solution for open coasts (Stive et al., 2013).

Beach nourishments – in particular large and concentrated nourishments – can simultaneously lead to an increase of local fresh groundwater resources in coastal areas (Huizer et al., 2016). However, the potential effect of such nourishments has only been comprehensively investigated for the Sand Engine in the Netherlands. The growth of fresh groundwater resources – as a consequence of the construction of a beach nourishment – will strongly depend on the local conditions at a site. For instance, Huizer et al. (2017) showed that the Sand Engine in the Netherlands is particularly vulnerable to land-surface inundations and seawater intrusion. In addition, this vulnerability to land-surface inundations will likely increase over time, because of the inevitable geomorphological changes of the beach nourishment within the 'Building with Nature' approach. Based on this local study of Huizer et al. (2017) one can deduce that changes in beach slope, groundwater recharge and tidal ranges will likely result in substantial deviations in the increase of fresh groundwater resources at a coastal site. Taking these importance factors into account, this study aims to provide a first estimate of the effects of concentrated large-scale beach nourishments on fresh groundwater resources at coastal areas around the world.

First, the global suitability of coasts for beach nourishments is assessed, based on an evaluation of the presence of an open beach, coastal erosion, and (if available) previous nourishments. Secondly, for the potentially suitable coastal areas, the most essential (geological) properties and (hydrological) processes that affect fresh groundwater resources are analysed: groundwater recharge, beach slope, tides, storm surges, coastal erosion (morphological change). The variability of each property or process is estimated with global datasets, and the effects on fresh groundwater resources is assessed and demonstrated with conceptual 2-D model simulations. In this study we focus on the current conditions of sandy beaches, and have excluded future changes in sea-level or groundwater recharge due to climate change. While changes in both of these processes will affect coastal fresh groundwater resources (Huizer et al., 2016), the global variability and uncertainty in the predicted changes render it too complex for this conceptual study. Finally, based on the results of the simulations, the implications for sandy shorelines worldwide are discussed.

5.2 Methods

5.2.1 Suitable locations for large-scale beach nourishments

Recent research (Luijendijk et al., 2018) suggests that 31% of the ice-free shorelines in the world consist of sandy beaches including quartz and carbonate sands, and gravel and that 24% of these sandy beaches were subjected to coastal erosion of more than 0.50 m per year in the period 1984 to 2016. These eroding coastlines may satisfy the primary conditions for (large-scale) beach nourishments: a coastal environment that conforms to (beach) nourishments, and local communities or stakeholders that desire and benefit from coastal protection (e.g. prevent loss of land). Of course, beach nourishments could also be implemented to widen recreational beaches or to create new beaches in coastal areas where none existed before. However, in this study we focus on sites that suffer from beach erosion, in order to comply with the 'Building with Nature' philosophy (Slobbe et al., 2013).

Whether beach nourishments are applied in coastal areas, is dependent on numerous factors and circumstances. First the desired adaptation strategy: coastal protection, accommodate, (re)claiming land from the sea, limited intervention ("passive retreat"), non-intervention, managed retreat, or ecosystem conservation (Berry et al., 2013). Only if a coastal manager opts for coastal protection - the most common adaptation option - and has the knowledge and means to execute this strategy, nourishments are one of the possibilities. Overall, the options for the coastal protection of the shoreline position vary between hard structures (e.g. groins and seawalls) and soft engineering (i.e. nourishments). Environmental concerns and inefficiencies have led to a historical shift from predominantly hard to soft engineering solutions (Charlier et al., 2005; de Ruig, 1998), in particular if the beach serves multiple vital purposes.

Table 5.1 Important (technical) considerations for sustainable (large) beach nourishments

Nr	Attribute	Considerations for successful beach nourishments
1	Aeolian transport	Aeolian transport of the nourished sand is highly dependent on the median grain size, grain-size distribution, and the spatial variability of sand properties (e.g. presence of shell fragments) (van der Wal, 1998).
2	Erosion rate	Generally, nourished beaches erode at least as fast as the original or pre-nourished coastline, and often even faster (Finkl and Walker, 2005).
3	Natural habitat	Beach nourishments are a more ecologically sound alternative to hard engineered structures, but nourishments can also cause damage to habitat and biota. Negative effects should be mitigated, e.g. match pre-nourished conditions (Cooper and McKenna, 2008; Defeo et al., 2009).
4	Developed shores	Beach nourishments are predominantly applied on marine, developed, sandy beaches, where the beach also serves as protection of coastal infrastructure and as recreational site (Finkl and Walker, 2005).
5	Sediment grain-size	The grain-size of the nourished sediment is generally slightly coarser than the original sediment (Capobianco et al., 2002; Ruessink and Ranasinghe, 2014).
6	Sediment source	The sediment source (dredge site or terrestrial source) that can provide the required composition and quantity of sediment should be relatively close to site to be cost-effective (Pranzini, 2017).
7	Sediment transport	The redistribution of the nourished sediment is a complex process, which is dependent on coastal forcing, coastal characteristics (e.g. profile), and the nourishment shape and dimensions (Steijn, 2015).

The suitability of coastal areas for beach nourishments is complex and should be assessed with detailed local studies, which lies beyond the scope of this study. However, to provide some insight, we summarized the most important considerations for (large) beach nourishments in Table 5.1. In this study we focus on all (eroding) sandy beaches worldwide and assume that these beaches are technically suitable for large-scale beach nourishments.

5.2.2 Processes and properties

Huizer et al. (2016) showed that fresh groundwater resources can grow substantially as a consequence of the construction of a mega-scale beach nourishment. However, whether this growth will occur at a coastal site is dependent on the inflow rate, outflow rate, storage capacity, and losses of fresh groundwater in the coastal aquifer. Recent research (Huizer et al., 2017, 2018) demonstrated the significance of these dynamic processes to the development of fresh groundwater resources, and illustrated for example the considerable impact of wave exposure and storm surges. The combined hydrological, morphological, and ecological processes (arrows) that affect the growth of fresh groundwater in a (large) beach nourishment are illustrated in Figure 5.1, where for simplicity anthropogenic effects such as groundwater abstractions were neglected.

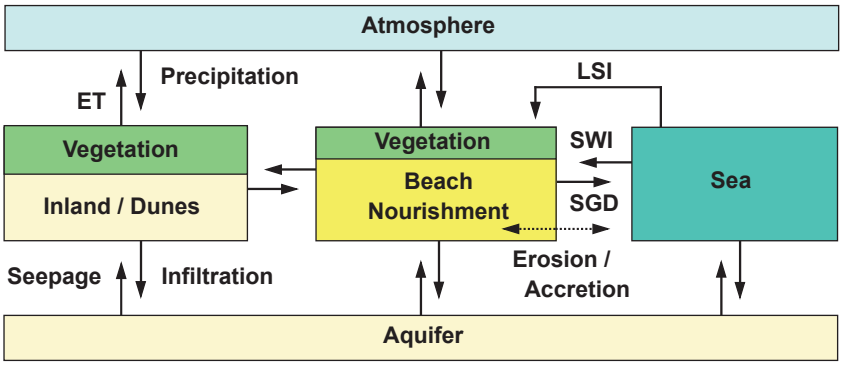

Figure 5.1 Hydrological, morphological, and ecological processes (arrows) that affect the growth of fresh groundwater resources in a (large) beach nourishment (LSI = land-surface inundations, ET = evapotranspiration, SGD = submarine groundwater discharge, and SWI = seawater intrusion).

It is important to note that these processes can affect one another, because each process can alter the groundwater head, hydraulic gradient, and the groundwater flow. For example, when land-surface inundations (LSI) lead to a substantial increase of the groundwater head, this in turn can lead to a larger evapotranspiration rate or more submarine groundwater discharge (SGD). Or, when a storm surge leads to extensive coastal flooding, this often also results in coastal erosion and can have a detrimental effect on flooded dune vegetation. Changes in surface elevation or loss of dune vegetation can in turn also alter the evapotranspiration rates.

While the hydrological processes shown in Figure 5.1 largely drive the (positive or negative) growth of fresh groundwater resources, the geological properties of the nourished sediment and the (local) coastal aquifer determine the infiltration rate, storage capacity, and groundwater flow rates. For example, the grain size and sorting of the nourished and original sediment will strongly determine the hydraulic conductivity and (effective) porosity of the coastal aquifer. Similarly, the geological properties will affect the (maximum) flow rate and flow direction of the groundwater fluxes, as for instance larger hydraulic conductivity will result in larger infiltration rates.

To assess the impact of hydrological processes and various other (geological) properties and, we have examined and described the effects of a selection of properties and processes on fresh groundwater resources individually (Table 5.2). For each of the listed (geological) properties and (hydrological) processes, the global range of variability of the particular property or process is characterized with low, average and high estimates. Clearly this selection is not comprehensive, and other properties or processes such as inland groundwater flow, geological heterogeneity, and sea-level rise will affect the built-up of fresh groundwater resources.

Table 5.2 Global variation in a selection of (hydrological) processes and (geological) properties of sandy beaches. The impact of each factor on fresh groundwater resources was evaluated with common estimates of low, average and high values within the noted limits.

Nr	Factor	Global variation	Low	Average	High	Source(s)
1	Groundwater recharge	Very low (<2 mm yr^{-1}) to very high (>300 mm yr^{-1}): highest in humid tropics, lowest in dry subtropics and arctic regions.	50 mm yr^{-1}	200 mm yr^{-1}	500 mm yr^{-1}	Döll and Fiedler (2008); Wada et al. (2010)
2	Hydraulic conductivity	Conductivity of coarse grained unconsolidated sediment varies from 0.7 m d^{-1} to 170 m d^{-1}.	10 m d^{-1}	20 m $^{-1}$	50 m d^{-1}	Wilson et al. (2008); Huscroft et al. (2018)
3	Specific yield	Storage in unconsolidated sediment varies between 0.11 and 0.36.	0.1	0.2	0.3	Gleeson et al. (2014); De Graaf et al. (2015)
4	Beach slope	Beach slope variability for sandy beaches varies between 1:5 to 1:80 (median 1:24).	1 : 10	1 : 30	1 : 50	McLachlan and Dorvlo (2005)
5	Tidal dynamics	Global tidal ranges: micro (<2 m), meso (2 – 4 m), to macro (>4 m).	0-2 m	2-4 m	4-5 m	PSMSL dataset (Holgate et al., 2013)
6	Coastal erosion	Beach erosion or shoreline retreat range from less than 1 m per year to several meters due to one storm surge event.	1 m yr^{-1}	2 m yr^{-1}	4 m yr^{-1}	Anthony (2005)
7	Storm surge / Inundation	Extreme sea levels caused by high tides, storm surges / hurricanes (return period of 100 years).	1 m	3 m	5 m	PSMSL dataset (Muis et al., 2016)

5.2.3 Model simulations

The effect of each (geological) property or (hydrological) process in Table 5.2 on the growth of fresh groundwater resources – in a sandy coast with a concentrated large-scale beach nourishment – was assessed with conceptual 2-D model simulations. The model simulations were executed with the computer code SEAWAT (Langevin et al., 2008) to simulate variable-density groundwater flow and coupled salt transport. The model scenarios were constructed, executed and processed with the Python package FloPy (Bakker et al., 2016), starting with a reference model that consists of a 2-D approximation of the average global sandy beach. The 2-D reference model (Figure 5.2) was discretized into 400 columns with horizontal cell sizes of 1 to 2 m, and 75 layers with thicknesses of 0.25 to 0.50 m. In each model scenario, the smallest cell sizes were positioned in the area close to the (intended) beach nourishment and sea boundary. The design of the model domain and geometry was based on designs from previous 2-D numerical modelling studies on sandy beaches (Abarca et al., 2013; Chui and Terry, 2013; Heiss and Michael, 2014; Ketabchi et al., 2014; Robinson et al., 2014). Similar to the design in these studies, the model comprises three sections: (1) constant berm height, (2) linear beach face, (3) constant bed level (Figure 5.2). In all model scenarios the berm elevation was defined above the highest prescribed sea-level – and accordingly the width of the (2) linear beach face was adapted – to avoid an inundation of the whole model domain due to tidal dynamics.

All model boundaries – besides the upper boundary – are defined as no-flow, to enable an unconstrained development of the fresh groundwater lens and fresh-salt groundwater mixing zone. Consequently, the reference model is in effect an elongated or strip island model with a width of 500 m and an aquifer thickness of 30 m. This is relatively small in comparison with real-world islands or sites, but this was a deliberate choice to cut-down the overall simulation time. For the simulation of the sea boundary the same method as in Huizer et al. (2017, 2018) was adopted, and for more information on the methodology we refer to these studies. In summary, the boundary was modelled as a time-variable specified head and concentration, equal to "General Head (head-dependent) Boundaries and Drains" as described by Mulligan et al. (2011). Wave setup and run-up were estimated with the parametrization for setup on dissipative sites of Stockdon et al. (2006).

The reference model was used a starting point for all model scenarios. For each scenario only the relevant model parameters were adapted in accordance with Table 5.2. First, all model scenarios were (repeatedly) simulated for a period of 50 years – without the intended beach nourishment – until a (dynamic) steady-state condition was reached. Steady state was defined in terms of the change in the volume of fresh, brackish and saline groundwater in the model domain, and attained when the changes oscillate around an equilibrium. Second, a beach nourishment with a width of 100 m and a crest elevation equal to the berm height, was added to each model scenario (Figure 5.2). Subsequently, each scenario was simulated for a period of 50 years to assess the impact on the volume of fresh groundwater.

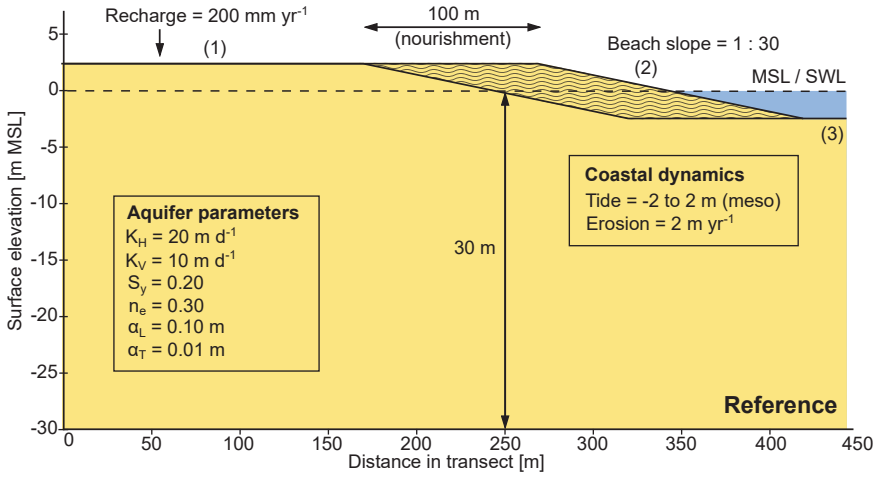

Figure 5.2 Schematic representation of the numerical model domain including aquifer parameters, recharge, beach slope, and coastal dynamics of the reference model (see 'average' column in Table 5.2).

5.2.4 Tidal dynamics

As stated in Table 5.2 a tidal regime with a meso tidal range (2 to 4 m) was implemented in the reference model, and tidal regime with micro (<2 m) and macro (>4 m) tidal ranges were included as model scenarios. Global representations of micro, meso and macro tidal regimes were obtained from the Research Quality Data Set of the University of Hawaii Sea Level Center, which is part of the Global Sea Level Observing System (GLOSS) Delayed Mode Higher Frequency dataset (Caldwell et al., 2015). This dataset contains tide gauge measurements of 547 stations around the world that have received quality control. Each tide gauge station was classified into a micro, meso or macro tidal range through the calculation of the mean tidal range of each timeseries. Only measurements after 01-01-1970 were included to ensure that the calculated tidal ranges were representative for present-day conditions.

Based on the measurement period and mean tidal range of each station, three tide gauge stations were selected to represent the micro, meso and macro tidal regimes in the model simulations (Table 5.3). The observed tidal behaviour at these three locations was extrapolated to the period 1970 to 2020, to fill time gaps in the measurements, and to obtain tide gauge data with a timestep of 10 minutes instead of one hour. For the extrapolation of the micro, meso and macro tidal regimes we used the Python package Pytides, which uses the method of harmonic constituents (Foreman and Henry, 1989). Sea-level rise was not incorporated in the extrapolation of the tidal regimes.

Table 5.3 Selection of tide gauge stations from the GLOSS Delayed Mode Higher Frequency dataset that signify micro, meso and macro tidal ranges.

Tide Class	GLOSS	Station	Country	Period	Tidal range
Micro	111	Kwajalein	Marshall Islands	1946 to 2014	1.01 m
Meso	284	Cuxhaven	Germany	1917 to 2014	2.93 m
Macro	040	Broome	Australia	1986 to 2015	5.51 m

5.2.5 Mapping global suitability

As described, conceptual 2-D model simulations were used to assess the effect of each (geological) property or (hydrological) process in Table 5.2 on the growth of fresh groundwater resources in a sandy coast with a (newly created) concentrated large-scale beach nourishment. For the properties or processes with the highest impact on fresh groundwater resources, the consequences of this analysis were translated and visualized to a global suitability map with help of global datasets. This map portrays the potential growth of fresh groundwater at a coastal site as result of the construction of a large-scale beach nourishment. As a rough estimate of the suitability of a coastal site for beach nourishments we focused on sandy beaches that suffer from coastal erosion.

For the identification of eroding sandy shorelines the data of a recent paper of Luijendijk et al. (2018) was used, which developed and implemented a procedure to detect sandy beaches from satellite images of 2016 (Sentinel-2) and shoreline changes from satellite images between 1984 – 2016 (Landsat 5, 7 and 8). All other shorelines were excluded from the analysis – 83% of all analysed coastal sites, and are visualized as either 'not required' (i.e. not-eroding sandy shore: 15% of sites) or 'not suitable' (i.e. not sandy shore: 68% of sites) in Figure 5.15. It should be noted that in some cases coastal erosion was obscured by human interventions between 1984 and 2016, and wrongly identified as 'not suitable'. One prime example is the widespread application of beach nourishments on the Dutch coast (Keijsers et al., 2015)

5.3 Results

For each of the top 6 of the listed processes or properties in Table 5.2, the simulated (1) initial condition or equilibrium state, and (2) impact of the beach nourishment on the fresh groundwater resources (as a function of time) are described and visualized in section 5.3.1 to 5.3.6. Extensive land-surface inundations due to storm surges, tropical cyclones or tsunamis were excluded (nr. 7 in Table 5.2), as simulating these events is beyond the scope of this study. Nonetheless, as previously shown by Huizer et al. (2017, 2018), frequent to occasional inundations – especially beyond the intertidal area – have a strong impact on the growth of the fresh groundwater volume. Therefore, it is treated as one of the paramount factors of the growth of fresh groundwater resources in coastal areas and included in Table 5.2.

Every model scenario contained an addition of a 100 m wide beach nourishment at the start of the simulation period, which slowly erodes to the original setup. In all model scenarios the application of the specified nourishment leads to an enlargement of the existent fresh groundwater lens, regardless of the changes in the processes or properties. The placement of the beach nourishment results in a seaward shift of the intertidal zone, and consequently – if extensive land-surface inundations are neglected – to a wider area in which the fresh groundwater lens can advance. The gradual erosion of the beach nourishment – or retreat of the shoreline – subsequently leads to a decline of the beach width. This in turn, ensures that the maximum growth in fresh groundwater (i.e. optimum) occurs before the end of the simulation period. Since this pattern is similar in all scenarios, the evaluation of the impact of each process or property will focus on the (relative) growth rate and the change in time.

It must be noted that the inland boundary was a no-flow boundary, to minimize the (external) impact on the development of the fresh groundwater lens. Previous studies have shown that a decrease in fresh groundwater flow at the inland boundary increases the effect of tidal forcing, leading to larger salt groundwater plumes or tidal circulation (Li et al., 2008; Robinson et al., 2007a). Therefore – as a consequence of the adopted model setup – tidal forcing becomes the dominant force in the model simulations. Tidal circulations cause the fresh to salt groundwater interface to expand, which results in relatively large mixing zones. As in most real-world coastal environments, a groundwater flux – with varying levels of salinity – will occur.

5.3.1 Groundwater recharge

Increases in groundwater recharge lead to higher groundwater levels, larger fresh groundwater lenses (Figure 5.3), and larger absolute growth rates of the volume of fresh groundwater (Figure 5.4a). However, low groundwater recharge rates result in considerably higher relative growth rates, and a longer period in which the fresh groundwater lens expands (Figure 5.4b). This is because larger (absolute) growth rates result in an earlier attainment of the maximum size (i.e. growth equals losses) of the fresh groundwater lens. However, this is only true when the (phreatic) aquifer is thick enough to allow for a continued growth of the fresh groundwater lens. In all model simulations the thickness of the phreatic aquifer was extended accordingly to avoid an impeded growth of the fresh groundwater lens (Figure 5.3c).

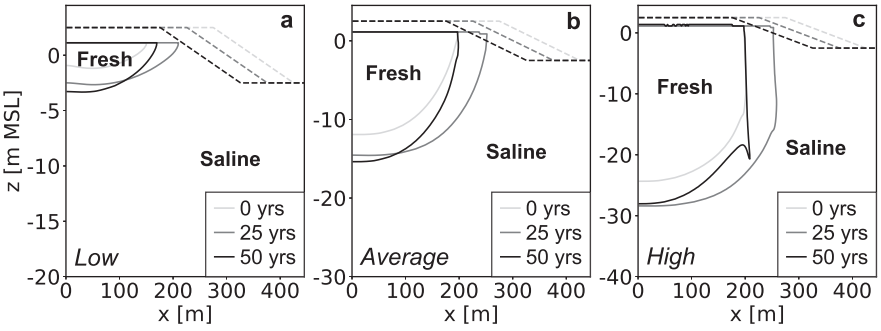

Figure 5.3 Simulated growth of the fresh groundwater lens for low (left), average (centre), and high (right) groundwater recharge rates. All images contain the fresh-salt groundwater interface of 1 g TDS L^{-1} (solid lines) and the surface elevation (dashed lines) at the start (light grey), middle (dark grey) and end (black) of the simulation period.

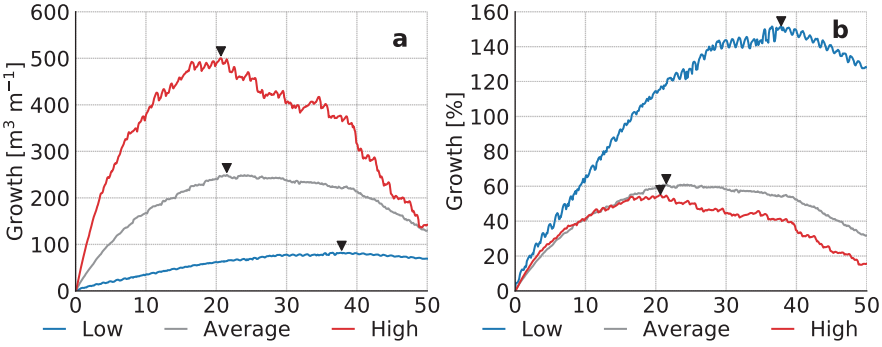

Figure 5.4 Simulated growth of fresh groundwater for low (blue line), average (dark grey line), and high (red line) estimates of the global groundwater recharge. The graphs represent the change in volume (left) and percentage (right) with respect to the initial conditions (i.e. equal to equilibrium state without beach nourishment).

5.3.2 Hydraulic conductivity

Low to average hydraulic conductivities lead to the highest groundwater levels, largest fresh groundwater lenses (Figure 5.5a and b), and the highest absolute growth rates of the fresh groundwater volume (Figure 5.6a). However, shores with high hydraulic conductivities result in considerably higher relative growth rates (Figure 5.6b). In a shore with a high hydraulic conductivity the growth remains relatively small in volume, but large in comparison with the initial volume of fresh groundwater. The period in which the volume of fresh groundwater increases also changes with the hydraulic conductivity, because shores with higher hydraulic conductivities are more strongly influenced by tidal forcing. This additionally leads to higher loss rates, and a steeper decline in the volume of fresh groundwater.

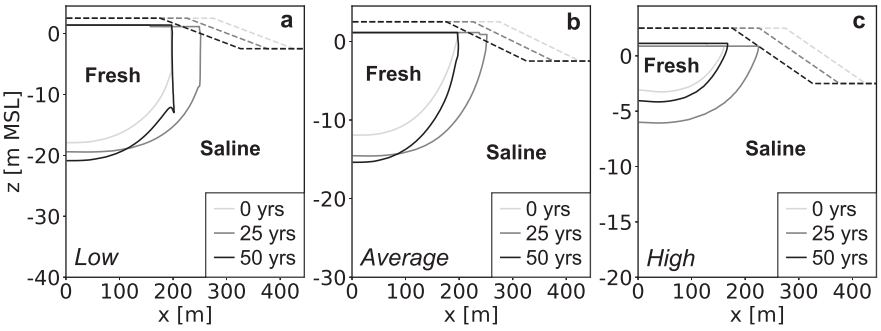

Figure 5.5 Simulated growth of the fresh groundwater lens for low (left), average (centre), and high (right) hydraulic conductivities. All images contain the fresh-salt groundwater interface of 1 g TDS L^{-1} (solid lines) and the surface elevation (dashed lines) at the start (light grey), middle (dark grey) and end (black) of the simulation period.

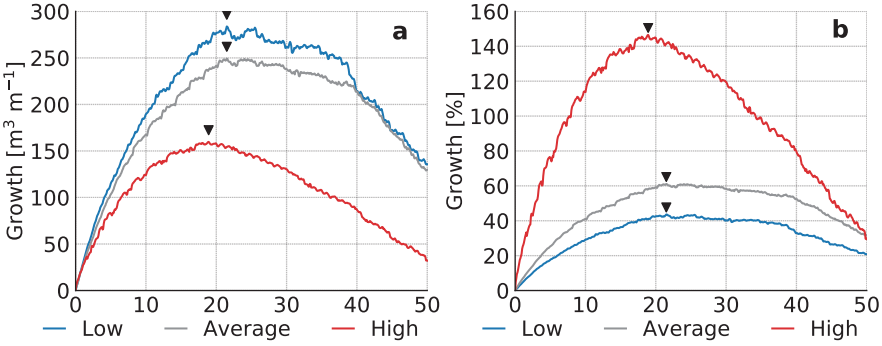

Figure 5.6 Simulated growth of fresh groundwater for low (blue line), average (dark grey line), and high (red line) estimates of the global hydraulic conductivities. The graphs represent the change in volume (left) and percentage (right) with respect to the initial conditions (i.e. equal to equilibrium state without beach nourishment).

5.3.3 Specific yield

The simulations show that a smaller specific yield leads to a larger fresh groundwater lens (Figure 5.7). However, as a result of the reduced storage capacity a smaller specific yield – despite the larger fresh groundwater lens – results in a decrease of the absolute growth of the fresh groundwater volume (Figure 5.8a). The relative growth rates for low, average, and high values of the specific yield confirm that sites with larger specific yields result in a higher growth rate (Figure 5.8b). Therefore, shores with a higher specific yield are generate the largest growth in fresh groundwater resources.

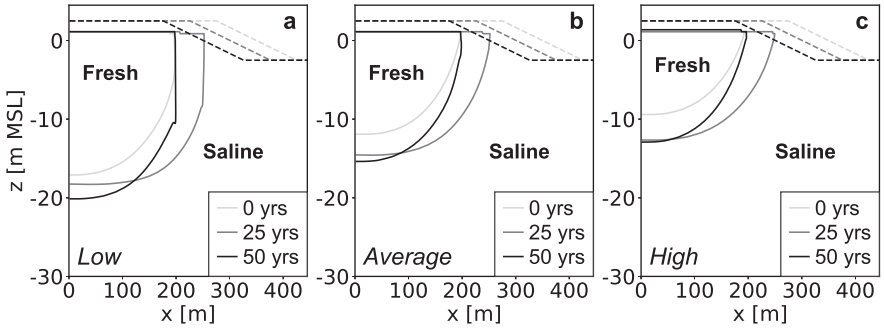

Figure 5.7 Simulated growth of the fresh groundwater lens for low (left), average (centre), and high (right) estimates of the specific yield. All images contain the fresh-salt groundwater interface of 1 g TDS L^{-1} (solid lines) and the surface elevation (dashed lines) at the start (light grey), middle (dark grey) and end (black) of the simulation period.

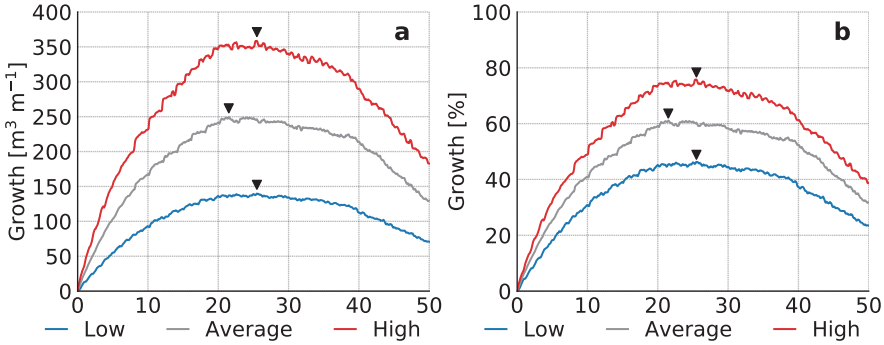

Figure 5.8 Simulated growth of fresh groundwater for low (blue line), average (dark grey line), and high (red line) estimates of the global specific yield in sandy shores. The graphs represent the change in volume (left) and percentage (right) with respect to the initial conditions (i.e. equal to equilibrium state without beach nourishment).

5.3.4 Beach slope

Increases in the beach slope result in narrower intertidal zones, which lead to a reduction of the area in which seawater infiltrates (within the same tidal range). The decrease in infiltration leads to lower groundwater levels (Figure 5.9), and subsequently the maximum (potential) depth of the fresh-salt groundwater interface becomes smaller. However, the relation between the beach slope and the groundwater level is non-linear: in beaches with lower slopes the increase in the infiltration of seawater will have a stronger impact on the fresh groundwater volume at some stage. This is the reason for the larger fresh groundwater lens in the simulation with an average beach slope (Figure 5.9b). In addition, a narrower intertidal zone and decrease in infiltration of seawater leads to a longer period of growth (Figure 5.10a), with a substantially higher relative growth rate (Figure 5.10b).

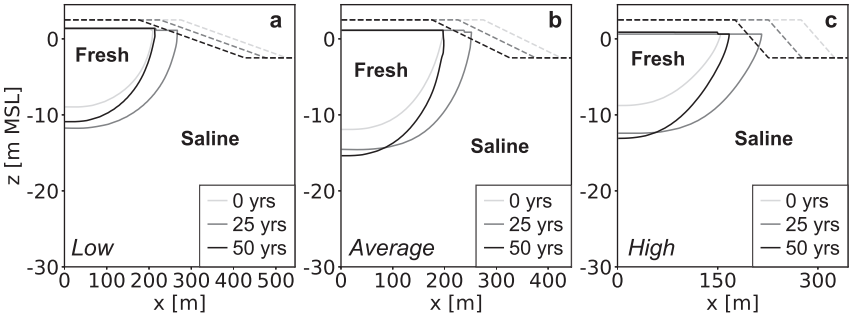

Figure 5.9 Simulated growth of the fresh groundwater lens for low (left), average (centre), and high (right) estimates of the beach slope. All images show the fresh-salt groundwater interface of 1 g TDS L^{-1} (solid lines) and surface elevation (dashed lines) at the start (light grey), middle (dark grey) and end (black) of the simulation period.

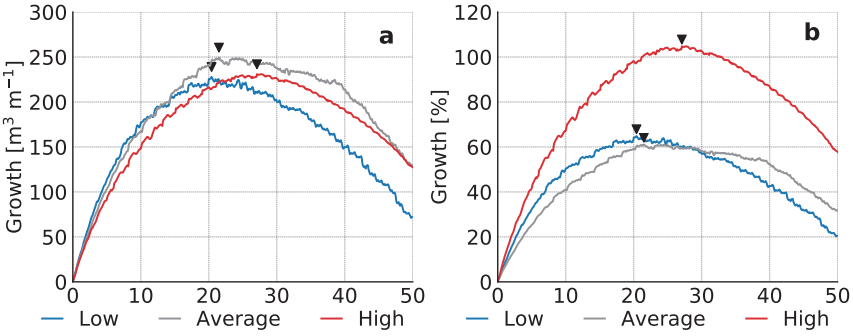

Figure 5.10 Simulated growth of fresh groundwater for low (blue line), average (dark grey line), and high (red line) estimates of the global beach slope in sandy shores. The graphs represent the change in volume (left) and percentage (right) with respect to the initial conditions (i.e. equal to equilibrium state without beach nourishment).

5.3.5 Tidal range

Sites with intermediate tidal ranges attain the largest fresh groundwater lens (Figure 5.11b) and highest absolute growth during the simulation period (Figure 5.12a). This is a result of two counteracting processes that are related to the increase in (net) seawater intrusion for sites with larger tidal ranges. Increases in the infiltration of seawater in the intertidal zone leads (1) to higher groundwater levels and therefore a larger potential depth of the fresh-salt groundwater interface, but (2) also result in a salinization of fresh groundwater resources within and near the intertidal zone. The optimum with respect to fresh groundwater resources, occurs therefore in intermediate tidal ranges. The longer growth curves for the meso and macro tidal ranges are a result of a larger potential depth of the fresh-salt groundwater interface. Smaller tidal ranges lead to lower groundwater levels. Thus, taking more time to produce fresh groundwater lenses.

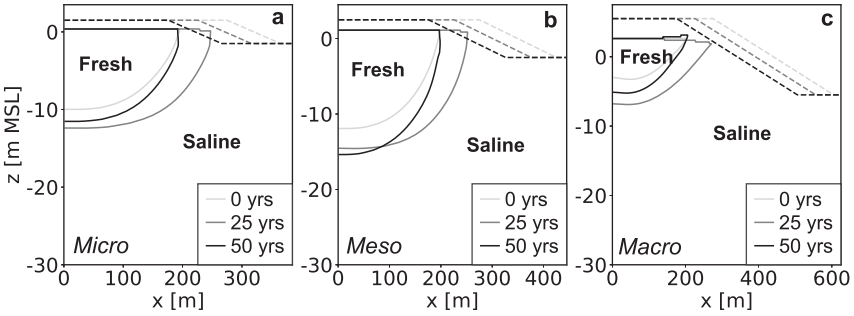

Figure 5.11 Simulated growth of the fresh groundwater lens for micro (left), meso (centre), and macro (right) tidal ranges. All images show the fresh-salt groundwater interface of 1 g TDS L^{-1} (solid lines) and the surface elevation (dashed lines) at the start (light grey), middle (dark grey) and end (black) of the simulation period.

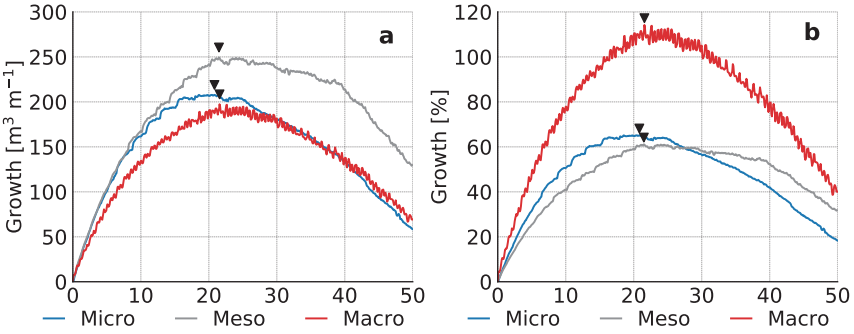

Figure 5.12 Simulated growth of fresh groundwater for micro (blue line), meso (dark grey line), and macro (red line) tidal ranges. The graphs represent the change in volume (left) and percentage (right) with respect to the initial conditions.

5.3.6 Coastal erosion

The development of the fresh groundwater lens is initially equal, and only starts to diverge when the varying erosion rates start to limit the growth rates or cause a loss in fresh groundwater (Figure 5.13a and b). Obviously, lower erosion rates result in larger fresh groundwater lens and the largest growth rates, reaching a maximum volume of fresh groundwater after 16 (after first nourishment), 21.5, and 38.5 years respectively (Figure 5.14). This shows that erosion is an important limiting factor the growth of fresh groundwater resources. It should be noted that in the simulation with a high erosion rate included two beach nourishments – at the start and after 25 years – to prevent an erosion beyond the initial shoreline. This shows that two consecutive nourishments lead to a larger growth of the fresh groundwater lens.

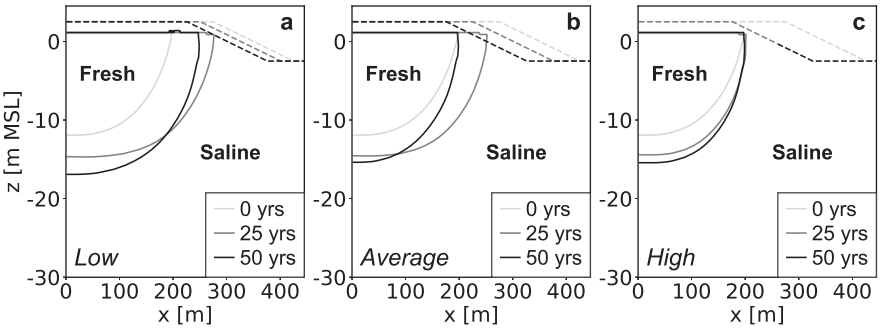

Figure 5.13 Simulated growth of the fresh groundwater lens for low (left), average (centre), and high (right) estimates of coastal erosion. All images show the fresh-salt groundwater interface of 1 g TDS L^{-1} (solid lines) and the surface elevation (dashed lines) at the start (light grey), middle (dark grey) and end (black) of the simulation period.

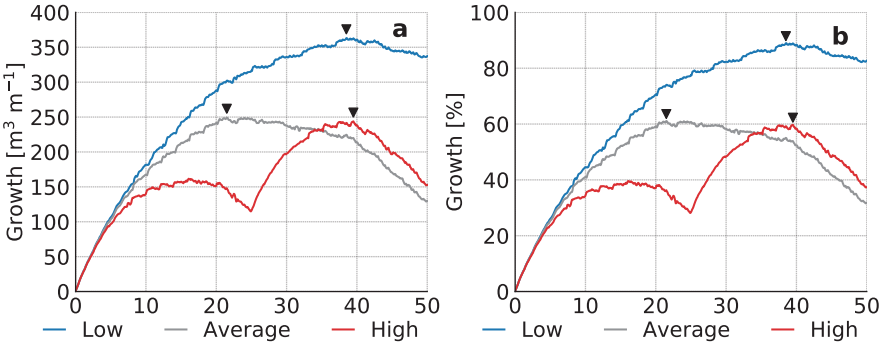

Figure 5.14 Simulated growth of fresh groundwater for low (blue line), average (dark grey line), and high (red line) estimates of the global coastal erosion in sandy shores. The graphs represent the change in volume (left) and percentage (right) with respect to the initial conditions (i.e. equal to equilibrium state without beach nourishment).

5.4 Global suitability

In all model scenarios, the addition of a beach nourishment to the coast results in a (temporary) increase of fresh groundwater resources. The growth rate is highest in the first years after the nourishment is added to the site. But over time the (simulated) retreat of the shoreline leads to a decrease of the growth rate, which eventually turns in to a decrease in the attained fresh groundwater volume. This pattern is to be expected, and likely for most cases where a beach is widened. Over a wide range of processes and properties, the simulations show that more groundwater recharge, smaller hydraulic conductivities, a larger specific yield (i.e. storage capacity), and less coastal erosion, in particular lead to a large growth of the fresh groundwater volume. However, it should be noted that larger hydraulic conductivities and smaller groundwater recharge rates bring about larger relative increases in fresh groundwater resources (i.e. relative to the initial condition or equilibrium state). Changes in the beach slope, and tidal dynamics have a relatively small impact on the attained growth in fresh groundwater.

Previous research has shown that extensive land-surface inundations – caused by storm surges or hurricanes – will likely have a substantial impact on coastal fresh groundwater in sandy beaches (Huizer et al., 2017, 2018)). Dependent on the extent and duration of the inundation, a portion or all of the accumulated fresh groundwater could be lost due to salinization. In addition, the design of the beach nourishment (e.g. crest elevation or nourishment volume) will also determine the susceptibility of a site for land-surface inundations. Therefore, when reflecting on the global suitability of coasts with respect to fresh groundwater resources, we believe that extensive land-surface inundations should be included.

With respect to the hydraulic conductivity, the global permeability map of Huscroft et al. (2018) indicates that most of the unconsolidated sediment has a hydraulic conductivity smaller than 25 m d^{-1}. Therefore, the hydraulic conductivity in most sandy beaches is likely low to average, and similarly we expect that most sandy beaches will have a specific yield close to the average (see Table 5.2). While both hydraulic conductivity and specific yield remain important factors for the growth of the fresh groundwater volume, we argue that (on a global scale) the most decisive factors for the growth of fresh groundwater resources by large beach nourishments are groundwater recharge, (extensive) land-surface inundations, and coastal erosion. Based on this assertion we created a global map that depicts the potential suitability of sandy shores for the growth of coastal fresh groundwater resources by large beach nourishments (Figure 5.15). The potential suitability was defined as the extent to which the characteristics of a coastal site can potentially lead to a growth of the fresh groundwater volume, and simultaneously reduce the likelihood of losses due to extensive inundations or coastal erosion.

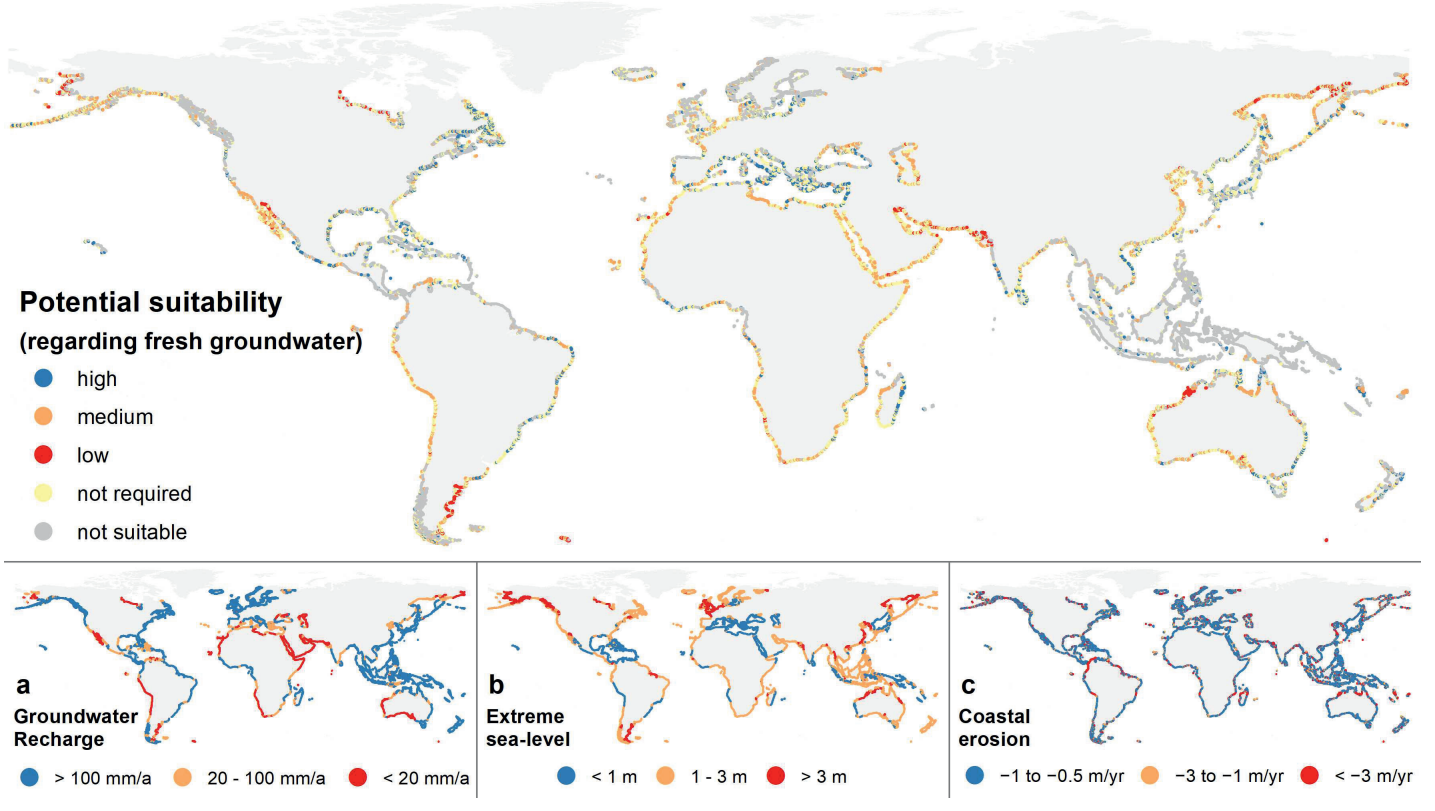

Figure 5.15 Global map of the potential suitability (high, medium, low) of eroding sandy shores for the growth of coastal fresh groundwater resources by large beach nourishments, based on the combination of global suitability maps for (a) groundwater recharge, (b) extreme sea-levels, (c) and hydraulic conductivity (see Table 5.4).

Focusing only on the eroding sandy shores – 17% of all analysed coastal sites, the subsequent potential suitability was assessed with global maps of (a) groundwater recharge (Döll and Fiedler, 2008), (b) height of extreme sea-levels with a return period of 100 years (Muis et al., 2016), and (c) coastal erosion (Luijendijk et al., 2018). The height of extreme sea-levels was used as an indication of the risk of extensive land-surface inundations at a particular coastal site on a global scale. Three classes of increasing suitability – low, medium, and high – were defined, based on the combination of global suitability maps for (a) groundwater recharge, (b) extreme sea-levels, and (c) coastal erosion (Figure 5.15). To each of these global maps weights were assigned ranging from -2 to +2, as shown in brackets in Table 5.4, and the summation of the weights (a+b+c) were used to define the potential suitability: high for weights equal or larger than 3, medium for weights between -3 and 3, and low for weights equal or smaller than -3. Coastal erosion was assigned a 50% lower weight, in accordance with the simulation results and the expected deviation in the impact on the growth of fresh groundwater resources.

Table 5.4 Weights assigned to (a) groundwater recharge, (b) extreme sea-levels, and (c) coastal erosion, which combined result in the suitability (low, medium, high) of eroding sandy shores for a growth of fresh groundwater resources by large beach nourishments.

Suitability Class	**a : Groundwater recharge**	**b : Extreme sea-level**	**c : Coastal erosion**
High ($\geq$ 3)	$>$ 100 mm yr^{-1} (+2)	$<$ 1 m MSL (+2)	-1 to -0.5 m yr^{-1} (+1)
Medium (-3 to 3)	20 to 100 mm yr^{-1} (0)	1 to 3 m MSL (0)	-3 to -1 m yr^{-1} (0)
Low ($\leq$ -3)	$<$ 20 mm yr^{-1} (-2)	$>$ 3 m MSL (-2)	$<$ -3 m yr^{-1} (-1)

The potential suitability map shows that on 17% of the analysed coastal sites large beach nourishments can lead to a growth in fresh groundwater resources, and of these sites 50% have a high potential suitability, 46% have a medium potential suitability, and 4% have a low potential suitability. This analysis suggests that on most of the eroding sandy sites, large beach nourishments can lead to growth of the (local) fresh groundwater volume.

5.5 Discussion

An unambiguous deficiency of the adopted methodology lies in the simplified 2-D model setup, because real sandy beaches exhibit 3-D variability in surface elevation, geology, heterogeneity, and aquifer thickness. For instance, most beaches exhibit heterogeneity in sediment grain size (Wilson et al., 2008) and therefore in hydraulic conductivity, which can lead to substantial changes in the fresh – salt groundwater distribution in the coastal aquifer. Besides space, also in time a coastal site may experience larger fluctuations of the surface elevation, inundated area, and (annual) groundwater recharge than were included in the model scenarios. One prime example is the impact of sea-level rise, which will lead to an increase in the extent and likely frequency of land-surface inundations. Another example is that over time beach slopes can change significantly due to varying concentrations of suspended sediment or seasonal differences in coastal forcing (e.g. erosion in winter, accretion in summer). Therefore, while in general the conclusions are probably true for most sandy shores, (local) variations in space and time can lead to substantially different outcomes in terms of growth in fresh groundwater resources.

Besides the higher complexity of real-world sandy beaches, the model setup excluded a flow of (fresh) groundwater across the inland model boundary. Most sites in the world will have a flow of groundwater towards the sea, and most islands in the world are wider or not shaped as strip-island as implemented in the model simulations. An inflow of fresh groundwater or an increase of the island width will both increase the growth of fresh groundwater resources, resulting a higher growth rate. When a specific coastal site is considered for beach nourishments, it is strongly recommended to conduct additional research.

5.6 Conclusion

In many coastal sites the application of a beach nourishment will likely lead to a (temporary) increase of fresh groundwater resources. To improve the likelihood of a (substantial) growth of the volume of fresh groundwater, a coastal site should get sufficient groundwater recharge, preferable have a low to medium hydraulic conductivity, and have limited number of extensive land-surface inundations. Coastal sites with high erosion rates will result in a lower maximum growth of fresh groundwater resources and may be more vulnerable to land-surface inundations. A global analysis revealed that an estimated 17% of the coasts consists of eroding sandy shores, which may be suitable for large-scale beach nourishments. Of these eroding sandy shores 50% have a high suitability with regard to the growth of fresh groundwater resources by large beach nourishments. However, these results provide only a first assessment of the possibility of an increase of the fresh groundwater resources by beach nourishments. For a detailed and more reliable prediction of the growth of the fresh groundwater volume on a site, additional site-specific research should be conducted.

Acknowledgements

This research is supported by the Dutch Technology Foundation STW, which is part of the Netherlands Organization for Scientific Research (NWO), and which is partly funded by the Ministry of Economic Affairs. This work was carried out within the Nature-driven nourishment of coastal systems (NatureCoast) program. The data used to produce the results of this paper may be obtained by contacting the corresponding author.

6 Synthesis

6.1 Introduction

The main objective of this research was to assess the impact of mega-scale beach nourishments on fresh groundwater resources, where the Sand Engine (also called Sand Motor) served as the primary study area. Chapters 2 to 5 have addressed several aspects of this main research objective along different temporal and spatial scales. In this synthesis the obtained outcomes are evaluated for each of the four research questions that were posed in section 1.2, and recommendations for further research are given.

6.2 Research questions

1. *What is the potential increase in fresh groundwater resources over a long period?*

The construction of a mega-scale nourishments such as the Sand Engine results in a (local) extension of the beach, and thus an expansion of the coastal area, which creates an opportunity for a growth in fresh groundwater resources. However, in a dynamic coastal environment the long-term potential increase in fresh groundwater resources will strongly depend on the morphological evolution of the nourishment. For example, if the nourishment erodes relatively quickly, the potential for a long period of growth of fresh groundwater is evidently small. As presented in chapter 2, we performed model simulations with projections of the morphological change of the Sand Engine between 2011 and 2050 to assess the potential effect of the Sand Engine on the volume of coastal fresh groundwater. The morphological evolution of the Sand Engine in this period was simulated with the hydrodynamics and morphodynamics model code Delft3D. Besides morphological changes, another important source of uncertainty for long-term projections is the impact of climate change on groundwater recharge and sea-level rise. To assess the potential impact of climate change in this period on fresh groundwater resources, we have conducted simulations with all of the KNMI'14 climate change scenarios (G_L, G_H, W_L and W_H) (KNMI, 2014).

The model simulations showed – for all climate scenarios – that the construction of the Sand Engine can potentially lead to a gradual growth of 0.3 to 0.5 million m^3 fresh groundwater per year. This growth is manifested as an expansion of the fresh groundwater lens in the adjacent dunes and the formation of a fresh groundwater lens in the Sand Engine. The simulated persistent growth in fresh groundwater over a long period is mainly a result of the projected gradual changes in morphology, which lead to a slow reversal to the original state of the coastal area.

Understandably such long-term projections of the morphological change contain considerable uncertainties, despite the extensive calibration and validation and large number of hydrodynamic processes that were included in the morphological simulations. For example, the lack of understanding of the highly-dynamic processes (related to sediment transport) and the absence of aeolian transport in the Delft3D simulations, can lead to incremental differences with reality. Measurements between 2011 – 2016 showed a reasonable fit with the model projections of the sediment volume changes and erosion patterns. However, future morphological changes can still turn out to be significantly different from these long-term projections (de Schipper et al., 2016). Besides the uncertainties about the morphological evolution, the subsequent chapters have shown the detrimental effect of land-surface inundations on coastal fresh groundwater. Therefore, the construction of the Sand Engine can lead to long period of gradual growth of the volume of fresh groundwater, but this growth will be constrained (in time and space) by the actual morphological change of the coastal area and limited by salinization processes of which coastal flooding is the predominant cause.

2. *What is the impact of tides, waves and storms on the fresh groundwater lens in the Sand Engine?*

One of the main purposes of the Sand Engine is coastal safety, which entails that it was designed to promote sand transport by natural forces (e.g. tides, wind, waves and storms). As alluded to in the previous paragraph, this design makes the Sand Engine prone to coastal flooding and thus salinization. To assess the impact of these natural forces on the fresh groundwater in the nourishment, measurements were conducted to observe the response of the groundwater head and salinity to tides, waves and storm surges. As described in chapter 3, the measurements consisted of (automated) time-lapse ERT measurements along a 2-D transect close to the shoreline, combined with various groundwater head measurements. This enabled us to obtain a series of 2-D resistivity images for a period of two months (November 2014 to January 2015), with time intervals of 15 to 30 minutes.

Subsequently, groundwater salinity images were derived from these measurements, which served as effective observations of the salinization of fresh groundwater under a variety of conditions (calm to storm) and the succeeding recovery of the fresh groundwater lens. For the analysis of the images we developed a 2-D variable-density groundwater model for the observation site and simulated the conditions of the measurement period as good as possible. These simulations served as a comparison with the observations to test to what extent observed changes in groundwater head and salinity could be reproduced.

The observed changes in groundwater head and salinity could be reproduced reasonably accurately with the groundwater model. This indicates that with a thorough understanding of the prevailing processes and a sufficient amount of monitoring data, the impact of tides, waves and even storm surges on fresh groundwater can be reproduced with a variable-density groundwater model. One of the processes that was important to incorporate in these simulations were wave set-up and wave run-up. Simulations with both processes – in particular wave run-up – showed a substantial improvement in the estimation of the extent of the land-surface inundations and related seawater intrusion. In more extreme conditions (i.e. storm surges) the impact became more extensive, suggesting that in areas with gently sloping beach profiles (estimations of) the wave set-up and run-up height need to be included to avoid underestimations of the impact of tides, waves and storm surges.

3. *What were the changes in the volume of fresh groundwater in the study area since its construction, and which processes drove these changes?*

Combining the answers to the preceding research questions, we can conclude that mega-scale nourishments such as the Sand Engine can lead to a gradual growth in fresh groundwater resources, but the potential growth is limited by coastal erosion and land-surface inundations. This raised the question to what extent an actual growth in the volume of fresh groundwater could be observed at the study site, and how large the relative (positive or negative) contribution of (1) land-surface inundations, (2) geomorphological changes, and (3) groundwater recharge was to this growth.

To answer this question, the growth of the fresh groundwater lens between 1 June 2011 (completion Sand Engine) to 31 May 2016 in the study area was reconstructed with measurements and model simulations. For the overall reconstruction we developed and implemented a 3-D variable-density groundwater model, which was calibrated with (transient) groundwater head and salinity measurements that were taken on or near the Sand Engine between 2014 and 2016. The relative contributions of land-surface inundations, geomorphological changes, and groundwater recharge were evaluated separately, by simplifications or variations of the calibrated reference model. For example, simulations without tidal fluctuations or without morphological changes were compared with the calibrated model to analyse the significance of a process with respect to the (total) volume of fresh groundwater.

The model simulations showed a substantial increase in the volume of fresh groundwater in the study area between 2011 and 2016, proving that the construction of a mega-nourishment can lead to an increase in fresh groundwater resources. Periods with high groundwater recharge rates led to substantial increases in the fresh groundwater volume, while periods with little or no rainfall led to a net loss of fresh groundwater. Land-surface inundations resulted in the salinization of the intertidal and supra-tidal areas, and geomorphological changes led to a gradual decline of the area that was not affected by seawater intrusion. Storm surges in particular were important for the determination of the growth of the freshwater lens, because these were the primary drivers of coastal erosion and led to the most extensive land-surface inundations. It is important to note that the observed growth of fresh groundwater resources in the Sand Engine between 2011 and 2016 was smaller than suggested by the simulations in chapter 2, demonstrating the importance of coastal forcing for an accurate reproduction of the growth of the freshwater lens.

4. *Which coastal sites are potentially suitable for large-scale beach nourishments, with regard to the growth of fresh groundwater resources?*

In chapters 2 to 4 we have shown that the Sand-Engine can lead to a gradual growth in fresh groundwater resources over a relatively long period, and has led to a growth of fresh groundwater resources between 2011 and 2016. In addition, research by de Schipper et al. (2016) has confirmed that in the first 18 months after the construction of the Sand Engine, the majority of the eroded sand on the Sand Engine ended up in adjacent coastal sections. Thus, the initial indications as for the transport of the nourished sediment (i.e. coastal safety) and for the growth of fresh groundwater resources are positive, and lead to the question which other shorelines in the world might be suitable for large to mega-scale beach nourishments. This is a complex multi-disciplinary question, which depends for example on the impact of the nourishment on the natural habitat, the transport of the nourished sediment, and the availability of a (cost-effective) sediment source. In chapter 5 we have made a first attempt to answer this question from an hydrogeological perspective – focusing on the growth of fresh groundwater resources, and assumed that all eroding sandy beaches are technically suitable for large beach nourishments.

Recent research of Luijendijk et al. (2018) showed that approximately 41% of the coastlines in the world consist of open beaches with sand, gravel or a mixture of both, of which 47% were subjected to substantial coastal erosion in the period 1984 to 2016. For these sites the growth in fresh groundwater resources by a large-scale beach nourishment depends on the prevailing characteristics of a coastal site. This was analysed for a selection of the most important (hydrological) processes and (geological) properties of sandy beaches: groundwater recharge, hydraulic conductivity, specific yield, beach slope, tidal dynamics, and morphodynamics. For each process or property the impact on the growth in fresh groundwater resources was evaluated with 2-D model simulations.

With low, average and high estimates (within the global variation), the absolute and relative contribution of each process or property on the fresh groundwater volume was simulated from 2020 to 2070. These simulations show that high groundwater recharge rates, small hydraulic conductivities and low coastal erosion rates generate the largest volumes of fresh groundwater. Combined with previous research (Huizer et al., 2017, 2018), it is concluded that the growth of fresh groundwater resources by large beach nourishments is determined mostly by: groundwater recharge, coastal erosion rates, (extensive) land-surface inundations, and to lesser extent hydraulic conductivity. Based on global maps of groundwater recharge (Döll and Fiedler, 2008), height of extreme sea-levels with a return period of 100 years (Muis et al., 2016), and permeability / hydraulic conductivity (Huscroft et al., 2018), most of the eroding sandy sites appear to be medium to highly suitable for the growth of coastal fresh groundwater resources by large beach nourishments. However, this analysis was only meant to portrait the global variability and should only be used as a first order assessment. For a reliable prediction of the growth of the fresh groundwater volume on a particular coastal site, additional site-specific research should be conducted.

6.3 Recommendations

For future research into the growth of fresh groundwater resources in dynamic coastal environments, and in particular for mega-scale beach nourishments, a number of challenges remain:

Extent of land-surface inundations
Coastal flooding is an important salinization process in (low-lying) coastal environments and – as shown in this thesis – in mega-scale beach nourishments. When an inundation coincides with little to negligible morphological change, the inundated area can be assessed with accurate estimations or measurements of the wave run-up height. Deviations can result in under- or overestimations of the (remaining) volume of coastal fresh groundwater. In more extreme circumstances – such as storm surges – inundations can coincide with substantial morphological changes, which can subsequently lead to variations in the inundated area. In this research the impact of land-surface inundations was successfully simulated with a combination of frequent topographic surveys, tide gauge measurements, and empirical equations for wave set-up and run-up (see chapter 3 and 4). Despite the overall resemblance between the observations and simulations, the model simulations underestimated the maximum extent of the inundations (Figure 3.8) and the increase of the groundwater level during some of the storm surges (see Figure 4.6 and 4.7).

Simulations that underestimate the salinization by land-surface inundations will evidently lead to overestimations of the available volume of fresh groundwater, especially for the most extensive inundation events. It is unclear whether this is a result of underestimations in the inundated area and the infiltration of seawater, underestimations of the lateral flow of infiltrated seawater, or a combination of both. Therefore, for future studies that adopt a similar approach as used in this thesis, we recommended to monitor the wave run-up height and morphological changes, and evaluate the approach under various conditions. Another option is to compare the outcomes of this approach to a simulation that is (fully) coupled with an hydrodynamic models, preferably for a coastal site with monitoring data.

Infiltration of seawater in the unsaturated zone
Another aspect, which is closely related to the preceding recommendation, is the infiltration of seawater into to the coastal aquifer. In areas with groundwater levels close to the surface or in areas that are (semi-)continuously saturated, such as the intertidal zone, the infiltration of seawater generally results in a fully saturated zone. In these (predominantly saline) areas a precise estimation of the infiltrated volume of seawater will likely have a limited impact on the overall uncertainty about fresh groundwater resources in the coastal system. However, in areas with deeper groundwater levels and larger unsaturated zones (e.g. supra-tidal zone), detailed knowledge on volume of seawater that infiltrates can be significant for (long-term) and accurate predictions of the growth of fresh groundwater resources in coastal areas. More importantly, these areas are often less frequently subjected to coastal flooding, and more likely to contain fresh groundwater.

In this research (see chapter 3 and 4), all model simulations were executed with (density-dependent) saturated groundwater flow, and assumptions were made for the infiltration of seawater up to the wave run-up height (see 3.2.3). The infiltration rate at the wave set-up height was estimated to be equal to the vertical hydraulic conductivity, which was subsequently linearly reduced to 10% at the wave run-up height. It is uncertain to what extent this best guess corresponds with reality, but with this approach we were able to obtain a reasonable fit with measurements. Similar to the preceding recommendation, for future studies we recommend to monitor inundation events and measure the impact on groundwater levels and salinity. As shown in this thesis, one possibility is the use of time lapse ERT (see section 3.2.2) in 2-D or 3-D, in combination with observation wells in which the groundwater level and sea-level is monitored. Subsequently, these measurements can be used to test and improve the adopted approach in this research, or to experiment with an approach that includes unsaturated flow.

Unsaturated zone modelling

As stated in the previous recommendation all model simulations in this thesis used density-dependent saturated groundwater flow with the model code SEAWAT. Besides assumptions on the infiltration rate of seawater through the unsaturated zone, this entails an approximation of evapotranspiration. Within the measurement period of this research (2011 – 2016) there was little to negligible dune vegetation present on the Sand Engine, and the groundwater recharge was predominantly dependent on the precipitation and soil evaporation. As shown in section 4.3.5, even for this relatively simple case, systematic over- or underestimations in the groundwater recharge rates will lead to substantial deviations in long-term predictions of the growth in fresh groundwater. Over the years, which has become especially apparent in recent years, the dune vegetation has expanded from the adjacent dune area to centre of the Sand Engine (van Puijenbroek, 2018). If this trend continues or stabilizes, evapotranspiration will become an important factor controlling the growth of fresh groundwater resources. Dependent on the desired accuracy of (long-term) projections of the volume of fresh groundwater and the susceptibility of a particular coastal site for the growth of (dune) vegetation, it is recommended to include unsaturated flow in the simulations to reduce the uncertainty in the estimated groundwater recharge rate. For further improvements in the estimation of the groundwater recharge rates it is recommended to conduct long-term monitoring programs, which focus on delineating the soil evaporation and evapotranspiration at coastal sites.

References

Abarca, E., H. Karam, H. F. Hemond and C. F. Harvey (2013), Transient groundwater dynamics in a coastal aquifer: The effects of tides, the lunar cycle, and the beach profile. Water Resources Research 49, 2473–2488. url: https://doi.org/10.1002/wrcr.20075.

Allen, R. G., L. S. Pereira, D. Raes and M. Smith (1998), Crop evapotranspiration: guidelines for computing crop water requirements. Tech. Rep., United Nations Food and Agriculture Orginization, Rome, Italy. url: http://www.kimberly.uidaho.edu/water/fao56/fao56.pdf.

Anthony, E. J. (2005), Beach Erosion. In: M. Schwartz, ed., The Encyclopedia of Coastal Science, Dordrecht: Springer, 140–145.

Anthony, E. J. (2013), Storms, shoreface morphodynamics, sand supply, and the accretion and erosion of coastal dune barriers in the southern North Sea. Geomorphology 199, 8–21. url: https://doi.org/10.1016/j.geomorph.2012.06.007.

Armstrong, S. B., E. D. Lazarus, P. W. Limber, E. B. Goldstein, C. Thorpe and R. C. Ballinger (2016), Indications of a positive feedback between coastal development and beach nourishment. Earth's Future 4, 626–635. url: https://doi.org/10.1002/2016EF000425.

Ataie-Ashtiani, B., R. Volker and D. Lockington (1999), Tidal effects on sea water intrusion in unconfined aquifers. Journal of Hydrology 216, 17–31. url: https://doi.org/10.1016/S0022-1694(98)00275-3.

Ataie-Ashtiani, B., A. D. Werner, C. Simmons, L. K. Morgan and C. Lu (2013), How important is the impact of land-surface inundation on seawater intrusion caused by sea-level rise? Hydrogeology Journal 21, 1673–1677. url: https://doi.org/10.1007/s10040-013-1021-0.

Bakhtyar, R., D. Barry, L. Li, D. Jeng and A. Yeganeh-Bakhtiary (2009), Modeling sediment transport in the swash zone: A review. Ocean Engineering 36, 767–783. url: https://doi.org/10.1016/j.oceaneng.2009.03.003.

Bakker, M., V. Post, C. D. Langevin, J. D. Hughes, J. T. White, J. J. Starn and M. N. Fienen (2016), Scripting MODFLOW Model Development Using Python and FloPy. Ground Water 54, 733–739. url: https://doi.org/10.1111/gwat.12413.

Bakker, M. A., S. van Heteren, L. M. Vonhögen, A. J. van der Spek and B. van der Valk (2012), Recent Coastal Dune Development: Effects of Sand Nourishments. Journal of Coastal Research 282, 587–601. url: https://doi.org/10.2112/jcoastres-d-11-00097.1.

Beaujean, J., F. Nguyen, A. Kemna, A. Antonsson and P. Engesgaard (2014), Calibration of seawater intrusion models: Inverse parameter estimation using surface electrical resistivity tomography and borehole data. Water Resources Research 50, 6828–6849. url: https://doi.org/10.1002/2013WR014020.

Beets, D., L. van der Valk and M. Stive (1992), Holocene evolution of the coast of Holland. Marine Geology 103, 423–443. url: https://doi.org/10.1016/0025-3227(92)90030-L.

Beets, D. J. and A. J. F. van der Spek (2000), The Holocene evolution of the barrier and the back-barrier basins of Belgium and the Netherlands as a function of late Weichselian morphology, relative sea-level rise and sediment supply. Netherlands Journal of Geosciences 79, 3–16. url: https://doi.org/10.1017/S0016774600021533.

Berry, A., S. Fahey and N. Meyers (2013), Changing of the Guard: Adaptation Options That Maintain Ecologically Resilient Sandy Beach Ecosystems. Journal of Coastal Research 289, 899–908. url: https://doi.org/10.2112/jcoastres-d-12-00150.1.

Brown, S., R. J. Nicholls, S. Hanson, G. Brundrit, J. A. Dearing, M. E. Dickson, S. L. Gallop, S. Gao, I. D. Haigh, J. Hinkel, J. a. Jiménez, R. J. Klein, W. Kron, A. N. Lázár, C. F. Neves, A. Newton, C. Pattiaratachi, A. Payo, K. Pye, A. Sánchez-Arcilla, M. Siddall, A. Shareef, E. L. Tompkins, A. T. Vafeidis, B. van Maanen, P. J. Ward and C. D. Woodroffe (2014), Shifting perspectives on coastal impacts and adaptation. Nature Climate Change 4, 752–755. url: https://doi.org/10.1038/nclimate2344.

Buma, J. (2013), Monitoring plan drainage measure Solleveld; Monitoring of groundwater and effectiveness of drainage measure (in Dutch). Tech. Rep., Deltares, Utrecht, The Netherlands.

Caldwell, P., M. Merrifield and P. Thompson (2015), Sea level measured by tide gauges from global oceans the Joint Archive for Sea Level holdings (NCEI Accession 0019568), Version 5.5. url: https://doi.org/10.7289/V5V40S7W.

Capobianco, M., H. Hanson, M. Larson, H. Steetzel, M. J. Stive, Y. Chatelus, S. Aarninkhof and T. Karambas (2002), Nourishment design and evaluation: Applicability of model concepts. Coastal Engineering 47, 113–135. url: https://doi.org/10.1016/S0378-3839(02)00123-0.

CBS, PBL and WUR (2016), Sea level: Dutch coast and worldwide, 1890-2014 (indicator 0229, version 09, 16 November 2016). url: https://www.clo.nl/en/indicators/en0229-sea-level-dutch-coast-and-worldwide.

Chang, S. W., T. P. Clement, M. J. Simpson and K. K. Lee (2011), Does sea-level rise have an impact on saltwater intrusion? Advances in Water Resources 34, 1283–1291. url: https://doi.org/10.1016/j.advwatres.2011.06.006.

Charlier, R. H., M. C. P. Chaineux and S. Morcos (2005), Panorama of the History of Coastal Protection. Journal of Coastal Research 211, 79–111. url: https://doi.org/10.2112/03561.1.

Chui, T. F. M. and J. P. Terry (2013), Influence of sea-level rise on freshwater lenses of different atoll island sizes and lens resilience to storm-induced salinization. Journal of Hydrology 502, 18–26. url: https://doi.org/10.1016/j.jhydrol.2013.08.013.

Colombani, N., A. Osti, G. Volta and M. Mastrocicco (2016), Impact of Climate Change on Salinization of Coastal Water Resources. Water Resources Management 30, 2483–2496. url: https://doi.org/10.1007/s11269-016-1292-z.

Comte, J. C. and O. Banton (2007), Cross-validation of geo-electrical and hydrogeological models to evaluate seawater intrusion in coastal aquifers. Geophysical Research Letters 34, 1–5. url: https://doi.org/10.1029/2007GL029981.

Cooke, B. C., A. R. Jones, I. D. Goodwin and M. J. Bishop (2012), Nourishment practices on Australian sandy beaches: A review. Journal of Environmental Management 113, 319–327. url: https://doi.org/10.1016/j.jenvman.2012.09.025.

Cooper, J. and J. McKenna (2008), Working with natural processes: the challenge for coastal protection strategies. Geographical Journal 174, 315–331. url: https://doi.org/10.1111/j.1475-4959.2008.00302.x.

Crain, C. M., B. S. Halpern, M. W. Beck and C. V. Kappel (2009), Understanding and managing human threats to the coastal marine environment. Annals of the New York Academy of Sciences 1162, 39–62. url: https://doi.org/10.1111/j.1749-6632.2009.04496.x.

De Bruin, H. A. R. and J. N. M. Stricker (2000), Evaporation of grass under non-restricted soil moisture conditions. Hydrological Sciences Journal 45, 391–406. url: https://doi.org/10.1080/02626660009492337.

de Franco, R., G. Biella, L. Tosi, P. Teatini, A. Lozej, B. Chiozzotto, M. Giada, F. Rizzetto, C. Claude, A. Mayer, V. Bassan and G. Gasparetto-Stori (2009), Monitoring the saltwater intrusion by time lapse electrical resistivity tomography: The Chioggia test site (Venice Lagoon, Italy). Journal of Applied Geophysics 69, 117–130. url: http://dx.doi.org/10.1016/j.jappgeo.2009.08.004.

De Graaf, I. E., E. H. Sutanudjaja, L. Van Beek and M. Bierkens (2015), A high-resolution global-scale groundwater model. Hydrology and Earth System Sciences 19, 823–837. url: https://doi.org/10.5194/hess-19-823-2015.

de Lange, W. J., G. F. Prinsen, J. C. Hoogewoud, A. A. Veldhuizen, J. Verkaik, G. H. Oude Essink, P. E. van Walsum, J. R. Delsman, J. C. Hunink, H. T. Massop and T. Kroon (2014), An operational, multi-scale, multi-model system for consensus-based, integrated water management and policy analysis: The Netherlands Hydrological Instrument. Environmental Modelling & Software 59, 98–108. url: https://doi.org/10.1016/j.envsoft.2014.05.009.

de Louw, P., S. Eeman, B. Siemon, B. Voortman, J. Gunnink, E. van Baaren and G. Oude Essink (2011), Shallow rainwater lenses in deltaic areas with saline seepage. Hydrology and Earth System Sciences 15, 3659–3678. url: https://doi.org/10.5194/hess-15-3659-2011.

de Ronde, J. (2008), Future long-term demand for nourishment (in Dutch). Tech. Rep., Deltares, Deltares, Delft.

de Ruig, J. H. M. (1998), Seaward coastal defence: limitations and possibilities. Journal of Coastal Conservation 4, 71–78. url: https://doi.org/10.1007/BF02806492.

de Ruig, J. H. M. and R. Hillen (1997), Developments in Dutch coastline management: Conclusions from the second governmental coastal report. Journal of Coastal Conservation 3, 203–210. url: https://doi.org/10.1007/BF02908195.

de Schipper, M. A., S. De Vries, M. Stive, R. De Zeeuw, J. Rutten, G. Ruessink, S. G. Aarninkhof and C. Van Gelder-Maas (2014), Morphological development of a mega-nourishment; first observations at the Sand Engine. In: Proceedings of Conference on Coastal Engineering, vol. 34, Seoul, Korea, 1–6. url: https://doi.org/10.9753/icce.v34.sediment.73.

de Schipper, M. A., S. de Vries, G. Ruessink, R. C. de Zeeuw, J. Rutten, C. van Gelder-Maas and M. J. Stive (2016), Initial spreading of a mega feeder nourishment: Observations of the Sand Engine pilot project. Coastal Engineering 111, 23–38. url: https://doi.org/10.1016/j.coastaleng.2015.10.011.

de Sherbinin, A., K. Warner and C. Ehrhart (2011), Casualties of Climate Change. Scientific American 304, 64–71. url: https://doi.org/10.1038/scientificamerican0111-64.

de Vriend, H., S. G. Aarninkhof and M. van Koningsveld (2014), Building with nature': the new Dutch approach to coastal and river works. Proceedings of the ICE - Civil Engineering 167, 18–24. url: https://doi.org/10.1680/cien.13.00003.

de Vries, S., M. Radermacher, M. A. de Schipper and M. J. Stive (2015), Tidal dynamics in the Sand Motor lagoon. In: E-proceedings of the 36th IAHR World Congress, The Hague, Netherlands, 1–6. url: http://resolver.tudelft.nl/uuid:e49d8911-72c2-4f6c-a8b4-7009954134c0.

Defeo, O., A. McLachlan, D. S. Schoeman, T. A. Schlacher, J. Dugan, A. Jones, M. Lastra and F. Scapini (2009), Threats to sandy beach ecosystems: A review. Estuarine, Coastal and Shelf Science 81, 1–12. url: https://doi.org/10.1016/j.ecss.2008.09.022.

Delsman, J. R., K. Hu-a ng, P. Vos, P. de Louw, G. Oude Essink, P. Stuyfzand and M. F. Bierkens (2014), Paleo-modeling of coastal saltwater intrusion during the Holocene: an application to the Netherlands. Hydrology and Earth System Sciences 18, 3891–3905. url: https://doi.org/10.5194/hess-18-3891-2014.

Deltacommissie (2008), Working Together with Water: A Living Land Builds for its Future, Findings of the Deltacommissie. Tech. Rep., Rotterdam, the Netherlands.

Döll, P. and K. Fiedler (2008), Global-scale modeling of groundwater recharge. Hydrology and Earth System Sciences 12, 863–885. url: https://doi.org/10.5194/hess-12-863-2008.

Draak, R. (2012), Water extraction in the Dunes (in Dutch). Holland's Duinen 60, 50–54.

Droogers, P. (2009), Improvement of the determination of actual evaporation for strategic water management (in Dutch). Tech. Rep., STOWA, Utrecht, The Netherlands.

Ebbens, E. and J. Fiselier (2010), Monitoring and evaluation plan Sand Engine (in Dutch). Tech. Rep., DHV B.V., Amersfoort, The Netherlands.

Eeman, S., A. Leijnse, P. Raats and S. van der Zee (2011), Analysis of the thickness of a fresh water lens and of the transition zone between this lens and upwelling saline water. Advances in Water Resources 34, 291–302. url: https://doi.org/10.1016/j.advwatres.2010.12.001.

Falkland, A. and C. Woodroffe (2004), Geology and Hydrogeology of Tarawa and Christmas Island, Kiribati. In: H. Vacher and T. Quinn, eds., Developments in Sedimentology, vol. 54, chap. 19, Elsevier, 577–610. url: https://doi.org/10.1016/S0070-4571(04)80041-4.

Famiglietti, J. S. (2014), The global groundwater crisis. Nature Climate Change 4, 945–948. url: https://doi.org/10.1038/nclimate2425.

Ferguson, G. and T. Gleeson (2012), Vulnerability of coastal aquifers to groundwater use and climate change. Nature Climate Change 2, 342–345. url: https://doi.org/10.1038/nclimate1413.

Few, R. and F. Matthies (2006), Flood Hazards and Health. London, United Kingdom: Routledge. url: https://doi.org/10.4324/9781849771351.

Finkl, C. and H. Walker (2005), Beach Nourishment. In: M. Schwartz, ed., The Encyclopedia of Coastal Science, Dordrecht: Springer, 147–161. url: https://doi.org/10.1007/978-3-319-48657-4{%}0D.

Fiselier, J. (2010), Project plan/EIA: Construction and extraction of sand, Sand Engine Delfland coast (in Dutch). Tech. Rep., DHV BV, Amersfoort, The Netherlands.

FitzGerald, D. M., M. S. Fenster, B. A. Argow and I. V. Buynevich (2008), Coastal Impacts Due to Sea-Level Rise. Annual Review of Earth and Planetary Sciences 36, 601–647. url: https://doi.org/10.1146/annurev.earth.35.031306.140139.

Fofonoff, N. and R. Millard Jr. (1983), Algorithms for computation of fundamental properties of seawater. Unesco Technical Papers in Marine Science 44, 58.

Foreman, M. G. G. and R. F. Henry (1989), The harmonic analysis of tidal model time series. Advances in Water Resources 12, 109–120. url: https://doi.org/10.1016/0309-1708(89)90017-1.

Friedman, S. P. (2005), Soil properties influencing apparent electrical conductivity: A review. Computers and Electronics in Agriculture 46, 45–70.

Giardino, A., J. Mulder, J. de Ronde and J. Stronkhorst (2011), Sustainable Development of the Dutch Coast: Present and Future. Journal of Coastal Research 61, 166–172. url: https://doi.org/10.2112/SI61-001.11.

Gingerich, S. B., C. I. Voss and A. G. Johnson (2017), Seawater-flooding events and impact on freshwater lenses of low-lying islands: Controlling factors, basic management and mitigation. Journal of Hydrology 551, 676–688. url: https://doi.org/10.1016/j.jhydrol.2017.03.001.

Giosan, L., J. Syvitski, S. Constantinescu and J. Day (2014), Protect the world's deltas. Nature 516, 31–33. url: https://doi.org/10.1038/516031a.

Gleeson, T., Y. Wada, M. Bierkens and L. van Beek (2012), Water balance of global aquifers revealed by groundwater footprint. Nature 488, 197–200. url: https://doi.org/10.1038/nature11295.

Gleeson, T., N. Moosdorf, J. Hartmann and L. van Beek (2014), A glimpse beneath earth's surface: GLobal HYdrogeology MaPS (GLHYMPS) of permeability and porosity. Geophysical Research Letters 41, 3891–3898. url: https://doi.org/10.1002/2014GL059856.

Goes, B., G. H. Oude Essink, R. Vernes and F. Sergi (2009), Estimating the depth of fresh and brackish groundwater in a predominantly saline region using geophysical and hydrological methods, zeeland, the netherlands. Near Surface Geophysics 7, 401–412. url: https://doi.org/10.3997/1873-0604.2009048.

Goodhew, T. (2014), Coastal Flood Defences - Strategies for Protection in the United Kingdom. In: C. A. Booth and S. M. Charlesworth, eds., Water Resources in the Built Environment: Management Issues and Solutions, Chichester, United Kingdom: John Wiley & Sons, Ltd, 233–248. url: https://doi.org/10.1002/9781118809167.

Gubler, S., S. Gruber and R. S. Purves (2012), Uncertainties of parameterized surface downward clear-sky shortwave and all-sky longwave radiation. Atmospheric Chemistry and Physics 12, 5077–5098. url: https://doi.org/10.5194/acp-12-5077-2012.

Guo, W. and C. D. Langevin (2002), User's Guide to SEAWAT : A Computer Program For Simulation of Ground-Water Flow. In: U.S. Geological Survey Techniques of Water-Resources Investigations 6, chap. A7, Tallahassee, Florida, USA: US Geological Survey, 6 edn., 87. url: https://pubs.water.usgs.gov/TWRI6a7.

Habel, S., C. H. Fletcher, M. Barbee and T. R. Anderson (2016), The influence of seasonal patterns on a beach nourishment project in a complex reef environment. Coastal Engineering 116, 67–76. url: https://doi.org/10.1016/j.coastaleng.2016.06.006.

Hallegatte, S., C. Green, R. J. Nicholls and J. Corfee-Morlot (2013), Future flood losses in major coastal cities. Nature Climate Change 3, 802–806. arXiv:1011.1669v3, url: https://doi.org/10.1038/nclimate1979.

Hanson, H., A. Brampton, M. Capobianco, H. H. Dette, L. Hamm, C. Laustrup, A. Lechuga and R. Spanhoff (2002), Beach nourishment projects, practices, and objectives - A European overview. Coastal Engineering 47, 81–111. url: https://doi.org/10.1016/S0378-3839(02)00122-9.

Heiss, J. W. and H. A. Michael (2014), Saltwater-freshwater mixing dynamics in a sandy beach aquifer over tidal, spring-neap, and seasonal cycles. Water Resources Research 50, 6747–6766. url: https://doi.org/10.1002/2014WR015574.

Henderson, R. D., F. D. Day-Lewis, E. Abarca, C. F. Harvey, H. N. Karam, L. Liu and J. W. Lane (2010), Marine electrical resistivity imaging of submarine groundwater discharge: sensitivity analysis and application in Waquoit Bay, Massachusetts, USA. Hydrogeology Journal 18, 173–185. url: https://doi.org/10.1007/s10040-009-0498-z.

Herckenrath, D., C. D. Langevin and J. Doherty (2011), Predictive uncertainty analysis of a saltwater intrusion model using null-space Monte Carlo. Water Resources Research 47, W05504. url: https://doi.org/10.1029/2010WR009342.

Hermans, T., A. Vandenbohede, L. Lebbe, R. Martin, A. Kemna, J. Beaujean and F. Nguyen (2012), Imaging artificial salt water infiltration using electrical resistivity tomography constrained by geostatistical data. Journal of Hydrology 438-439, 168–180. url: https://doi.org/10.1016/j.jhydrol.2012.03.021.

Hill, K. D., T. M. Dauphinee and D. J. Woods (1986), The extension of the Practical Salinity Scale 1978 to low salinities. IEEE Journal of Oceanic Engineering 11, 1–4. url: https://doi.org/10.1109/JOE.1986.1145154.

Hoggart, S., M. Hanley, D. Parker, D. Simmonds, D. Bilton, M. Filipova-Marinova, E. Franklin, I. Kotsev, E. Penning-Rowsell, S. Rundle, E. Trifonova, S. Vergiev, A. White and R. Thompson (2014), The consequences of doing nothing: The effects of seawater flooding on coastal zones. Coastal Engineering 87, 169–182. url: https://doi.org/10.1016/j.coastaleng.2013.12.001.

Holding, S. and D. M. Allen (2015a), From days to decades: numerical modelling of freshwater lens response to climate change stressors on small low-lying islands. Hydrology and Earth System Sciences 19, 933–949. url: https://doi.org/10.5194/hess-19-933-2015.

Holding, S. and D. M. Allen (2015b), Wave overwash impact on small islands: Generalised observations of freshwater lens response and recovery for multiple hydrogeological settings. Journal of Hydrology 529, 1324–1335. url: https://doi.org/10.1016/j.jhydrol.2015.08.052.

Holgate, S. J. J., A. Matthews, P. L. L. Woodworth, L. J. J. Rickards, M. E. E. Tamisiea, E. Bradshaw, P. R. R. Foden, K. M. M. Gordon, S. Jevrejeva and J. Pugh (2013), New Data Systems and Products at the Permanent Service for Mean Sea Level. Journal of Coastal Research 288, 493–504. url: https://doi.org/10.2112/jcoastres-d-12-00175.1.

Hoofs, J. and Y. van der Pijl (2002), Kartobibliografie van de Waterstaatskaart (1865-1991). Tech. Rep., Ministerie van Verkeer en Waterstaat, Rijkswaterstaat, Meetkundige Dienst (RWS, MD), afd. IEBD, Delft, The Netherlands.

Hooghart, J. and W. Lablans (1988), From Penman to Makkink: a new calculation method for the climatological numbers of evaporation (in Dutch). Tech. Rep., KNMI, De Bilt, The Netherlands.

Huizer, S., G. H. P. Oude Essink and M. F. P. Bierkens (2016), Fresh groundwater resources in a large sand replenishment. Hydrology and Earth System Sciences 20, 3149–3166. url: https://doi.org/10.5194/hess-20-3149-2016.

Huizer, S., M. Karaoulis, G. Oude Essink and M. Bierkens (2017), Monitoring and simulation of salinity changes in response to tide and storm surges in a sandy coastal aquifer system. Water Resources Research 53, 6487–6509. url: https://doi.org/10.1002/2016WR020339.

Huizer, S., M. Radermacher, S. de Vries, G. H. P. Oude Essink and M. F. P. Bierkens (2018), Impact of coastal forcing and groundwater recharge on the growth of a fresh groundwater lens in a mega-scale beach nourishment. Hydrology and Earth System Sciences 22, 1065–1080. url: https://doi.org/10.5194/hess-22-1065-2018.

Huscroft, J., T. Gleeson, J. Hartmann and J. Börker (2018), Compiling and Mapping Global Permeability of the Unconsolidated and Consolidated Earth: GLobal HYdrogeology MaPS 2.0 (GLHYMPS 2.0). Geophysical Research Letters 45, 1897–1904. arXiv:1011.1669v3, url: https://doi.org/10.1002/2017GL075860.

IOC, SCOR and IAPSO (2010), Appendix E: Algorithm for calculating Practical Salinity. In: The international thermodynamic equation of seawater - 2010: Calculation and use of thermodynamic properties, Intergovernmental Oceanographic Commision, UNESCO, manuals an edn., 147–151.

IPCC (2014), Climate Change 2013: The Physical Science Basis. Contribution of Working Group I to the Fifth Assessment Report of the Intergovern- mental Panel on Climate Change. Cambridge, United Kingdom and New York, NY, USA: Cambridge University Press. url: https://doi.org/10.1017/CBO9781107415324.

Jensen, J., J. Hofstede, H. Kunz, J. de Ronde, P. Heinen and W. Siefent (1993), Long term water level observations and variations. In: Proceedings of the Symposium on Coastal and Ocean Management, New Orleans, LA, USA, 110–130.

Kabat, P., L. O. Fresco, M. J. Stive, C. P. Veerman, J. S. van Alphen, B. W. Parmet, W. Hazeleger and C. A. Katsman (2009), Dutch coasts in transition. Nature Geoscience 2, 450–452. url: https://doi.org/10.1038/ngeo572.

Karaoulis, M., J.-H. Kim and P. Tsourlos (2011), 4D active time constrained resistivity inversion. Journal of Applied Geophysics 73, 25–34. url: https://doi.org/10.1016/j.jappgeo.2010.11.002.

Keijsers, J. G., A. Poortinga, M. J. Riksen and J. Maroulis (2014), Spatio-Temporal Variability in Accretion and Erosion of Coastal Foredunes in the Netherlands: Regional Climate and Local Topography. PLoS ONE 9, 1–11. url: https://doi.org/10.1371/journal.pone.0091115.

Keijsers, J. G., A. Giardino, A. Poortinga, J. P. Mulder, M. J. Riksen and G. Santinelli (2015), Adaptation strategies to maintain dunes as flexible coastal flood defense in The Netherlands. Mitigation and Adaptation Strategies for Global Change 20, 913–928. url: https://doi.org/10.1007/s11027-014-9579-y.

Ketabchi, H., D. Mahmoodzadeh, B. Ataie-Ashtiani, A. D. Werner and C. T. Simmons (2014), Sea-level rise impact on fresh groundwater lenses in two-layer small islands. Hydrological Processes 28, 5938–5953. url: https://doi.org/10.1002/hyp.10059.

Ketabchi, H., D. Mahmoodzadeh, B. Ataie-ashtiani and C. T. Simmons (2016), Sea-level rise impacts on seawater intrusion in coastal aquifers : Review and integration. Journal of Hydrology 535, 235–255. url: https://doi.org/10.1016/j.jhydrol.2016.01.083.

Khan, S. J., D. Deere, F. D. Leusch, A. Humpage, M. Jenkins and D. Cunliffe (2015), Extreme Weather Events: Should Drinking Water Quality Management Systems Adapt to Changing Risk Profiles? Water Research 85, 124–136. url: https://doi.org/10.1016/j.watres.2015.08.018.

Kim, J. H., M. J. Yi, S. G. Park and J. G. Kim (2009), 4-D inversion of DC resistivity monitoring data acquired over a dynamically changing earth model. Journal of Applied Geophysics 68, 522–532. url: https://doi.org/10.1016/j.jappgeo.2009.03.002.

Kim, J. H., R. Supper, P. Tsourlos and M. J. Yi (2013), Four-dimensional inversion of resistivity monitoring data through Lp norm minimizations. Geophysical Journal International 195, 1640–1656. url: https://doi.org/10.1093/gji/ggt324.

KNMI (2014), KNMI'14 : Climate Change scenarios for the 21st Century - A Netherlands perspective. Tech. Rep., KNMI, KNMI, De Bilt, The Netherlands. url: www.climatescenario.nl.

Kooi, H., J. Groen and A. Leijnse (2000), Modes of seawater intrusion during transgressions. Water Resources Research 36, 3581–3589. url: https://doi.org/10.1029/2000WR900243.

Kuan, W. K., G. Jin, P. Xin, C. Robinson, B. Gibbes and L. Li (2012), Tidal influence on seawater intrusion in unconfined coastal aquifers. Water Resources Research 48, 1–11. url: https://doi.org/10.1029/2011WR010678.

Kuras, O., J. D. Pritchard, P. I. Meldrum, J. E. Chambers, P. B. Wilkinson, R. D. Ogilvy and G. P. Wealthall (2009), Monitoring hydraulic processes with automated time-lapse electrical resistivity tomography (ALERT). Comptes Rendus - Geoscience 341, 868–885. url: https://doi.org/10.1016/j.crte.2009.07.010.

Langevin, C. D., W. Barclay and W. Guo (2003), MODFLOW-2000, the U.S. Geological Survey Modular Ground-Water Model Documentation of the SEAWAT-2000 Version with the Variable-Density Flow Process (VDF) and the Integrated MT3DMS Transport Process (IMT). Tech. Rep., US Geological Survey, Tallahassee, Florida, USA.

Langevin, C. D., D. T. Thorne Jr., A. Dausman, M. C. Sukop and W. Guo (2008), SEAWAT version 4: A Computer Program for Simulation of Multi-Species Solute and Heat Transport. In: U.S. Geological Survey Techniques and Methods 6, chap. A22, Reston, Virginia, USA: US Geological Survey, 39.

Lesser, G., J. Roelvink, J. van Kester and G. Stelling (2004), Development and validation of a three-dimensional morphological model. Coastal Engineering 51, 883–915. url: https://doi.org/10.1016/j.coastaleng.2004.07.014.

Levanon, E., E. Shalev, Y. Yechieli and H. Gvirtzman (2016), Fluctuations of fresh-saline water interface and of water table induced by sea tides in unconfined aquifers. Advances in Water Resources 96, 34–42. url: https://doi.org/10.1016/j.advwatres.2016.06.013.

Li, H., M. C. Boufadel and J. W. Weaver (2008), Tide-induced seawatergroundwater circulation in shallow beach aquifers. Journal of Hydrology 352, 211–224. url: https://doi.org/10.1016/j.jhydrol.2008.01.013.

Liu, Y., S.-h. Shang and X.-m. Mao (2012), Tidal effects on groundwater dynamics in coastal aquifer under different beach slopes. Journal of Hydrodynamics, Ser. B 24, 97–106. url: http://linkinghub.elsevier.com/retrieve/pii/S1001605811602230.

Luijendijk, A., G. Hagenaars, R. Ranasinghe, F. Baart, G. Donchyts and S. Aarninkhof (2018), The State of the World's Beaches. Scientific Reports 8, 6641. url: https://doi.org/10.1038/s41598-018-24630-6.

Luijendijk, A. P., R. Ranasinghe, M. A. de Schipper, B. A. Huisman, C. M. Swinkels, D. J. Walstra and M. J. Stive (2017), The initial morphological response of the Sand Engine: A process-based modelling study. Coastal Engineering 119, 1–14. url: https://doi.org/10.1016/j.coastaleng.2016.09.005.

Luo, S., F. Cai, H. Liu, G. Lei, H. Qi and X. Su (2015), Adaptive measures adopted for risk reduction of coastal erosion in the People's Republic of China. Ocean & Coastal Management 103, 134–145. url: https://doi.org/10.1016/j.ocecoaman.2014.08.008.

Mahmoodzadeh, D., H. Ketabchi, B. Ataie-Ashtiani and C. T. Simmons (2014), Conceptualization of a fresh groundwater lens influenced by climate change: A modeling study of an arid-region island in the Persian Gulf, Iran. Journal of Hydrology 519, 399–413. url: https://doi.org/10.1016/j.jhydrol.2014.07.010.

Mao, X., P. Enot, D. Barry, L. Li, A. Binley and D. Jeng (2006), Tidal influence on behaviour of a coastal aquifer adjacent to a low-relief estuary. Journal of Hydrology 327, 110–127. url: https://doi.org/10.1016/j.jhydrol.2005.11.030.

McDonald, M. G., A. W. Harbaugh, B. R. Orr and D. J. Ackerman (1992), A method of converting no-flow cells to variable- head cells for the U.S. Geological Survey modular finite-difference ground-water flow model. Tech. Rep., U.S. Geological Survey Open-File Report 91-536, Reston, Virginia, USA.

McGranahan, G., D. Balk and B. Anderson (2007), The rising tide: assessing the risks of climate change and human settlements in low elevation coastal zones. Environment and Urbanization 19, 17–37. url: https://doi.orgi/10.1177/0956247807076960.

McLachlan, A. and A. Dorvlo (2005), Global Patterns in Sandy Beach Macrobenthic Communities. Journal of Coastal Research 214, 674–687. url: https://doi.org/10.2112/03-0114.1.

Meinardi, C. (1994), Groundwater recharge and travel times in the sandy regions of the Netherlands. Ph.d. thesis, Ph.D. Thesis, VU University Amsterdam, Amsterdam, The Netherlands.

Michael, H. A., C. J. Russoniello and L. A. Byron (2013), Global assessment of vulnerability to sea-level rise in topography-limited and recharge-limited coastal groundwater systems. Water Resources Research 49, 2228–2240. url: https://doi.org/10.1002/wrcr.20213.

Millero, F. (2003), Physicochemical Controls on Seawater. In: H. Elderfield, ed., Treatise on Geochemistry, Chapter 6.01, i, chap. 6.01, Amsterdam: Elsevier, 1–21. url: https://doi.org/10.1016/B0-08-043751-6/06154-5.

Millero, F. J., R. Feistel, D. G. Wright and T. J. McDougall (2008), The composition of Standard Seawater and the definition of the Reference-Composition Salinity Scale. Deep Sea Research Part I: Oceanographic Research Papers 55, 50–72. url: https://doi.org/10.1016/j.dsr.2007.10.001.

Morgan, L. K. and A. D. Werner (2014), Seawater intrusion vulnerability indicators for freshwater lenses in strip islands. Journal of Hydrology 508, 322–327. url: https://doi.org/10.1016/j.jhydrol.2013.11.002.

Morrow, F. J., M. R. Ingham and J. A. McConchie (2010), Monitoring of tidal influences on the saline interface using resistivity traversing and cross-borehole resistivity tomography. Journal of Hydrology 389, 69–77. url: https://doi.org/10.1016/j.jhydrol.2010.05.022.

Muis, S., M. Verlaan, H. C. Winsemius, J. C. Aerts and P. J. Ward (2016), A global reanalysis of storm surges and extreme sea levels. Nature Communications 7, 11969. url: https://doi.org/10.1038/ncomms11969.

Mulder, J. P. and P. K. Tonnon (2011), " Sand Engine " : Background and Design of a Mega-Nourishment pilot in the Netherlands. In: Proceedings of Conference on Coastal Engineering, vol. 32, Shanghai, China, 1–10. url: https://doi.org/10.9753/icce.v32.management.35.

Mulligan, A. E., C. Langevin and V. E. Post (2011), Tidal Boundary Conditions in SEAWAT. Ground Water 49, 866–879. url: https://doi.org/10.1111/j.1745-6584.2010.00788.x.

Neumann, B., A. T. Vafeidis, J. Zimmermann and R. J. Nicholls (2015), Future coastal population growth and exposure to sea-level rise and coastal flooding - A global assessment. PLoS ONE 10. url: https://doi.org/10.1371/journal.pone.0118571.

Nguyen, F., A. Kemna, A. Antonsson, P. Engesgaard, O. Kuras, R. D. Ogilvy, J. Gisbert, S. Jorreto and A. Pulido-Bosch (2009), Characterization of seawater intrusion using 2D electrical imaging. Near Surface Geophysics 7, 377–390. url: https://doi.org/10.3997/1873-0604.2009025.

Nicholls, R. (2011), Planning for the Impacts of Sea Level Rise. Oceanography 24, 144–157. url: https://doi.org/10.5670/oceanog.2011.34.

Nicholls, R. J. (2010), Impacts of and responses to Sea-Level Rise. In: J. Church, P. Woodworth, T. Aarup and W. Wilson, eds., Understanding Sea-Level Rise and Variability, Wiley-Blackwell., 17–51. url: https://doi.org/10.1002/9781444323276.

Nicholls, R. J. and A. Cazenave (2010), Sea-Level Rise and Its Impact on Coastal Zones. Science 328, 1517–1520. url: https://doi.org/10.1126/science.1185782.

Nicholls, R. J., S. Brown, S. Hanson and J. Hinkel (2010), Economics of Coastal Zone Adaptation to Climate Change. Tech. Rep. october, The International Bank for Development and Reconstruction / The World Bank, Washington D.C., USA.

Ogilvy, R. D., P. I. Meldrum, O. Kuras, P. B. Wilkinson, J. E. Chambers, M. Sen, A. Pulido-Bosch, J. Gisbert, S. Jorreto, I. Frances and P. Tsourlos (2009), Automated Monitoring of Coastal Aquifers with Electrical Resistivity Tomography. Near Surface Geophysics 7, 367–375. url: https://doi.org/10.1007/s13398-014-0173-7.2.

Oude Essink, G., E. van Baaren and P. de Louw (2010), Effects of climate change on coastal groundwater systems: A modeling study in the Netherlands. Water Resources Research 46, W00F04. url: https://doi.org/10.1029/2009WR008719.

Oude Essink, G. H. (2001), Improving fresh groundwater supply - problems and solutions. Ocean & Coastal Management 44, 429–449. url: https://doi.org/10.1016/S0964-5691(01)00057-6.

Passeri, D. L., S. C. Hagen, S. C. Medeiros, M. V. Bilskie, K. Alizad and D. Wang (2015), The dynamic effects of sea level rise on low-gradient coastal landscapes: A review. Earth's Future 3, 159–181. url: https://doi.org/10.1002/2015EF000298.

Pauw, P., G. H. Oude Essink, A. Leijnse, A. Vandenbohede, J. Groen and S. E. van der Zee (2014), Regional scale impact of tidal forcing on groundwater flow in unconfined coastal aquifers. Journal of Hydrology 517, 269–283. url: https://doi.org/10.1016/j.jhydrol.2014.05.042.

Post, V., H. Van der Plicht and H. Meijer (2003), The origin of brackish and saline groundwater in the coastal area of the Netherlands. Netherlands Journal of Geosciences 82, 133–147. url: https://doi.org/10.1017/S0016774600020692.

Post, V. E. and G. J. Houben (2017), Density-driven vertical transport of saltwater through the freshwater lens on the island of Baltrum (Germany) following the 1962 storm flood. Journal of Hydrology 551, 689–702. url: https://doi.org/10.1016/j.jhydrol.2017.02.007.

Post, V. E. A. (2012), Electrical Conductivity as a Proxy for Groundwater Density in Coastal Aquifers. Ground Water 50, 785–792. url: https://doi.org/10.1111/j.1745-6584.2011.00903.x.

Pranzini, E. (2017), Shore protection in Italy: From hard to soft engineering ... and back. Ocean & Coastal Management , 1–15url: https://doi.org/10.1016/j.ocecoaman.2017.04.018.

Rasmussen, P., T. O. Sonnenborg, G. Goncear and K. Hinsby (2013), Assessing impacts of climate change, sea level rise, and drainage canals on saltwater intrusion to coastal aquifer. Hydrology and Earth System Sciences 17, 421–443. url: https://doi.org/10.5194/hess-17-421-2013.

Revil, A., M. Karaoulis, T. Johnson and A. Kemna (2012), Review: Some low-frequency electrical methods for subsurface characterization and monitoring in hydrogeology. Hydrogeology Journal 20, 617–658. url: https://doi.org/10.1007/s10040-011-0819-x.

Rijkswaterstaat (2012), Salinity in the North Sea along the coast (in Dutch). url: http://www.noordzeeloket.nl/en/spatial-management/north-sea-atlas/watersysteem/zoutgehalte.aspx.

Roache, P. (1994), Perspective: A Method for Uniform Reporting of Grid Refinement Studies. Journal of Fluids Engineering 116, 405–413. url: https://doi.org/10.1115/1.2910291.

Robinson, C., L. Li and D. Barry (2007a), Effect of tidal forcing on a subterranean estuary. Advances in Water Resources 30, 851–865. url: https://doi.org/10.1016/j.advwatres.2006.07.006.

Robinson, C., L. Li and H. Prommer (2007b), Tide-induced recirculation across the aquifer-ocean interface. Water Resources Research 43, 1–14. url: https://doi.org/10.1029/2006WR005679.

Robinson, C., P. Xin, L. Li and D. A. Barry (2014), Groundwater flow and salt transport in a subterranean estuary driven by intensified wave conditions. Water Resources Research 50, 165–181. url: https://doi.org/10.1002/2013WR013813.

Rosenzweig, C. and W. Solecki (2010), Introduction to Climate Change Adaptation in New York City: Building a Risk Management Response. Annals of the New York Academy of Sciences 1196, 13–17. url: https://doi.org/10.1111/j.1749-6632.2009.05415{_}1.x.

Rotzoll, K. and C. H. Fletcher (2012), Assessment of groundwater inundation as a consequence of sea-level rise. Nature Climate Change 3, 477–481. url: https://doi.org/10.1038/nclimate1725.

Ruessink, G. and R. Ranasinghe (2014), Beaches. In: G. Masselink and R. Gehrels, eds., Coastal Environments and Global Change, vol. 28, chap. 7, John Wiley & Sons, Ltd, first edn., 149–177. url: https://doi.org/10.1002/9781119117261.ch7.

Rutten, J., S. M. de Jong and G. Ruessink (2017), Accuracy of Nearshore Bathymetry Inverted From X -Band Radar and Optical Video Data. IEEE Transactions on Geoscience and Remote Sensing 55, 1106–1116. url: https://doi.org/10.1109/TGRS.2016.2619481.

Schneider, J. C. and S. E. Kruse (2003), A comparison of controls on freshwater lens morphology of small carbonate and siliciclastic islands: Examples from barrier islands in Florida, USA. Journal of Hydrology 284, 253–269. url: https://doi.org/10.1016/j.jhydrol.2003.08.002.

Shah, N., M. Nachabe and M. Ross (2007), Extinction Depth and Evapotranspiration from Ground Water under Selected Land Covers. Ground Water 45, 329–338. url: https://doi.org/10.1111/j.1745-6584.2007.00302.x.

Shibutani, Y., M. Kuroiwa and Y. Matsubara (2016), Effect of the Coastal Protection using the Beach Nourishment at Tottori Sand Dune Coast, Japan. Journal of Coastal Research 75, 695–699. url: https://doi.org/10.2112/SI75-139.1.

Slobbe, E., H. Vriend, S. G. Aarninkhof, K. Lulofs, M. Vries and P. Dircke (2013), Building with Nature: in search of resilient storm surge protection strategies. Natural Hazards 65, 947–966. url: https://doi.org/10.1007/s11069-012-0342-y.

Stafleu, J., D. Maljers, F. Busschers, J. Gunnink, J. Schokker, R. Dambrink, H. Hummelman and M. Schijf (2013), GeoTop construction (in Dutch). Tech. Rep., TNO, Utrecht, The Netherlands.

Steijn, P. W. V. (2015), Global Assessment on the Lifetime of Mega Nourishments. Msc thesis, Delft University.

Sterr, H. (2008), Assessment of Vulnerability and Adaptation to Sea-Level Rise for the Coastal Zone of Germany. Journal of Coastal Research 242, 380–393. url: https://doi.org/10.2112/07A-0011.1.

Stive, M. J., M. A. de Schipper, A. P. Luijendijk, S. G. Aarninkhof, C. van Gelder-Maas, J. S. van Thiel de Vries, S. de Vries, M. Henriquez, S. Marx and R. Ranasinghe (2013), A New Alternative to Saving Our Beaches from Sea-Level Rise: The Sand Engine. Journal of Coastal Research 290, 1001–1008. url: https://doi.org/10.2112/jcoastres-d-13-00070.1.

Stockdon, H. F., R. A. Holman, P. A. Howd and A. H. Sallenger (2006), Empirical parameterization of setup, swash, and runup. Coastal Engineering 53, 573–588. url: https://doi.org/10.1016/j.coastaleng.2005.12.005.

Stuurman, R. (2010), Conclusions drainage meeting MOS-Boskalis/Van Oord/Deltares (in Dutch). Tech. Rep., Deltares, Utrecht, The Netherlands.

Stuyfzand, P. J. (1993), Hydrochemistry and Hydrology of the Coastal Dune area of the Western Netherlands. Ph.d. thesis, Ph.D. Thesis, VU University Amsterdam, Amsterdam, The Netherlands.

Stuyfzand, P. J. (2014), Predicting the effects of sea spray deposition and evapoconcentration on shallow coastal groundwater salinity under various vegetation types. In: Proceedings of the 23rd Salt Water Intrusion Meeting, Husum, Germany, 401–404.

Syvitski, J. P. M., A. J. Kettner, I. Overeem, E. W. H. Hutton, M. T. Hannon, G. R. Brakenridge, J. Day, C. Vörösmarty, Y. Saito, L. Giosan and R. J. Nicholls (2009), Sinking deltas due to human activities. Nature Geoscience 2, 681–686. url: https://doi.org/10.1038/ngeo629.

Taylor, R. G., B. Scanlon, P. Döll, M. Rodell, R. van Beek, Y. Wada, L. Longuevergne, M. Leblanc, J. S. Famiglietti, M. Edmunds, L. Konikow, T. R. Green, J. Chen, M. Taniguchi, M. F. Bierkens, A. MacDonald, Y. Fan, R. M. Maxwell, Y. Yechieli, J. J. Gurdak, D. M. Allen, M. Shamsudduha, K. Hiscock, P. J.-F. Yeh, I. Holman, H. Treidel, R. van Beek, Y. Wada, M. Leblanc, Laurent Longuevergne, J. S. Famiglietti, M. Edmunds, L. Konikow, T. R. Green, J. Chen, M. Taniguchi, A. MacDonald, Y. Fan, R. M. Maxwell, Y. Yechieli, J. J. Gurdak, D. M. Allen, M. Shamsudduha, K. Hiscock, P. J.-F. Yeh, I. Holman and H. Treidel (2013), Ground water and climate change. Nature Climate Change 3, 322–329. url: https://doi.org/10.1038/nclimate1744.

Temmerman, S., P. Meire, T. J. Bouma, P. M. J. Herman, T. Ysebaert and H. J. de Vriend (2013), Ecosystem-based coastal defence in the face of global change. Nature 504, 79–83. url: https://doi.org/10.1038/nature12859.

Terry, J. P. and A. C. Falkland (2010), Responses of atoll freshwater lenses to storm-surge overwash in the Northern Cook islands. Hydrogeology Journal 18, 749–759. url: https://doi.org/10.1007/s10040-009-0544-x.

Tonnon, P. K., J. van der Werf and J. P. Mulder (2009), Morphological simulations, Environmental Impact Assesment Sand Engine (in Dutch). Tech. Rep. November, Deltares, Delft, The Netherlands.

Tonnon, P. K., L. van der Valk, H. Holzhauer, M. Baptist, J. Wijsman, C. Vertegaal and S. Arens (2011), Execution program Monitoring and Evaluation Pilot Sand Engine (in Dutch). Tech. Rep., Deltares and Imares.

Vallejos, A., F. Sola and A. Pulido-Bosch (2014), Processes Influencing Groundwater Level and the Freshwater-Saltwater Interface in a Coastal Aquifer. Water Resources Management 29, 679–697. url: https://doi.org/10.1007/s11269-014-0621-3.

Valverde, H. R., A. C. Trembanis and O. H. Pilkey (1999), Summary of beach nourishment episodes on the U.S. East Coast barrier islands. Journal of Coastal Research 15, 1100–1118. url: https://www.jstor.org/stable/4299028.

van der Wal, D. (1998), The impact of the grain-size distribution of nourishment sand on aeolian sand transport. Journal of Coastal Research 14, 620–631.

van Koningsveld, M. and J. P. Mulder (2004), Sustainable Coastal Policy Developments in The Netherlands. A Systematic Approach Revealed. Journal of Coastal Research 202, 375–385.

van Koningsveld, M., J. Mulder, M. Stive, L. Van Der Valk and A. van der Weck (2008), Living with Sea-Level Rise and Climate Change: A Case Study of the Netherlands. Journal of Coastal Research 242, 367–379. url: https://doi.org/10.2112/07A-0010.1.

van Puijenbroek, M. E. (2018), Dunes, above and beyond. The interactions between ecological and geomorphological processes. Phd thesis, Wageningen University & Research.

Vandenbohede, A. and L. Lebbe (2007), Effects of tides on a sloping shore: groundwater dynamics and propagation of the tidal wave. Hydrogeology Journal 15, 645–658. url: https://doi.org/10.1007/s10040-006-0128-y.

Vandenbohede, A. and L. Lebbe (2012), Groundwater chemistry patterns in the phreatic aquifer of the central Belgian coastal plain. Applied Geochemistry 27, 22–36. url: https://doi.org/10.1016/j.apgeochem.2011.08.012.

Vernes, R. and T. van Doorn (2005), From Guide layer to Hydrogeological Unit, Description of the construction of the data set (in Dutch). Tech. Rep., TNO, Utrecht, The Netherlands.

Vitousek, S., P. L. Barnard, C. H. Fletcher, N. Frazer, L. Erikson and C. D. Storlazzi (2017), Doubling of coastal flooding frequency within decades due to sea-level rise. Scientific Reports 7, 1399. url: https://doi.org/10.1038/s41598-017-01362-7.

Voortman, B., R. Bartholomeus, S. Van Der Zee, M. F. Bierkens and J. Witte (2015), Quantifying energy and water fluxes in dry dune ecosystems of the Netherlands. Hydrology and Earth System Sciences 19, 3787–3805. url: https://doi.org/10.5194/hess-19-3787-2015.

Vos, P. and S. de Vries (2013), Second generation of palaeogeographical maps of the Netherlands (version 2.0). Tech. Rep., Deltares, Deltares, Utrecht. url: www.archeologieinnederland.nl.

Wada, Y., L. van Beek, C. M. van Kempen, J. W. Reckman, S. Vasak and M. Bierkens (2010), Global depletion of groundwater resources. Geophysical Research Letters 37, 1–5. url: https://doi.org/10.1029/2010GL044571.

Wahl, T., I. Haigh, P. Woodworth, F. Albrecht, D. Dillingh, J. Jensen, R. Nicholls, R. Weisse and G. Wöppelmann (2013), Observed mean sea level changes around the North Sea coastline from 1800 to present. Earth-Science Reviews 124, 51–67. url: https://doi.org/10.1016/j.earscirev.2013.05.003.

Watson, T. A., A. D. Werner and C. T. Simmons (2010), Transience of seawater intrusion in response to sea level rise. Water Resources Research 46, 1–10. url: https://doi.org/10.1029/2010WR009564.

Waxman, M. and L. Smits (1968), Electrical conductivities in oil-bearing shaly sands. Society of Petroleum Engineers Journal 8, 107–122.

Webb, M. D. and K. W. Howard (2011), Modeling the Transient Response of Saline Intrusion to Rising Sea-Levels. Ground Water 49, 560–569. url: https://doi.org/10.1111/j.1745-6584.2010.00758.x.

Werner, A. D., M. Bakker, V. E. Post, A. Vandenbohede, C. Lu, B. Ataie-Ashtiani, C. T. Simmons and D. Barry (2013), Seawater intrusion processes, investigation and management: Recent advances and future challenges. Advances in Water Resources 51, 3–26. url: https://doi.org/10.1016/j.advwatres.2012.03.004.

Werner, A. D., H. K. Sharp, S. C. Galvis, V. E. Post and P. Sinclair (2017), Hydrogeology and management of freshwater lenses on atoll islands: Review of current knowledge and research needs. Journal of Hydrology 551, 819–844. url: https://doi.org/10.1016/j.jhydrol.2017.02.047.

White, I. and T. Falkland (2010), Management of freshwater lenses on small Pacific islands. Hydrogeology Journal 18, 227–246. url: https://doi.org/10.1007/s10040-009-0525-0.

Wilson, A. M., M. Huettel and S. Klein (2008), Grain size and depositional environment as predictors of permeability in coastal marine sands. Estuarine, Coastal and Shelf Science 80, 193–199. url: https://doi.org/10.1016/j.ecss.2008.06.011.

Wilson, A. M., W. S. Moore, S. B. Joye, J. L. Anderson and C. A. Schutte (2011), Storm-driven groundwater flow in a salt marsh. Water Resources Research 47, 1–11. url: https://doi.org/10.1029/2010WR009496.

Wong, P., I. Losada, J.-P. Gattuso, J. Hinkel, A. Khattabi, K. McInnes, Y. Saito and A. Sallenger (2014), Coastal systems and low-lying areas. In: Climate Change 2014: Impacts, Adaptation, and Vulnerability., chap. Part A: Gl, Cambridge, United Kingdom and New York, NY, USA: Cambridge University Press, 361–409.

Wösten, J., G. Veerman, W. DeGroot and J. Stolte (2001), Water retention and conductivity parameters of soils in the Netherlands: The Staring series (in Dutch). Tech. Rep., Alterra, Research Institute voor de Groene Ruimte, Wageningen.

Yang, J., T. Graf, M. Herold and T. Ptak (2013), Modelling the effects of tides and storm surges on coastal aquifers using a coupled surfacesubsurface approach. Journal of Contaminant Hydrology 149, 61–75. url: https://doi.org/10.1016/j.jconhyd.2013.03.002.

Yang, J., T. Graf and T. Ptak (2015), Sea level rise and storm surge effects in a coastal heterogeneous aquifer: a 2D modelling study in northern Germany. Grundwasser 20, 39–51. url: https://doi.org/10.1007/s00767-014-0279-z.

Yi, M.-J., J.-H. Kim and S.-H. Chung (2003), Enhancing the resolving power of least squares inversion with active constraint balancing. Geophysics 68, 931–941. url: https://doi.org/10.1190/1.1581045.

Zhang, K., B. C. Douglas and S. P. Leatherman (2004), Global Warming and Coastal Erosion. Climatic Change 64, 41–58. url: https://doi.org/10.1023/B:CLIM.0000024690.32682.48.

Zhang, Y., L. Li, D. V. Erler, I. R. Santos and D. Lockington (2016), Effect of alongshore morphology on groundwater flow and solute transport in a nearshore aquifer. Water Resources Research 52, 990–1008. url: https://doi.org/10.1002/2014WR015716.

Zwamborn, M. and J. Peters (2000), Expansion of water extraction Solleveld, Environmental Impact Assessment report (in Dutch). Tech. Rep., Kiwa N.V., Nieuwegein, The Netherlands.

Dankwoord

Om te beginnen wil ik Marc en Gu bedanken dat ze mij de kans hebben gegeven om dit promotieonderzoek te doen. Sinds de start van het promotietraject heb ik geen moment spijt gehad van deze keus, en er volop van genoten. Het heeft me de mogelijkheidheid gegeven om me verder te verdiepen in de kunst van het modelleren, het programmeren, en het schrijven en publiceren van wetenschappelijk onderzoek. Verder wil ik ze bedanken voor hun geduld, vertrouwen, en de vrijheid die ze me gaven om ook mijn eigen weg te gaan. Daarnaast natuurlijk ook voor de goede ideeen en suggesties op moeilijke momenten, en het uitgebreide en scherpe commentaar op de artikelen, zeker op al die keren dat het eigenlijk niet pastte in de drukke agenda's. Hopelijk kunnen we in de toekomst nog meer samenwerken!

Naast de hulp van Marc en Gu was een aanzienlijk deel van dit onderzoek niet mogelijk geweest zonder Marios, Mike, Pieter, Pieter, Max, Sierd, Arjen, Carlos, Nefeli, Lisa, Bas, Joost, en Perry. Hen ik wil ook allemaal bedanken voor de ondersteuning bij (geofysische) metingen, het modelleren, en programmeren!

Hoewel ik er erg van genoten heb, was het promotietraject een behoorlijk stuk eenzamer geweest zonder het gezelschap van met name Maria, René, Eelco, Joost, Yoshi, Jantien, Anouk, Daan, Daniel, Jude en Joeri! Een deel daarvan hadden eigenlijk geen keus omdat de kamers zo waren ingedeeld, maar desondanks ontzettend bedankt voor hun hulp, interesse en openheid. Dan denk ik ook aan de vele Gutenberg cappuccino's en wandelingen door de botanische tuin, die het leven ook een stuk aangenamer en smakelijker maakten. Naast de gezelligheid onder werktijd, denk ik natuurlijk ook aan de heerlijke Japanse diners onder de inspirerende leiding van Yoshi, reizen door de VS en Mexico met Jantien, Joost en Daan, en de vele bordspellen! Als het aan mij ligt gaan er nog vele volgen na de promotie.

Naast het gezelschap op de campus, had ik ook het geluk om deel uit te maken van NatureCoast (i.e. het collectief van PhD's en postdoc's die onderzoek doen/deden op/bij de Zandmotor). Daardoor heb ik mogen kennis maken met vele andere interessante onderzoeksvelden, zoals o.a. geochemie, ecologie (breed spectrum), morfologie. De NatureCoast bijeenkomsten waren vanaf begin af aan gezellig, met een open en genteresseerde houding van iedereen naar elkaar. Alle PhD's bedankt, in het bijzonder Iris, Jantien, Corjan, Marinka, Max, Simeon, Emily, Lotte, Marjolein, Ewert, Lianne en Isaac. Ook de postdoc's Arjen, Timothy, Vera, en Alexander: ontzettend bedankt voor het trekken, motiveren, stimuleren van ons als groep! Ik ben ook erg nieuwsgierig naar het aankomende NatureCoast boek! Aansluitend wil ik ook de eindgebruikers Arie, Hein, Patrick, en Jaap en de Satellietgroep (Jacqueline, Ronald, Francois) bedanken voor hun interesse, inspirate, tijd en scherpe vragen bij de NatureCoast bijeenkomsten.

Tenslotte wil ik ook mijn familie en vrienden die nog niet zijn genoemd bedanken voor hun interesse en betrokkenheid bij mijn promotie. Zelfs tot en met een bezoek aan de Zandmotor (uiteraard met gids, zie voorkant). Daarbij wil ik ook Daan en Sjoerd bedanken voor hun hulp, tijd en energie als paranimf. Sjoerd nog in het bijzonder bedankt voor het ontwerp, en de laatste aanpassingen!

Sebastian Huizer
Wageningen, Maart 2019

Summary

Most coastal regions around the world rely on groundwater as their primary source of fresh water. Excessive groundwater abstraction, population growth, sea-level rise, and increases in storm surges threaten the availability of fresh water in many (densely populated) coastal communities. Coastal lowlands and small islands are particularly at risk, because these areas are most susceptible to coastal flooding. One of the potential responses to protect these communities, is to actively protect the coast against erosion and flooding with beach nourishments. As discussed in chapter 1, the Sand Engine is one prime example of this strategy, and one of a few adaptation approaches that additionally might lead to an increase of the fresh groundwater volume. Since the Sand Engine is the first of its kind, little is known about the influence of mega-scale beach nourishment on fresh groundwater resources. This raises the question: What is the impact of the Sand Engine on fresh groundwater resources?

Where the direct impact of the construction of the Sand Engine on fresh groundwater is predictable and limited, the indirect impact of the creation of the Sand Engine is complex and extensive. The complexity is a result of the morphological evolution of the Sand Engine and the exposure to tides, waves, and storm surges. In other words, the growth of fresh groundwater resources is to a large extent controlled by highly dynamic processes, which are hard to predict. To answer and specify the various aspects of the impact of the Sand Engine on fresh groundwater resources, the main research question was split into three sub-questions:

1. What is the potential increase in fresh groundwater resources over a long period (chapter 2)?

2. What is the impact of tides, waves and storms on the fresh groundwater lens in the Sand Engine (chapter 3)?

3. What were the changes in the volume of fresh groundwater in the study area since the construction of the Sand Engine, and which processes drove these changes (chapter 4)?

To accurately assess the effects of the Sand Engine on fresh groundwater resources, a comprehensive analysis of the groundwater system was conducted. First, data from local water authorities was collected (e.g. boreholes, pumping rates, historical maps, groundwater levels, analyses of the groundwater salinity), and groundwater levels and salinities were monitored on the Sand Engine. Subsequently, this data was used to reconstruct the spatial distribution of groundwater levels and salinities, before and after the construction of the Sand Engine. This included reconstructions of the historical landscape evolution (1500–2010) and the historical pumping rates in the dune area Solleveld (chapter 2).

This reconstruction was implemented in a three-dimensional groundwater model, which was used to predict and reconstruct the growth in fresh groundwater resources in the study area. Model simulations with predictions of the morphological change of the Sand Engine up to 2050 confirmed that the construction of the Sand Engine could lead to an increase of fresh groundwater of approximately 0.3 to 0.5 million m^3 yr^{-1}. However, reconstructions of the growth in fresh groundwater resources for 2011 to 2016 showed that this volume was smaller in reality, because of coastal flooding and underestimations of the actual geomorphological changes. The growth of the freshwater lens between 2011 and 2016 was primarily determined by the groundwater recharge, (maximum) land-surface inundations due to storm surges, groundwater in- and outflow, and to a lesser extent by geomorphological changes. Naturally, larger deviations between projections and reality in the future could lead to larger errors in the actual and predicted growth in fresh groundwater resources and are therefore important for accurate predictions of the impact of the Sand Engine.

The impact of tides, waves and storm surges on fresh groundwater was successfully monitored with a technique called 'electrical resistivity tomography'. This technique uses differences in the electrical resistivity (or conductivity) of for instance sand and salt to attain two dimensional images of the groundwater salinity. The measurements were employed near the shoreline on the outer perimeter of the Sand Engine. Over a period of several months we were able to observe changes in the thickness of the fresh groundwater lens every 30 minutes, in calm to turbulent weather conditions. In addition, most of the measured changes in groundwater head and salinity could be imitated with a numerical groundwater model. This proved that with a thorough understanding of the local system, groundwater models can be used to make accurate predictions of the impact of tides and storm surges on fresh groundwater resources.

Thus, mega-scale beach nourishments such as the Sand Engine can lead to a substantial increase in fresh groundwater resources. A first attempt to map the global potential – presuming all eroding sandy beaches are suitable for large beach nourishments – showed that large beach nourishments will likely lead to a (temporary) increase of fresh groundwater resources in most settings. However, for a substantial growth in fresh groundwater, the coastal site should receive sufficient groundwater recharge, consist of sediment with a low to medium hydraulic conductivity, and be subject to a limited number of land-surface inundations. Our global analysis shows that 17% of the shorelines – excluding Arctic regions – may consist of such erosive sandy beaches, and of these sites 50% have a high potential suitability. This suggests that local mega-scale beach nourishments may become an interesting solution for some (sandy) coastal areas, to protect the inhabitants and fresh groundwater resources.

Samenvatting

De meeste kustgebieden in de wereld zijn afhankelijk van grondwater als primaire bron van zoet water. Grondwateronttrekkingen, bevolkingsgroei, zeespiegelstijging en stormen bedreigen echter de beschikbaarheid van zoet water in veel (dichtbevolkte) kustgemeenschappen in toenemende mate. Hierbij lopen vooral kleine eilanden en laaggelegen kustgebieden gevaar, omdat deze gebieden het meest vatbaar zijn voor overstromingen. Eén van de mogelijke beheersmaatregelen is om de kust actief te beschermen tegen erosie en overstromingen met behulp van zandsuppleties. Zoals besproken in hoofdstuk 1 is de Zandmotor een goed voorbeeld van deze strategie, en bovendien één van de weinige maatregelen die kan leiden tot een vergroting van de voorraad zoet grondwater. Omdat de Zandmotor de eerste in zijn soort is, is er weinig bekend over de invloed van een mega-suppletie op zoet grondwater. Dit roept de vraag op: wat is de impact van de Zandmotor op de voorraad zoet grondwater?

Waar de directe impact van de constructie van de Zandmotor op zoet grondwater voorspelbaar en beperkt in omvang is, is de indirecte impact van de aanleg van de Zandmotor complex en mogelijk uitgebreid. De complexiteit is het gevolg van de morfologische veranderingen van de Zandmotor en de blootstelling aan getijden, golven en stormen. Met andere woorden, de groei van de voorraad zoet grondwater wordt grotendeels beheerst door dynamische processen, die moeilijk te voorspellen zijn. Om de verschillende aspecten van de impact van de Zandmotor op zoet grondwater te beantwoorden en te specificeren, is de hoofdonderzoeksvraag opgesplitst in drie deelvragen:

1. Wat is de potentiële toename van de voorraad zoet grondwater over een lange periode (hoofdstuk 2)?

2. Wat is de invloed van getijden, golven en stormen op de zoete grondwaterlens in de Zandmotor (hoofdstuk 3)?

3. Wat waren de veranderingen in het volume zoet grondwater in het studiegebied sinds de constructie van de Zandmotor, en welke processen hebben deze veranderingen veroorzaakt (hoofdstuk 4)?

Om de effecten van de Zandmotor op de voorraad zoet grondwater nauwkeurig te bepalen, is een grondige analyse van het grondwatersysteem uitgevoerd. Eerst zijn gegevens van lokale waterschappen verzameld (e.g. boorstaten, grondwaterstanden, analyses van het zoutgehalte van het grondwater) en zijn grondwaterstanden en zoutgehaltes op de Zandmotor gemonitord. Vervolgens zijn deze gegevens gebruikt om een ruimtelijke verdeling van grondwaterstanden en zoutgehaltes voor en na de bouw van de Zandmotor te reconstrueren. Dit betekende onder meer een reconstructie van de historische evolutie van het kustgebied (1500-2010) en van de onttrekkingen in het duingebied Solleveld (hoofdstuk 2).

Deze reconstructie is gemplementeerd in een driedimensionaal grondwatermodel, dat is gebruikt om de groei van de voorraad zoet grondwater in het studiegebied te voorspellen. Modelsimulaties met voorspellingen van de morfologische verandering van de Zandmotor tot 2050 bevestigden dat de bouw van de Zandmotor zou kunnen leiden tot een toename van zoet grondwater van ongeveer 0.3 tot 0.5 miljoen m^3 yr^{-1}. Uit reconstructies van de groei van de hoeveelheid zoet grondwater tussen 2011 en 2016 bleek echter dat dit volume in werkelijkheid kleiner was vanwege overstromingen aan de kust en onderschatting van de feitelijke geomorfologische veranderingen. De groei van de zoetwaterlens tussen 2011 en 2016 werd voornamelijk bepaald door de neerslag, verdamping, overstromingen van het landoppervlak als gevolg van stormen, grondwater in- en uitstroming, en in mindere mate door geomorfologische veranderingen. Uiteraard kunnen grotere afwijkingen tussen projecties en de werkelijkheid in de toekomst leiden tot grotere fouten in de feitelijke en voorspelde groei van nieuwe grondwatervoorraden en zijn daarom van belang voor nauwkeurige voorspellingen van de impact van de Zandmotor.

De invloed van getijden, golven en stormen op zoet grondwater zijn met succes gemonitord met een techniek genaamd 'electro resistivity tomography'. Deze techniek maakt gebruik van verschillen in de elektrische weerstand (of geleidbaarheid) van bijvoorbeeld zand en zout om tweedimensionale beelden van het zoutgehalte van het grondwater te krijgen. De metingen zijn dichtbij de kustlijn uitgevoerd, aan de buitenrand van de Zandmotor. Gedurende een periode van enkele maanden konden we elke 30 minuten veranderingen in de dikte van de verse grondwaterlens waarnemen, in rustige tot turbulente weersomstandigheden. Bovendien konden de meeste gemeten veranderingen in grondwaterstand en zoutgehalte worden gereproduceerd met een numeriek grondwatermodel. Dit toont aan dat met grondige kennis van het lokale systeem grondwatermodellen kunnen worden gebruikt om nauwkeurige voorspellingen te doen van de invloed van getijden en stormvloeden op nieuwe grondwatervoorraden.

Mega-suppleties zoals de Zandmotor kunnen dus leiden tot een substantile toename van zoet grondwater. Een eerste poging om het wereldwijde potentieel in kaart te brengen - ervan uitgaande dat alle eroderende zandstranden geschikt zijn voor grote strandsuppleties – toonde aan dat grote strandsuppleties waarschijnlijk zullen leiden tot een (tijdelijke) toename van zoet grondwater in de meeste omstandigheden. Voor een substantiële groei in zoet grondwater moet de kustlocatie voldoende grondwater bijladen, bestaan uit sediment met een lage tot gemiddelde hydraulische geleidbaarheid en zijn onderworpen aan een beperkt aantal overstromingen van het landoppervlak. Onze wereldwijde analyse laat zien dat 17% van de stranden – met uitzondering van Arctische gebieden – uit dergelijke erosieve zandstranden kan bestaan, en van deze locaties hebben 50% een hoge potentile geschiktheid. Dit betekent dat grote zandsuppleties mogelijk wereldwijd een interessante oplossing kunnen vormen voor de bescherming van (zandige) kustgebieden en het aanwezige zoet grondwater.

About the author

Sebastian Huizer was born on the 17^{th} of May 1985 in the city of Gorinchem. Sebastian attended high school (VWO) in Leerdam, both at the Heerenlanden College. At the age of 18, Sebastian moved to the city of Wageningen and started studying Soil, Water, Atmosphere at Wageningen University. In September 2008, Sebastian finished his masters in the field of geohydrology. Directly following his master, Sebastian started working at Arcadis. In June 2013, Sebastian started on a PhD project focused on fresh groundwater in the Sand Engine (also called Sand Motor, or 'Zandmotor' in Dutch). Sebastian now returned to Arcadis and holds the position of specialist in the field of geohydrology.

List of publications

Journal papers

Huizer, S., Oude Essink, G. H. P., and Bierkens, M. F. P. (2016), Fresh groundwater resources in a large sand replenishment, Hydrology and Earth System Sciences 20, 3149–3166, doi:10.5194/hess-20-3149-2016.

Huizer, S., Karaoulis, M. C., Oude Essink, G. H. P., and Bierkens, M. F. P. (2017), Monitoring and simulation of salinity changes in response to tide and storm surges in a sandy coastal aquifer system, Water Resources Research 53, 6487–6509, doi:10.1002/2016WR020339.

Huizer, S., Radermacher, M., de Vries, S., Oude Essink, G. H. P., and Bierkens, M. F. P. (2018), Impact of coastal forcing and groundwater recharge on the growth of a fresh groundwater lens in a mega-scale beach nourishment, Hydrology and Earth System Sciences 22, 1065–1080, doi:10.5194/hess-22-1065-2018.

Huizer, S., Luijendijk, A. P., Bierkens, M. F. P., and Oude Essink, G. H. P., (under review) Global potential for the growth of fresh groundwater resources with large beach nourishments, submitted to Scientific Reports.

Conference contributions

Huizer, S., Bierkens, M. F. P., and Oude Essink, G. H. P. (2014), Can a large sand suppletion lead to a substantial increase in fresh water resources?: The Sand Motor Project, 23rd Saltwater Intrusion Meeting (SWIM), Husum, Germany (oral).

Huizer, S., Bierkens, M. F. P., and Oude Essink, G. H. P. (2014), Modelling Changing Morphology and Density Dependent Groundwater Flow in a Dynamic Environment: Sand Motor, AGU Fall meeting, San Francisco, USA (poster).

Huizer, S., Bierkens, M. F. P., and Oude Essink, G. H. P. (2015), Modeling Changing Morphology and Density Dependent Groundwater Flow in a Dynamic Environment: case study, EGU General Assembly, Vienna, Austria (oral).

Huizer, S., Karaoulis, M. C., Oude Essink, G. H. P., and Bierkens, M. F. P. (2016), Monitoring the effect of tides and storm surges on coastal fresh groundwater lenses, 24th Saltwater Intrusion Meeting (SWIM) and the 4th Asia-Pacific Coastal Aquifer Management Meeting (APCAMM), Cairns, Queensland, Australia (oral).

Huizer, S., Radermacher, M., de Vries, S., Oude Essink, G. H. P., and Bierkens, M. F. P. (2018), Impact of coastal forcing and groundwater recharge on the growth of a fresh groundwater lens in a mega-scale beach nourishment, 25th Saltwater Intrusion Meeting (SWIM), Gdansk, Poland (oral).